



Ludwig-Maximilians-Universität München

Fakultät für Biologie

Lehrstuhl für Zell- und Entwicklungsbiologie

**Functional characterization of the BRCT domains of the  
RhoA GEF Ect2 during cell division**

Dissertation

zur

Erlangung des akademischen Grades eines Doktors der  
Naturwissenschaften (Dr. rer. nat.)

vorgelegt von Kristina Maria Buchner

Neufahrn, Dezember 2018



Erstgutachterin: Dr. Esther Zanin

Zweitgutachter: Prof. Dr. Heinrich Leonhardt

Tag der Abgabe: 11.12.2018

Tag der mündlichen Prüfung: 29.05.2019

## **ERKLÄRUNG**

Ich versichere hiermit an Eides statt, dass meine Dissertation selbständig und ohne unerlaubte Hilfsmittel angefertigt worden ist. Die vorliegende Dissertation wurde weder ganz, noch teilweise bei einer anderen Prüfungskommission vorgelegt. Ich habe noch zu keinem früheren Zeitpunkt versucht, eine Dissertation einzureichen oder an einer Doktorprüfung teilzunehmen.

München, den 11.07.2019

Kristina Buchner



# Table of Contents

Abstract .....	1
Zusammenfassung .....	3
1. Introduction .....	14
1.1. Cytokinesis in animal cells.....	14
1.2. The mitotic spindle positions the contractile ring .....	15
1.3. RhoA GTPase and its role in contractile ring formation.....	18
1.4. Contractile ring composition and molecular control of ring constriction .....	20
1.5. Abscission as the last step of cytokinesis.....	22
1.6. The GEF Ect2 and its role in cytokinesis .....	23
1.7. Ect2 regulation by centralspindlin.....	25
1.8. Regulation of Ect2 by mitotic kinases.....	28
1.9. Aims of the thesis .....	30
2. Methods and materials .....	33
2.1. Methods.....	33
2.1.1. <i>C. elegans</i> techniques .....	33
2.1.1.1. Maintenance of <i>C. elegans</i> worm strains .....	33
2.1.1.2. Freezing of <i>C. elegans</i> worm strains .....	33
2.1.1.3. Generation of transgenic worm strains by MosSCI insertion .....	34
2.1.1.4. Insertion of transgenes and validation of integration in <i>C. elegans</i> .....	34
2.1.1.5. Verification of homozygous insertion events in <i>C. elegans</i> .....	35
2.1.1.6. Verification of GOI insertion by genotyping .....	36
2.1.1.7. Worm crosses .....	36
2.1.1.8. dsRNA production for the depletion of endogenous ECT-2 in <i>C. elegans</i> .....	37
2.1.1.9. <i>ect-2(RNAi)</i> , lethality tests and measurement of brood size in <i>C. elegans</i> strains .....	38
2.1.1.10. <i>gfp(RNAi)</i> feeding approach to deplete the <i>gfp::ect-2<sup>ΔBRCT0+1+2</sup></i> transgene during strain generation.....	38

2.1.1.11. Live imaging of embryos in <i>C. elegans</i> by confocal spinning disk microscopy .....	39
2.1.2. Tissue culture techniques .....	39
2.1.2.1. Maintenance of HeLa FRT cell lines .....	39
2.1.2.2. Freezing of HeLa FRT cell lines .....	39
2.1.2.3. Generation of transgenic HeLa cell lines .....	40
2.1.2.4. Depletion of endogenous Ect2 by RNAi in human cells.....	40
2.1.2.5. Live Imaging in cells.....	41
2.1.2.6. Analysis of expression levels of Ect2 transgenes by Live Imaging .....	41
2.1.2.7. Quantification methods of HsEct2 fluorescence intensities at the cell periphery and at the spindle midzone by Live Imaging .....	41
2.1.2.8. Immunostainings in cells.....	42
2.1.2.9. C3 Rho inhibitor experiments .....	43
2.1.3. Molecular biology techniques .....	43
2.1.3.1. Polymerase chain reaction for cloning by Gibson Assembly .....	43
2.1.3.2. Agarose gel electrophoresis for PCR products .....	43
2.1.3.3. Dpn1 digest of PCRs amplified from bacterial templates.....	44
2.1.3.4. Purification of PCR products by spin-column .....	44
2.1.3.5. Purification of PCR products by gel excision .....	44
2.1.3.6. Cloning by Gibson Assembly .....	44
2.1.3.7. Transformation in the competent <i>E. coli</i> strain DH5alpha.....	45
2.1.3.8. DNA preparations by alkaline lysis .....	46
2.1.3.9. DNA preparations by plasmid Mini Kit.....	46
2.1.3.10. Sequencing of candidates .....	47
2.1.3.11. Western Blot analysis in cells .....	47
2.2. Materials.....	48
3. Results .....	66

3.1. CeECT-2 BRCT0 and BRCT1 domains are not inhibiting GEF activity but are required for cytokinesis and viability .....	67
3.1.1. Establishing a molecular replacement system for CeECT-2 in <i>C. elegans</i> .....	67
3.1.2. Absence of CeECT-2 BRCT domains cause high sterility in <i>C. elegans</i> .....	70
3.1.3. CeECT-2 BRCT0 and BRCT1 domains are required for embryonic viability and cytokinesis .....	73
3.2 HsEct2 BRCT1 and BRCT2 domains are required for cytokinesis and inhibit GEF function <i>in-vivo</i> .....	81
3.2.2. The BRCT0 domain contributes to spindle midzone localization and is not required for cytokinesis .....	85
3.2.3. The BRCT1 domain is the major spindle midzone binding domain and is required for cytokinesis .....	93
3.2.4. The BRCT2 domain is required for cytokinesis and inhibits GEF activity .....	98
3.2.5. Membrane blebbing in HsEct2 <sup>ΔBRCT2</sup> is caused by hyperactive Rho .....	102
3.2.6. Deletion of BRCT2 domain results in increased anillin levels .....	103
3.2.7. The linker region between the BRCT2 and GEF domain is involved in regulating HsEct2 function.....	105
4. Discussion and outlook .....	109
Literature .....	129
Acknowledgement.....	139



## Abstract

Cytokinesis is the final step in cell division that is initiated by the formation of a cleavage furrow that partitions the contents of a single cell into two nascent daughter cells. The RhoA Guanine nucleotide exchange factor (GEF) Ect2 has been shown to be essential for the regulation of cleavage furrow formation, however how Ect2 is regulated in order to control proper cell division is incompletely understood. Current models propose an autoinhibitory mechanism by which the three N-terminal BRCT domains bind the C-terminal GEF domain of Ect2. It has not yet been tested whether the three BRCT domains act as one module or whether each BRCT domain has a distinct role during cytokinesis. Using structure-function studies in *C. elegans* and human cells we showed that the BRCT domains are required for spindle midzone localization and have distinct roles in regulating Ect2 localization and function. Our results demonstrate that each of the BRCT domains but not only BRCT1 as shown before contribute to midzone binding and enrichment at the equatorial plasma membrane. Importantly our data suggests that BRCT2 domain is the major inhibitory domain of human Ect2 and that deletion of BRCT2 leads to active RhoA dependent hypercontractility during mitosis. Furthermore, I found that phosphorylation of the linker region between the BRCT2 and the GEF domain of Ect2 is required to inhibit Ect2 GEF activity which is consistent with former findings that showed that phosphorylation is involved in Ect2 regulation. Moreover, with my work the function of BRCT0 and BRCT1 domain were characterized in *C. elegans* and I showed that BRCT0 and BRCT1 domains are important for embryonic viability and for cytokinesis. Moreover, I showed that BRCT0 is not required for cytokinesis in human cells but is essential in *C. elegans* whereas BRCT1 domain is required in both systems.

Together my findings suggest that Ect2 BRCT domains in human cells do not act as one module but rather have separate roles during cytokinesis in localizing HsEct2 to the spindle midzone, the equatorial plasma membrane, and in regulating Ect2 activity *in-vivo*. My results are consistent with a model where Ect2 is regulated in a two-step process: Ect2 is phosphorylated in the linker region by mitotic kinases to keep it inactive until anaphase onset. In anaphase the BRCT2 domain is released from the GEF domain due to dephosphorylation of the linker region. Ect2 is then targeted to the plasma membrane and enriched at the equatorial plasma membrane via the N-terminal BRCT domains. Once Ect2 is at the plasma membrane it can activate RhoA to initiate contractile ring formation and cell division.



## Zusammenfassung

Zytokinese ist der letzte Schritt der Zellteilung, bei dem die Bestandteile einer einzelnen Zelle auf zwei neue Zellen aufgeteilt werden. Es wurde bereits gezeigt, dass das RhoA-GEF (Guanine nucleotide exchange factor) Ect2 essentiell für die Bildung der Teilungsfurche während der Zytokinese ist. Allerdings ist nicht klar, wie Ect2 während der Zellteilung reguliert wird, um die korrekte Bildung der Teilungsfurche zu gewährleisten. Eine aktuelle Hypothese besagt, dass Ect2 über einen auto-inhibitorischen Mechanismus reguliert wird, bei dem die N-terminalen BRCT-Domänen die katalytische GEF Domäne binden und inhibieren. Ob die drei BRCT-Domänen als Einheit agieren, oder ob sie unabhängig voneinander, unterschiedliche Funktionen während der Zellteilung übernehmen wurde bisher nicht geklärt. Mit Hilfe von Struktur-Funktionsstudien in *Caenorhabditis elegans* und humanen Zellen konnte durch meine Arbeit gezeigt werden, dass die BRCT-Domänen unterschiedliche Aufgaben bezüglich Lokalisierung und Funktion von Ect2 haben. Meine Arbeit demonstriert, dass die BRCT0 Domäne zwar während der Embryonalentwicklung in *C. elegans* benötigt wird, jedoch keine Funktion während der Zellteilung in humanen Zellen hat. Die BRCT1 Domäne hingegen ist sowohl in *C. elegans* also auch in Humanzellen für die Zytokinese essentiell. Darüber hinaus konnte gezeigt werden, dass das Entfernen der BRCT2-Domäne zu einer erhöhten und RhoA-abhängigen Kontraktilität des Zellcortex führt was darauf hin deutet, dass die BRCT2-Domäne die GEF-Aktivität inhibiert. Zudem werden alle drei BRCT-Domänen für die Lokalisierung von Ect2 an der Zentralspindel benötigt, und nicht wie bisher vermutet nur die BRCT1-Domäne. Weiterhin wurde gezeigt, dass alle drei BRCT-Domänen für die Anreicherung an der äquatorialen Plasmamembran benötigt werden, und dass Phosphorylierungen in der Region zwischen den BRCT und der GEF-Domäne (Linker-Region) wichtig sind, um die GEF-Aktivität zu inhibieren. Dies ist konsistent mit früheren Erkenntnissen, dass Phosphorylierungen für die Regulierung von Ect2 wichtig sind. Zusammenfassend wurde gezeigt, dass die BRCT-Domänen von Ect2 nicht als Modul zusammenhängend agieren, sondern unterschiedliche Funktionen bezüglich der Lokalisierung und der Regulierung von Ect2 in der Zelle haben. Meine Ergebnisse sind im Einklang mit einer Hypothese, dass Ect2 über zwei verschiedene Schritte reguliert ist: die Linker-Region von Ect2 wird während der G2/M Phase von mitotischen Kinasen phosphoryliert und Ect2 wird dabei in einem inaktiven Zustand gehalten. In der Anaphase wird die BRCT2-Domäne durch das Entfernen der Phosphorylierungen in der Linker-Region von der GEF-Domäne gelöst und Ect2 wird mit Hilfe

der Ect2 BRCT-Domänen am Zelläquator angereichert, um RhoA zu aktivieren und den kontraktilen Ring zu bilden.



## List of figures

Fig. 1. Overview of cytokinesis. ....	15
Fig. 2. Models of cleavage furrow positioning. ....	18
Fig. 3. The RhoA signalling pathway during cytokinesis and composition of the contractile ring. .....	20
Fig. 4. HsEct2 and CeECT-2 localize differently in the cell.....	25
Fig. 5. Different models of Ect2 regulation during cytokinesis. ....	26
Fig. 6. RNAi resistant, transgenic GFP-CeECT-2WT rescues cytokinetic failure, lethality and brood size. ....	69
Fig. 7. Different experimental strategies to express GFP-CeECT-2 <sup>ΔBRCT0+1+2</sup> in the one-cell <i>C.</i> <i>elegans</i> embryo. ....	72
Fig. 8. CeECT-2 BRCT0 and BRCT1 are not required for membrane localization. ....	74
Fig. 9. CeECT-2 BRCT0 and BRCT1 domains are required for embryonic viability and cytokinesis. ....	76
Fig. 10. CeNMY-2 levels in CeECT-2 <sup>ΔBRCT0</sup> transgenic strains are decreased at the furrow tip. .....	78
Fig. 11. The BRCT0 domain promotes CeNMY-2 recruitment to the furrow in the absence of endogenous CeECT-2. ....	80
Fig. 12. Flp-In T-REx™ HeLa system to generate transgenic HsEct2 cell lines with single-copy insertions of the transgenes. ....	82
Fig. 13. Transgenic, RNAi resistant HsEct2WT rescues cytokinesis defect after depletion of endogenous HsEct2. ....	84
Fig. 14. Overview of generated transgenic HsEct2 cell lines. ....	85
Fig. 15. BRCT0 domain is not required for cytokinesis. ....	87
Fig. 16. HsEct2 transgenes are expressed at similar levels. ....	88
Fig. 17. BRCT0 domain contributes to spindle midzone localization and, is required to enrich HsEct2 at the cell equator.....	90
Fig. 18. Absence of BRCT0 domain does not increase membrane blebbing during mitosis... 92	
Fig. 19. The BRCT1 domain is required for cytokinesis and deletion of BRCT1 abolishes spindle midzone localization. ....	96
Fig. 20. BRCT1 domain is required to enrich HsEct2 at the equatorial membrane and deletion of BRCT1 induces mild membrane blebbing in anaphase. ....	97
Fig. 21. BRCT2 domain is required for cytokinesis and contributes to spindle midzone localization. ....	101

Fig. 22. BRCT2 domain is required to enrich HsEct2 at the equatorial plasma membrane and absence of BRCT2 causes severe membrane blebbing. ....	101
Fig. 23. Blebbing in HsEct2 <sup>ΔBRCT2</sup> expressing cells is reduced upon Rho inhibition. ....	103
Fig. 24. Cortical anillin levels are increased in metaphase when cells express HsEct2 <sup>ΔBRCT2</sup> . .....	104
Fig. 25. HsEct2 linker region is involved in inhibiting HsEct2 GEF activity.....	107
Fig. 26. BRCT domains are not required for plasma membrane targeting in <i>C. elegans</i> , but for equatorial enrichment in human cells.....	124
Fig. 27. Model of HsEct2 activity regulation.....	128

## List of tables

Table 1. Buffers and solutions.....	48
Table 2. Technical equipment .....	50
Table 3. Kits .....	52
Table 4. Drugs, Chemicals and Reagents.....	52
Table 5. Antibodies .....	53
Table 6. Enzymes and Enzyme Mixes .....	54
Table 7. DNA Primers.....	54
Table 8. Plasmids provided by the laboratory .....	59
Table 9. Generated plasmids .....	59
Table 10. Bacterial strains provided by the laboratory .....	60
Table 11. Received <i>C. elegans</i> strains.....	60
Table 12. Generated <i>C. elegans</i> strains .....	61
Table 13. Generated cell lines .....	62
Table 14. Components of the MosSCI Injection Mix .....	63
Table 15. Digestion mix for worm lysis.....	63
Table 16. PCR pipetting scheme and cycler settings for genotyping and RNA generation ....	63
Table 17. Pipetting scheme and cycler settings of PCR for Gibson assembly.....	64
Table 18. Pipetting scheme of Gibson Reaction .....	64
Table 19. Pipetting scheme of sequencing reaction according to the protocol “Cycle, Clean and Run BigDye v.3.1. from the LMU sequencing service .....	65
Table 20. Pipetting scheme of the transcription mix.....	65

Table 21. Thresholds of fluorescent intensity levels used for the different categories of HsEct2 transgene expression in cell lines analyzed by confocal microscopy images. .... 89

## General abbreviations

<b>Symbol</b>	<b>Full name</b>
AA	Amino acid
<i>A. marginale</i>	<i>Anaplasma marginale</i>
APS	Ammonium persulfate
<i>A. rusticana</i>	<i>Armoracia rusticana</i>
<i>A. victoria</i>	<i>Aequorea victoria</i>
bp	Base pair(s)
BRCT	BRCA1 C-terminus domain
BSA	Bovine serum albumin
CAAX motif	C= cysteine, A= aliphatic AA, X= any AA
cDNA	Complimentary DNA
<i>C. elegans</i>	<i>Caenorhabditis elegans</i>
Ce	<i>C. elegans</i>
CO <sub>2</sub>	Carbon dioxide
C-terminus	Carboxy-terminus/ end of a protein
Da	Dalton [g/mol]
DH	Dbl homology
DIC	Differential interference contrast microscopy
DNA	Deoxyribonucleic acid
DNase	Deoxyribonuclease
dNTP	Deoxyribonucleoside triphosphate
<i>D. melanogaster</i>	<i>Drosophila melanogaster</i>
DMSO	Dimethylsulfoxide
Ds	Double-stranded
EB	Elution buffer
<i>E. coli</i>	<i>Escherichia coli</i>
EDTA	Ethylenediaminetetraacetic acid
<i>E. quadricolor</i>	<i>Entacmaea quadricolor</i>

ER	Endoplasmic reticulum
EtOH	Ethanol
Flp-recombinase	Flip-in recombinase
FRT	Flp recognition target
g	gram
GAP	GTPase activating protein
GDP	Guanosine diphosphate
GEF	Guanine nucleotide exchange factor
GDI	Guanosine dissociation factor
GOI	Gene of interest
GTP	Guanosine triphosphate
GTPase	Guanosine triphosphatase
h	hour
HeLa cells	Human ovarian cancer cell line derived from the patient Henrietta Lacks
<i>H. sapiens</i>	<i>Homo sapiens</i>
Hs	<i>Homo sapiens</i>
H <sub>2</sub> O	Water
IPTG	Isopropylthiogalactoside
KCl	Potassium chloride
kDa	kilo Dalton
kg	kilogram
l	liter
LB	Lysogeny broth
LiCl	Lithium-chloride
MeOH	Methanol
μg	microgram
mg	Milligram
μl	Microliter
ml	Milliliter
min	minutes
MosSCI	Mos1-mediated single-copy insertion
ms	milliseconds
NaCl	Sodium Chloride

NEBD	Nucleic envelope break-down
NGM	Nematode growth medium
Ng	Nanogram
NLS	Nuclear localization signal
N-terminus	Amino-terminus/ end of a protein
O/N	Over night
ORF	Open reading frame
PAGE	Polyacrylamide gel electrophoresis
PBS	Polybasic sequence
PBS (buffer)	Phosphate-buffered saline
PCR	Polymerase chain reaction
PH domain	Pleckstrin homology domain
pH value	Logarithmic scale to specify the acidity or basicity of an aqueous solution
PVDF	Polyvinylidenfluorid
RNA	Ribonucleic acid
RNase	Ribonuclease
RNAi	RNA interference
RT	Room temperature
<i>S. cerevisiae</i>	<i>Saccharomyces cerevisiae</i>
P/S	Penicillin/Streptomycin
rNTP	Ribonucleoside triphosphate
s	second
SDS	Sodium dodecyl sulfate
siRNA	Small interfering RNA
Taq	<i>Thermus aquaticus</i> (polymerase)
TBS (buffer)	Tris-buffered saline
TAE	Tris-acetate-EDTA
TE	Tris-EDTA
TEMED	Tetramethylethylenediamine
Trans-light	Transmission-light
Tris	Tris(hydroxymethyl)aminomethane
UTR	Untranslated region
UV	Ultra-violet

WT

*X. laevis*

Wild type

*Xenopus laevis*

## Gene and protein abbreviations

Gene symbol	Protein symbol	Full name	Species
<i>Bcr</i>	BCR	Break-point cluster region	<i>H. sapiens</i>
<i>Cdc24</i>	Cdc24	Cell division control protein 24	<i>H. sapiens</i>
<i>Cdc42</i>	Cdc42	Cell division control protein 42 homolog	<i>H. sapiens</i>
<i>cdk-1</i>	CDK-1	Cyclin-dependent kinase 1	<i>C. elegans</i>
<i>Cdk1</i>	Cdk1	Cyclin-dependent kinase 1	<i>H. sapiens</i>
<i>cyk-4</i>	CYK-4	Cytokinesis defect 4	<i>C. elegans</i>
<i>dbl-1</i>	DBL-1	<i>C. elegans</i> orthologue of Dpp	<i>C. elegans</i>
<i>dpp</i>	Dpp	Decapentaplegic	<i>D. melanogaster</i>
<i>ect-2/let21</i>	ECT-2	Epithelial cell transforming sequence 2	<i>C. elegans</i>
<i>Ect2</i>	Ect2	Epithelial cell transforming sequence 2	<i>H. sapiens</i>
<i>ESCRT-III</i>	ESCRT-III	Endosomal sorting complex required for transport III	<i>H. sapiens</i>
<i>F-actin</i>	F-actin	Filamentous actin	<i>H. sapiens</i>
<i>gfp</i>	GFP	Green fluorescent protein	<i>A. victoria</i>
<i>hrp</i>	HRP	Horseradish peroxidase	<i>A. rusticana</i>
<i>mCherry</i>	mCherry	Monomeric red fluorescent protein derived from sea anemone	<i>A. marginale</i>
<i>MgcRacGAP</i>	MgcRacGAP	Male-germ-cell Rac GTPase-activating protein	<i>H. sapiens</i>
<i>Mklp1</i>	MKLP1	Mitotic kinesin-like protein 1	<i>H. sapiens</i>
<i>MP-GAP</i>	MP-GAP	Mitotic phase-GTP activating protein	<i>H. sapiens</i>
<i>mkate2</i>	Mkate2	Monomeric far-red fluorescent protein derived from sea anemone	<i>E. quadricolor</i>
<i>nmy-2</i>	NMY-2	Non-muscle myosin II	<i>C. elegans</i>

<i>nop-1</i>	NOP-1	Pseudocleavage protein 1	<i>C. elegans</i>
<i>pebble</i>	Pebble	<i>D. melanogaster</i> orthologue of Ect2	<i>D. melanogaster</i>
<i>PKC</i>	PKC	Protein-kinase C	<i>H. sapiens</i>
<i>Plk1</i>	Plk1	Polo-like kinase 1	<i>H. sapiens</i>
<i>plk-1</i>	PLK-1	Polo-like kinase 1	<i>C. elegans</i>
<i>PRC1</i>	PRC1	Protein regulator of cytokinesis 1	<i>H. sapiens</i>
<i>Rac</i>	Rac	Ras-related C3 botulinum toxin substrate (human cells)	<i>H. sapiens</i>
<i>rho-1</i>	RHO-1	Ras-like GTP-binding protein 1	<i>C. elegans</i>
<i>RhoA</i>	RhoA	Ras homolog gene family member A	<i>H. sapiens</i>
<i>RhoB</i>	RhoB	Ras homolog gene family member B	<i>H. sapiens</i>
<i>RhoC</i>	RhoC	Ras homolog gene family member C	<i>H. sapiens</i>
<i>ROCK</i>	ROCK	Rho kinase	<i>H. sapiens</i>
<i>rga-3/4</i>	RGA-3/4	Rho GTPase-activating proteins 3 and 4	<i>C. elegans</i>
<i>TopBP1</i>	TopBP1	DNA topoisomerase 2-binding protein 1	<i>H. sapiens</i>
<i>tpx2</i>	TPX2	Targeting protein for Xklp2	<i>X. laevis</i> , <i>H. sapiens</i>
<i>tpxl-1</i>	TPXL-1	<i>C. elegans</i> orthologue of Tpx2	<i>C. elegans</i>
<i>unc-119</i>	UNC-119	Uncoordinated-119	<i>C. elegans</i>
<i>Xklp2</i>	Xklp2	Xenopus kinesin-like protein 2	<i>X. laevis</i> , <i>H. sapiens</i>
<i>XRCC1</i>	XRCC1	X-ray repair cross-complementing protein 1/ DNA repair protein XRCC1	<i>H. sapiens</i>
<i>zen-4</i>	ZEN-4	<i>C. elegans</i> orthologue of Mklp1	<i>H. sapiens</i>



# 1. Introduction

## 1.1. Cytokinesis in animal cells

Cytokinesis is the final step in cell division that partitions the contents of a single cell into two newly formed daughter cells (D'Avino, 2015). Precise regulation of cell division is required for proper tissue growth and defects in cytokinesis can lead to severe diseases such as cancer (Lacroix and Maddox, 2012). Indeed, failure in cytokinesis leads to polyploidy and generates genetic instability that can lead to oncogenic transformations (Ganem et al., 2014). Thus, precise orchestration of cell division is of high importance and tightly controlled in eukaryotic cells. For successful cytokinesis, the chromatin and the cytoplasmic contents of the mother cell must be distributed between the newly formed daughter cells. In order to precisely achieve this, the division plane has to be set between the segregating chromosomes. During chromosome segregation, constriction of an actomyosin based structure called the contractile ring underneath the plasma membrane leads to the formation of a cleavage furrow that results in the formation of the two daughter cells (D'Avino, 2015). Formation of the contractile ring is dependent on the activation of the small GTPase Ras homolog gene family member A (RhoA, RHO-1 in *C. elegans*) (Bement et al., 2006).

Cytokinesis proceeds in three major steps: contractile ring formation, ring ingression and abscission. Moreover, cytokinesis is spatially controlled by a collaboration between the mitotic anaphase spindle and the cell cortex. After nuclear envelope break down (NEBD), the mitotic spindle is assembled and the spindle consists of i) astral microtubules that originate from the centrosomes and ii) the spindle midzone, an array of anti-parallel and overlapping microtubules between the segregating chromosomes which is also referred to as the central spindle (D'Avino, 2015; Green et al., 2012) (Fig. 1).

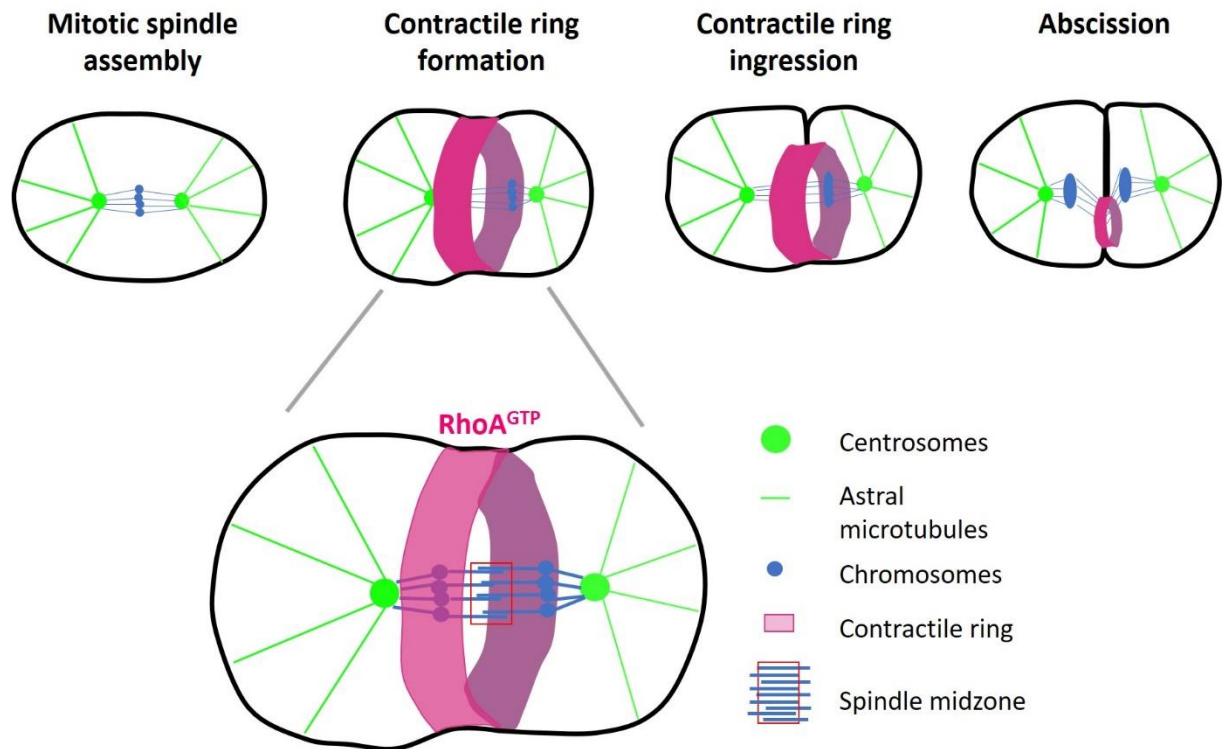


**Fig. 1. Overview of cytokinesis.** During anaphase, the constriction of the contractile ring leads to the formation of a cleavage furrow that partitions the contents of a single cell into two. In all animal cells cytokinesis is driven by the formation of the contractile ring whose position is determined by the mitotic spindle. The mitotic spindle induces the activation of the small GTPase RhoA at the equatorial plasma membrane.

## 1.2. The mitotic spindle positions the contractile ring

Multiple signals from the mitotic spindle determine the division plane between the segregating chromosomes and direct cleavage furrow formation to the equatorial cortex (D'Avino, 2015; Green et al., 2012). Already more than three decades ago, it was shown that the mitotic anaphase spindle plays a crucial role in positioning the cleavage furrow since replacement of the spindle in echinoderm eggs after cleavage furrow formation induced regression of the furrow and the formation of a new cleavage furrow at the site of the re-positioned spindle (Rappaport, 1985). Later on, it was shown that the mitotic spindle directs that activation of the small GTPase RhoA in the narrow equatorial zone and that active RhoA in turn is essential for the formation of the contractile ring and successful cytokinesis (Bement et al., 2006).

Different molecular signals from the mitotic spindle are thought to regulate contractile ring assembly and position. Several models have been proposed how positive and negative stimuli from the central spindle and astral microtubules orchestrate the precise localization of contractile ring proteins at the equatorial cortex during cytokinesis in order to induce cytokinetic furrow formation (Fig. 2). Two strong and opposing models have been initially suggested (Glotzer, 2005). The “astral stimulation model” proposed the concept that a specific population of astral microtubules that are in very close proximity to the equatorial cortex could stimulate furrow formation by directing factors or signals along the astral microtubules to the cortex. The opposing “astral relaxation model” however suggested that astral microtubules inhibit furrowing. The model predicts that higher abundance of astral microtubules at the cell poles leads to less contractility of the poles and lower quantities of astral microtubules at the cell equator allow furrowing and constriction of the membrane at the cell equator. Even though the two models were initially opposing each other, these days it is broadly concluded that both models can coexist and do not exclude each other, for example depending on different conditions like cell types or cell shapes (D’Avino, 2015).

Over time it became more and more evident that not only astral microtubules are important for cleavage furrow formation but also the central spindle (Fig. 1) and based on several observations, it was suggested that the central spindle is the major signaling site of furrow induction. Many important cytokinesis factors such as the centralspindlin complex and Epithelial cell transforming sequence 2 (Ect2) are enriched at the central spindle which suggested that the central spindle microtubules are essential for furrow formation (Glotzer, 2004). Centralspindlin is a conserved hetero-tetrameric complex that localizes to the spindle midzone during anaphase consisting of two types of proteins, the Mitotic Kinesin-Like Protein 1 (MKLP1, ZEN-4 in *C. elegans*) and the Male-germ-cell Rac GTPase-Activating Protein (MgcRacGAP, CYK-4 in *C. elegans*) (Mishima et al., 2002). Ect2 is a Guanine nucleotide exchange factor (GEF) for Rho GTPases (Kim et al., 2005; Rossman et al., 2005; Tatsumoto et al., 1999).

It has been shown that the RhoA activator Ect2 localizes and binds to MgcRacGAP in a phospho-dependent manner at the spindle midzone in *Drosophila* and human cells (Prokopenko et al., 1999; Su et al., 2011; Tatsumoto et al., 1999; Yüce et al., 2005). This suggested that the interaction is crucial for cytokinesis and it could lead to the transition of Ect2 to the plasma membrane where it activates RhoA. However, in *Caenorhabditis elegans* (*C. elegans*) ECT-2 does not localize to the spindle midzone but only to the cell

cortex which already questioned this model (Chan and Nance, 2013; Motegi and Sugimoto, 2006). In addition, another study published by Kotýnková et. al in 2016 showed that blocking the interaction of Ect2 and MgcRacGAP in human cells abolished Ect2 spindle midzone localization but did not interfere with successful furrowing and cytokinesis (Kotýnková et al., 2016). These findings already hinted that the suggested central spindle model requires revision and a new interpretation of results.

Even though it was demonstrated that the central spindle plays an important role in regulating furrow positioning, more and more studies were arising that astral microtubules inhibit contractility at the cell poles (Bement et al., 2006; von Dassow, 2009; Murthy and Wadsworth, 2008). It has recently been shown that polar clearing of contractile ring proteins is an active process regulated by Aurora A kinase that must be activated by TPXL-1 that concentrates on astral microtubules (Mangal et al., 2018).

In summary, the precise mechanisms of how the mitotic spindle regulates contractile ring position is still not entirely understood. However, these two signaling pathways, i.e. stimulating cues from the central spindle and inhibiting signals from the cell poles are thought to ensure the establishment of a confined zone of active RhoA only at the cell equator and prevents formation of several cleavage sites (Bringmann and Hyman, 2005).

Lastly it has been shown that there are ways to position the furrow independently of the spindle. The model arises from the examples of cells that show cortical contractility independent of the mitotic spindle, such as the pre-mitotic pseudocleavage formation in *C. elegans* 1-cell stage embryo or the metaphase furrow formation of syncytial cells during *D. melanogaster* development (Crest et al., 2012; Rose et al., 1995).

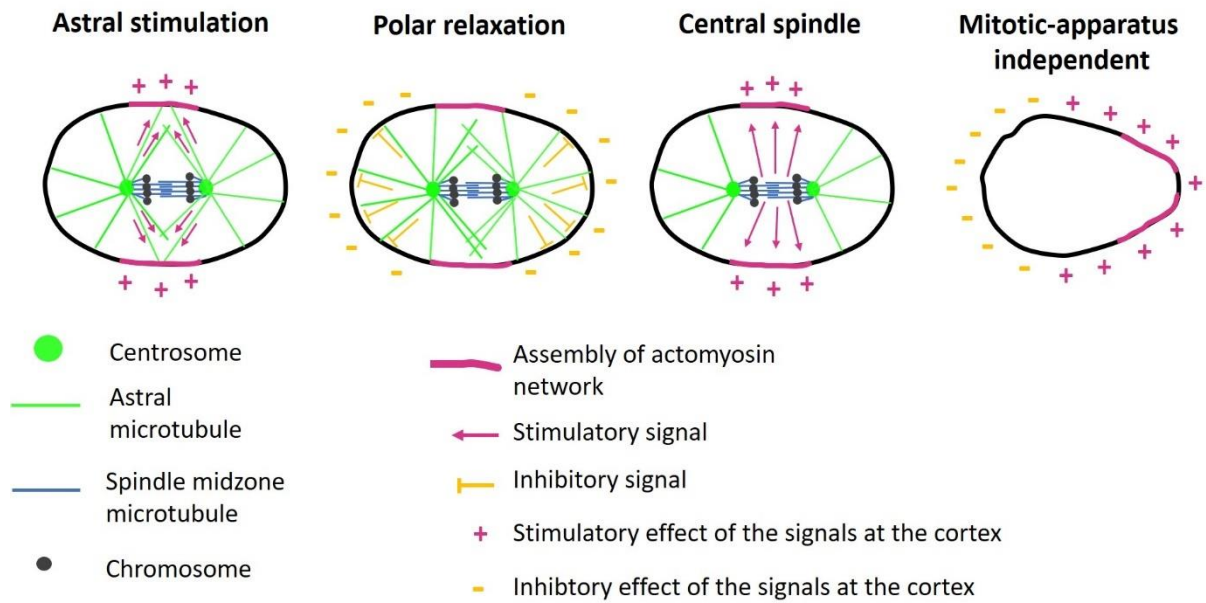


**Fig. 2. Models of cleavage furrow positioning.** Different models have been suggested how cues from the mitotic spindle regulate positioning of the cleavage furrow (reviewed in Mishima, 2016). In the astral stimulation model, positive cues from the astral microtubules stimulate cleavage furrow formation at the site of maximal stimulation at the cell cortex. In the polar relaxation model, astral microtubules induce relaxation of cortical contractility at the cell poles and thereby restrict the site of cleavage furrow ingression at the cell equator. In the central spindle model, positive stimulatory signals from the central spindle stimulate cleavage furrow formation at the adjacent plasma membrane and thereby define the site of constriction. Also, there is another model that describes cleavage furrow stimulation independent of the mitotic spindle but dependent on polarity cues (Mishima et al., 2016).

### 1.3. RhoA GTPase and its role in contractile ring formation

The formation of the contractile ring is essential for successful cytokinesis. The activation of the small GTPase RhoA is the key step in assembling the contractile ring (Bement et al., 2006; Piekny et al., 2005).

RhoA, like small GTPases in general, is a molecular switch that cycles between an inactive GDP-bound state and an active GTP-bound state. RhoA is part of the small Rho GTPase family which also includes Rac and Cdc42. Rho GTPases are involved in the regulation of the actin cytoskeleton during many cellular events, such as polarity establishment, cell migration, cell shape, adhesion, transcription and cytokinesis (D'Avino, 2015; Jordan and Canman, 2012).

Rho GTPases have an approximate size of around 20 kDa and harbor a classical GTPase domain and the C-terminus contains a CAAX motif (CAAX, C = cysteine, A = aliphatic and X = any amino acid) and a polybasic sequence (PBS). The CAAX site drives prenylation of Rho proteins at the endoplasmic reticulum (ER), that in turn adds a hydrophobic anchor that contributes to membrane binding (Hancock et al., 1990). The PBS motif is hypothesized to be important for plasma membrane association by binding of the positively charged amino acids to the negatively charges of the lipids within the plasma membrane (Heo et al., 2006).

In both higher and lower eukaryotes such as yeast, sand dollar, *Dictyostelium*, *Xenopus laevis* Rho GTPases have been reported to play an essential role in the formation of the contractile ring during cell division (Drechsel et al., 1997; Kishi, 1993; Larochelle et al., 1996; Mabuchi et al., 1993). In the budding yeast *Saccharomyces cerevisiae* the small GTPase Cdc42 is involved in bud site selection and Rho1 is important for contractile ring ingression (Casamayor, 2002). In *C. elegans*, RHO-1 (RhoA) regulates embryonic cell division and knock-down of RHO-1 by RNAi leads to inhibition of cytokinesis and in late stage to embryonic arrest (Jantsch-Plunger et al., 2000; Spencer et al., 2001). In vertebrates, there are two closely related Rho GTPases of RhoA, namely RhoB and RhoC. Genetic loss of RhoB leads to vascular growth defects in developing mice but does not result in mitotic defects (Liu et al., 2001). Genetic deletion of RhoC gene does not prevent cell proliferation but rather has a role in cell migration especially in metastasis of cancers (Hakem, 2005). In humans there are 22 different Rho proteins, however the major Rho GTPase involved in cytokinesis is RhoA (D'Avino, 2015).

In several studies and different model systems it has been shown, that RhoA plays an essential role during cytokinesis (Drechsel et al., 1997; Kishi, 1993; Prokopenko et al., 1999). Presence of RhoA or its orthologues are essential for successful cytokinesis and loss of function of RhoA prevents furrow formation in many different animal cells studied (Jordan and Canman, 2012). The RhoA protein and other orthologues of different species i.e. of *C. elegans* (RHO-1) localize to a narrow zone at the equatorial plasma membrane between the segregating chromosomes (Nishimura and Yonemura, 2006) and it has been shown that the accumulated pool of RhoA is indeed active RhoA (Bement et al., 2006).

RhoA cycles between an GDP-bound inactive and GTP-bound active state (Haeusler et al., 2003; Moon, 2003) and the flux between the two states is regulated by several classes of

proteins. GEFs are responsible for the exchange of GDP to GTP (Rossman et al., 2005). GTPase activating proteins (GAPs) promote intrinsic hydrolysis of GTP (Tcherkezian and Lamarche-Vane, 2007). Guanine nucleotide dissociation inhibitors (GDIs) stabilize the GDP-bound state of RhoA (Bement et al., 2006; Siderovski and Willard, 2005). Moreover, Mitotic-Phase GAP (MP-GAP, RGA-3/4 in *C. elegans*) was identified to be the major GAP of RhoA during cytokinesis (Zanin et al. 2013). In contrast, Epithelial cell transforming sequence 2 (Ect2; ECT-2 in *C. elegans*) is the major GEF for RhoA (Tatsumoto et al., 1999).

#### 1.4. Contractile ring composition and molecular control of ring constriction

Contractile ring assembly and constriction is crucial in order for cells to divide. The contractile ring consists of various components, most importantly filamentous actin (F-actin), myosin II, septins, RhoA and the scaffolding protein anillin (Fig. 3B). The latter can bind RhoA, F-actin and myosin II in order to form a complex meshwork of constricting filaments (Piekny and Glotzer, 2008).

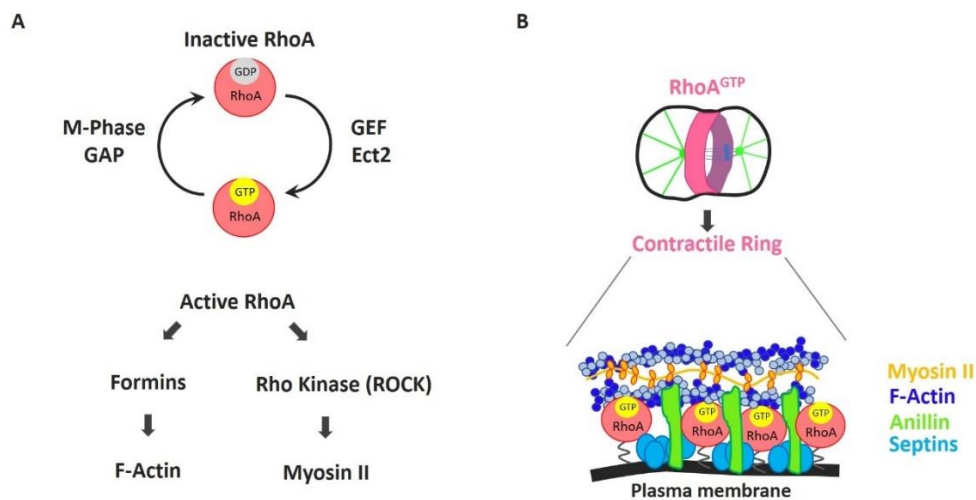


**Fig. 3. The RhoA signalling pathway during cytokinesis and composition of the contractile ring.** (A) RhoA cycles between an inactive GDP-bound state and an active GTP-bound state. The major activator of RhoA is the GEF Ect2 and the major inactivator is M-Phase GAP (MP-GAP). Once RhoA is active, it induces F-actin polymerization via formins and myosin II contractility via Rho kinase. (B) Major components of the contractile ring include F-actin, myosin II, septin filaments, the scaffolding protein anillin and active RhoA (

By immunohistochemical studies as well as in live-cell imaging, the small GTPase RhoA was shown to localize in a narrow-confined zone at the equatorial cortex before furrowing occurs in human cells and different model organisms (Bement et al., 2006; Takaishi et al., 1995; Yonemura et al., 2004; Yoshizaki et al., 2003). The Rho flux model suggests that GEFs and GAPs regulate the activity of RhoA through the GTPase cycle resulting in a flux of RhoA defining a narrow zone of active RhoA. Additionally, microtubule asters arising from the centrosomes are inhibiting contractility at the cell poles (Bement et al., 2006). Later on, M-Phase GAP in human cells and RGA-3/4 in *C. elegans* were identified as the major GAPs inactivating RhoA (Schonegg and Hyman, 2007, Zanin et al. 2013). Inhibition of M-Phase GAP resulted in excessive RhoA activation during M-phase and leads to late cytokinesis failure and uncontrolled cortical protrusions (Zanin et al., 2013). Together these two mechanisms synergistically define the narrow zone of active RhoA in order to ensure correct positioning of the contractile ring at the equatorial cortex.

Contractile ring formation is initiated by the small GTPase RhoA (Jordan and Canman, 2012). When sister chromatids start to separate, RhoA is activated by its activator. RhoA initiates contractile ring formation by triggering two independent pathways: one pathway involves diaphanous-related formins which polymerize actin filaments with the help of profilin (Carlson et al., 1977, Haugwitz et al., 1994, Severson, Baillie, and Bowerman 2002). The second pathway is stimulated by the activation of non-muscle myosin II via Rho-kinase (D'Avino, 2015; Green et al., 2012) (Fig. 3). In detail, active RhoA activates formins and releases them from an autoinhibitory state which in turn polymerize linear actin filaments that are crucial for the contractile ring to form (Otomo et al., 2005; Watanabe et al., 1997). Another factor called profilin promotes together with the formins actin polymerization. Profilins bind actin monomers and are thought to contribute to actin polymerization by keeping pre-polymerized monomeric actin in a pre-active state for providing them to active formins in order to polymerize actin filaments (Evangelista et al., 2002). Simultaneously RhoA activates the two serine-threonine kinases Rho-associated protein kinase (ROCK) thereby activating myosin II filament assembly. Then active myosin-II can bind F-actin and drives the contraction of the filaments resembling the sliding filament model of muscle contraction (D'Avino, 2015; Jordan and Canman, 2012). The scaffold protein anillin directly binds RhoA and the plasma membrane and also associates with the actomyosin meshwork which couples the contractile ring to the plasma membrane (A. J. Piekny and Glotzer 2008, D'Avino 2009, Piekny and Maddox 2010).

Moreover, it has been shown that anillin binds Ect2 (Frenette et al., 2012a). Constriction of the contractile ring then drives plasma membrane ingression that divides the mother cell into two newly formed daughter cells.

### **1.5. Abscission as the last step of cytokinesis**

Once RhoA is active the contractile ring forms and constricts and thereby promotes ingression of the plasma membrane. After constriction, an intercellular bridge is formed between the two daughter cells and at its center the midbody assembles. The midbody was first discovered by Walther Flemming in the 19<sup>th</sup> century, it was later on described as an electron-dense material containing microtubules evolving between nascent daughter cells during cell division (Mullins, 1977).

The midbody is the anchor point for the cleavage furrow and provides the molecular platform required for the assembly of the abscission machinery that is essential for the physical separation of the two newly formed daughter cells (Green et al., 2012). The cleavage furrow ingresses until a maximum diameter of 1-2 $\mu$ m and the formed midbody remains up to several hours until the abscission machinery is ready to divide the nascent daughter cells (Addi et al., 2018; Mierzwa and Gerlich, 2014). The midbody derives from the maturing spindle midzone and requires constriction of the plasma membrane (Hu et al., 2012; Kechad et al., 2012). During spindle midzone maturation in order to form the midbody, several contractile ring components, e.g. MKLP1, PRC1, anillin, septins, actin, myosin, RhoA and Ect2 are retained in the forming midbody structure (Gai et al., 2011; Hu et al., 2012; Kechad et al., 2012).

For abscission to occur the midbody has to be reorganized. First, cytoskeletal components are removed, and F-actin fibers are disassembled. Central spindle proteins such as for example centralspindlin complex and anillin stay associated with the microtubules within the midbody but PRC1 stays at the microtubule overlapping region (Elia et al., 2012; Hu et al., 2012). Thereby the midbody is linked to the plasma membrane. Other contractile ring proteins such as RhoA and septins are localizing to a ring-like structure next to the midbody (Hu et al., 2012). It has been also shown that phosphoinositide lipids that are present at the equatorial cortex and associate with contractile ring components when the cleavage furrow constricts are also enriched at sites nearby the midbody structure (Dambournet et al., 2011; Emoto et al., 2005; Field et al., 2005). During reorganization of the midbody two new

contraction sites both adjacent to the midbody occur, leading to a bow-like appearance of the midbody and its adjacent contraction sites. After cleavage furrow ingression the actin filaments are removed, and the endosomal sorting complex required for transport III (ESCRT-III) localizes to the midbody promoting the ultimate scission of the daughter cells (Guizetti and Gerlich, 2012). In most cases the midbody structure is inherited by one of the two cells (Addi et al., 2018; Mierzwa and Gerlich, 2014).

## **1.6. The GEF Ect2 and its role in cytokinesis**

Contractile ring formation depends on the activation of RhoA via the GEF Ect2. Ect2 was originally identified as a proto-oncogene in a screen for mitogenic signal transducers where a murine keratinocyte cDNA library was introduced into fibroblasts and cells that formed foci with altered morphology were isolated. Ect2 shows significant homology with the genes *Bcr*, *Dbl* and *Cdc24* genes that were reported to be involved in the signaling pathway of Rho-like proteins. Furthermore, it was shown that Ect2 interacts with RhoA, RhoC, and Rac1 *in-vitro* (Miki et al., 1991). These results already suggested a crucial role of Ect2 in the regulation of small GTP binding Rho family proteins. In later studies, it was shown that Ect2 is a GEF for RhoA, Rac1 and Cdc42 which promotes the exchange of GDP to GTP (Tatsumoto et al. 1999). Ect2 is required for cleavage furrow formation during cytokinesis and absence of Ect2 leads to cytokinetic failure (Chalamalasetty et al., 2006; Jantsch-Plunger et al., 2000; Tatsumoto et al., 1999). Another protein called NOP-1 was identified as playing a crucial role in the pseudocleavage furrow formation during polarity establishment and also mediates aster-induced furrowing in *C. elegans* (Tse et al., 2012).

*In-vivo* studies revealed that the gene Ect2 is the orthologue of *Pebble* in *Drosophila melanogaster* and of *let-21* (later on called *ect-2*) in *C. elegans* (Dechant and Glotzer 2003; Lehner 1992; Prokopenko, Saint, and Bellen 2000). In *D. melanogaster* and *C. elegans* similar phenotypic results were obtained suggesting that the role of Ect2 in regulating Rho family proteins during cell division is conserved (Canevascini et al. 2005; Glotzer 2005, Prokopenko et al. 2000).

Ect2 consists of a catalytic DH-type GEF domain, a PH domain at the C-terminus and three BRCT domains at the N-terminus (Fig. 4A) and in 2014 the crystal structure of the BRCT domains was resolved (Zou et al., 2014). The GEF domain catalyzes the exchange of GDP to GTP in RhoA and thereby activates it (Tatsumoto et al. 1999). A linker region of about

120 amino acids connects the N-terminal BRCT domains with the C-terminal part of Ect2. The C-terminus harbors a poly-basic sequence (PBS) required for membrane binding in human cells but not in *C. elegans* (Motegi and Sugimoto, 2006; Su et al., 2011). In human cells Ect2 binds to the plasma membrane with the PH domain and the PBS and plasma membrane binding of Ect2 is essential for cytokinesis (Su et al., 2011). In *C. elegans*, it was shown that the C-terminus is required for membrane targeting (Chan and Nance, 2013). Ect2 localizes to the spindle midzone and the plasma membrane in human cells (Tatsumoto et al. 1999). Interestingly in *Drosophila* and *C. elegans* embryos the Ect2 orthologues localize exclusively to the plasma membrane and not to the spindle midzone (Motegi and Sugimoto 2006; Jenkins et al., 2006; Prokopenko et al. 1999) (Fig. 4B).

It has been shown *in-vitro* that the BRCT domains bind the C-terminus including the GEF domain and thereby inhibit Ect2 activity (Kim et al., 2005; Saito et al., 2004). In addition, the mutation of W304R in BRCT2 domain cannot rescue multinucleation caused by depletion of endogenous HsEct2 other than expression of RNAi resistant HsEct2<sup>WT</sup>. This suggests that BRCT domains do not only have an inhibitory role for HsEct2 function but that they are also required for Ect2 function (Kim et al., 2005; Wolfe et al., 2009).

BRCT domains are phosphopeptide binding motifs that interact with their binding partners upon phosphorylation (Manke, 2009). Mostly BRCT domains occur in tandem repeats of two. The triple BRCT domains of Ect2 are similar to the triple BRCT domains in the protein DNA topoisomerase 2-binding protein 1 (TopBP1) (Zou et al., 2014). However, the BRCT domains of Ect2 (as well as the ones of TopBP1) are very different from the canonical tandem BRCT domains in other proteins and could resemble a new class of BRCT domains. Therefore it is unclear how the Ect2 BRCT domains function and whether they bind phosphopeptides (Zou et al., 2014).

Ect2 BRCT domains have shown to associate with centralspindlin which promotes activation and targeting of Ect2 to the spindle midzone (Wolfe et al. 2009, Burkard 2009). Next to the interaction of Ect2 with centralspindlin, it was shown that the Ect2 PH domain interacts with the anillin, a scaffold protein for the actomyosin network at the cell cortex. The interaction was suggested to stabilize central spindle microtubules and to cross link the central spindle with the cell cortex in order to position the contractile ring and to define a distinct zone of active RhoA that is activated by Ect2 (Frenette et al., 2012b).

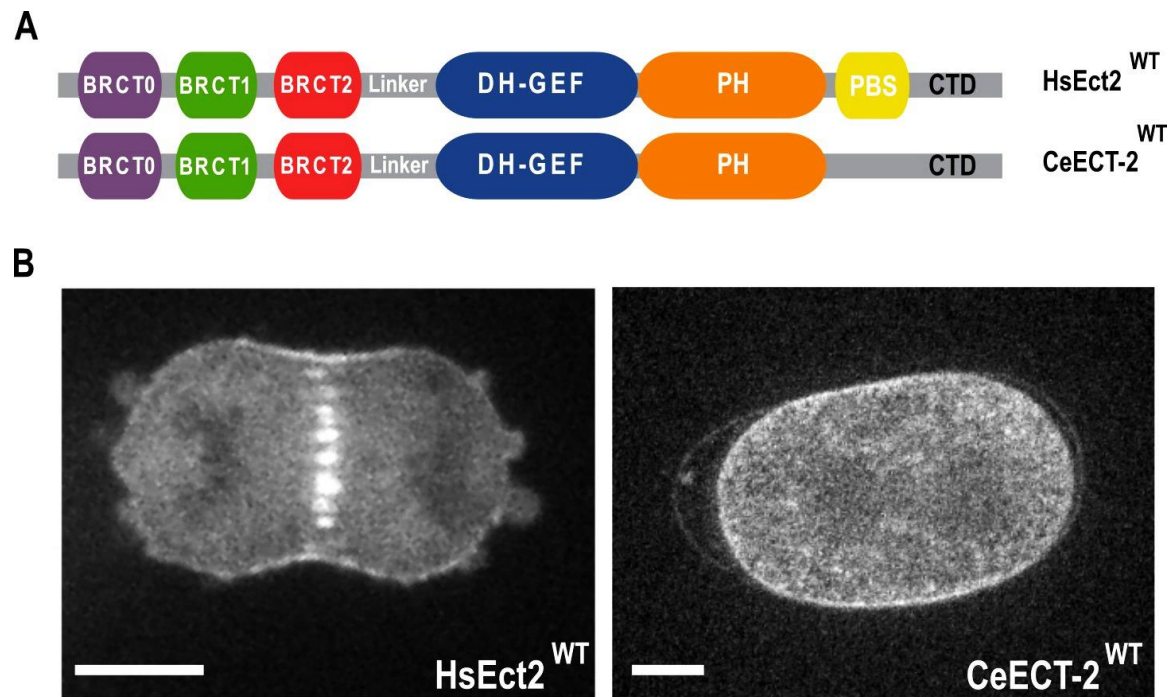


**Fig. 4. HsEct2 and CeECT-2 localize differently in the cell.** (A) Domain organization of *Homo sapiens* *Ect2* (HsEct2) and *C. elegans* *ECT-2* (CeECT-2). Both orthologues harbor three N-terminal BRCT domains, a DH-GEF domain which catalyzes the exchange of GDP to GTP in RhoA and a C-terminus containing a PH domain involved in plasma membrane binding. HsEct2 harbors an additional polybasic sequence (PBS) at the C-terminus. (B) Localization of HsEct2 in human cells and of CeECT-2 in *C. elegans* during cell division. HsEct2 localizes to the spindle midzone and to the plasma membrane in human cells. In *C. elegans*, CeECT-2 exclusively localizes to the plasma membrane. Scale bar = 10  $\mu$ M.

### 1.7. Ect2 regulation by centralspindlin

Another player in the signaling transduction cascade of contractile ring formation is the protein complex centralspindlin consisting of MKLP1 and MgcRacGAP (Mishima et al., 2002).

Centralspindlin recruits the GEF Ect2 to the spindle midzone by the binding of Ect2 to MgcRacGAP via its N-terminal BRCT domains (Nishimura and Yonemura, 2006; Yüce et al., 2005; Zhao and Fang, 2005).

The current model predicts that MgcRacGAP is phosphorylated by Polo-like kinase 1 (Plk1) and phosphorylation triggers the binding of BRCT domains to MgcRacGAP. Then, binding of the BRCT domains to MgcRacGAP releases Ect2 autoinhibition and thereby activates Ect2 GEF activity (Fig. 5A). Once recruited, Ect2 is activated and loaded onto the

adjacent plasma membrane where it in turn activates RhoA (Wolfe et al. 2009, Burkard 2009). How active Ect2 translocates from the midzone to the membrane has yet not been clarified.

A paper by Kotýnková et al. in 2016 challenged this model. The authors showed that neither the binding of MgcRacGAP to Ect2 nor Ect2 localization to the spindle midzone are required for successful cytokinesis and propose an activation of Ect2 independent of Ect2-MgcRacGAP interaction (Fig. 5B).

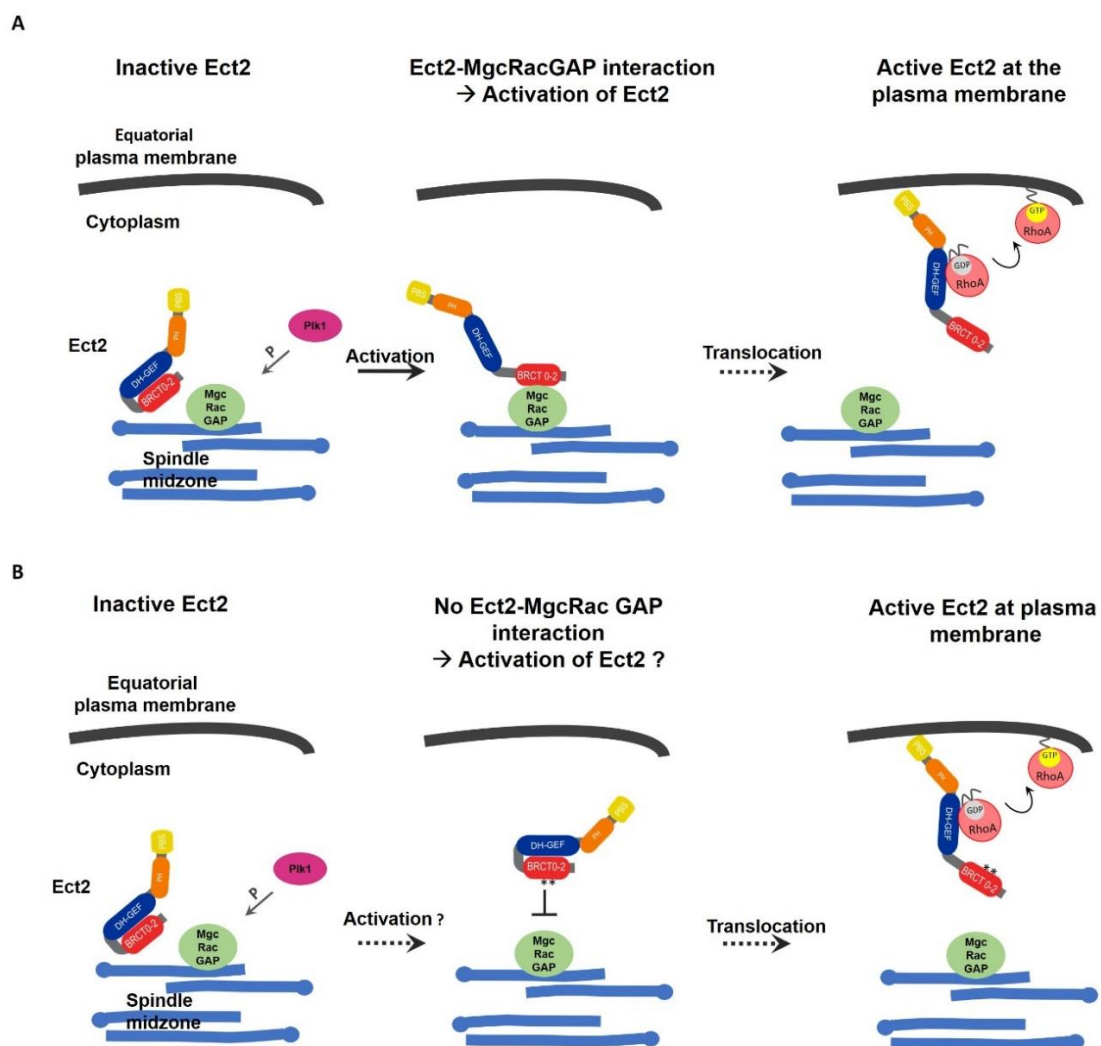


**Fig. 5. Different models of Ect2 regulation during cytokinesis.** (A) At anaphase onset, Plk1 phosphorylates spindle midzone localized MgcRacGAP, thereby creating a binding site for Ect2 N-terminal BRCT domains. Upon phosphorylation of MgcRacGAP by Plk1, Ect2 is recruited from the cytoplasm to the spindle midzone where it binds to MgcRacGAP. The Ect2 N-terminal BRCT domains are thereby released from inhibiting the GEF domain and active Ect2 then translocates from the spindle midzone to the plasma membrane by not yet identified mechanisms (Su et al., 2011), reviewed in (D’Avino, 2015). (B) Illustration

of the results by the study from Kotýnková et al., 2016. Two-point mutations in the BRCT1 domain of Ect2 block the interaction with MgcRacGAP and abolish Ect2 localization to the spindle midzone. Even though mutant Ect2 does not localize to the spindle midzone cytokinesis is successful. This suggests that Ect2 localization to the spindle midzone is not crucial for Ect2 activation (Kotýnková et al., 2016). Their results challenge the hypothesis shown in (A) that Ect2 is activated at the spindle midzone by the interaction of MgcRacGAP and Ect2.

The authors of Kotýnková et al., 2016 generated a stable, RNAi resistant cell line where they introduced two specific point mutations (T153A, K195M, called TK mutant) in the BRCT1 domain of Ect2. They state with biochemical assays the results from another study by Zou et al., 2014 that these point mutations abolish the interaction of Ect2 with MgcRacGAP (Zou et al., 2014). Then they performed live-imaging with the TK mutant in absence of endogenous Ect2. Ect2<sup>TK</sup> was not localizing to the spindle midzone, however cell division and cytokinesis was completely normal when compared to a cell line expressing Ect2<sup>WT</sup> in absence of endogenous Ect2. These results are consistent with other findings from the literature that spindle midzone localization of Ect2 is not important for cytokinesis. In *C. elegans*, CeECT-2 only localizes to the plasma membrane and not to the spindle midzone (Jenkins, 2006; Motegi and Sugimoto, 2006). Moreover, in human cells it was shown that displacement of endogenous HsEct2 from the spindle midzone by overexpression of transgenic N-terminal fragments does not interfere with cytokinesis (Chalamalasetty et al., 2006).

Furthermore, the authors enquired the function of the PH- and PBS domain of Ect2 during cytokinesis. Deletion of PH-PBS domain has been shown to strongly interfere with successful cytokinesis (Su et al., 2011). To exclude artifacts caused by the big deletions, Kotýnková et al., 2016 generated an Ect2 fusion protein where the PH-PBS domain was replaced with a C1B membrane targeting domain derived from human Protein Kinase C (PKC). The Ect2-C1B protein was artificially forced to the plasma membrane upon addition of TPA to the culture medium. Localization of Ect2-C1B lacking the PH-PBS domains to the plasma membrane could rescue the cytokinetic failure caused by deletion of PH-PBS domains. Then they generated a fusion protein of the GEF domain tagged with the C1B domain to enquire whether localization of the GEF domain alone to the plasma membrane is sufficient to induce cytokinesis. They show that membrane localization of the GEF-C1B domain upon TPA treatment alone was not sufficient for successful cytokinesis.

Together these findings of Kotýnková et al., 2016 showed that successful cytokinesis requires Ect2 membrane localization via its PH-PBS domains but not spindle midzone localization via MgcRacGAP interaction. Furthermore, the findings show that the membrane-localized GEF domain without the N-terminal BRCT domains of Ect2 is not sufficient for cytokinesis. These results strongly suggest that Ect2 activity must be regulated via the N-terminal BRCT domains at the equatorial plasma membrane and raise the question whether BRCT domains have additional roles in regulating Ect2 activity independently of spindle midzone localization. However, if and how Ect2 activity is controlled at the plasma membrane to achieve orderly RhoA activation is currently unknown.

Another study from Kim et al., 2005 that revealed that the N-terminal BRCT domains of Ect2 interact with the C-terminal GEF domain. They exchanged a highly conserved tryptophan for an arginine (W304R) in the BRCT2 domain that was suggested to be involved in the folding of the BRCT domain. Kim showed that the W304 mutation interferes with the interaction of the BRCT domains and the GEF domain. Furthermore, they showed that W304R mutations increased strongly the GEF activity of Ect2<sup>W304R</sup> *in-vitro* (GEF assays). However, there was one study that showed that mutating this residue does not abolish the binding of BRCA1 and XRCC1 (= represents part of the sequence of BRCT0 domain discovered in 2014 by Zou et al.) (Taylor et al., 2004). These findings are not conclusive, moreover they lack *in-vivo* analysis that could answer the question whether the W304R mutation interferes with cytokinesis since there are several contradictory results on this conserved residue.

## **1.8. Regulation of Ect2 by mitotic kinases**

Another possible mechanism by which Ect2 activity and localization is regulated could be through the mitotic kinases Cyclin-dependent kinase 1 and Plk1. The two major kinases Cdk1 and Plk1 have been suggested to phosphorylate Ect2 *in-vitro* and *in-vivo* (Niiya et al. 2006; Suzuki et al. 2015; Wolfe et al. 2009, Hara 2009). Cdk1 and Plk1 are serine/ threonine kinases that are active during G2/M phase and that have multiple crucial functions during mitosis.

Plk1 is a highly conserved eukaryotic serine/ threonine kinase and was first identified in *Drosophila* (Llamazares et al., 1991; Sunkel and Glover, 1988). It contains a polo-box

binding domain that serves as a phosphopeptide binding domain that recognizes serine/threonine consensus sites (Elia, 2003). Plk1 triggers metaphase to anaphase transition and is important for many mitotic events such as centrosome maturation and condensation, nuclear envelope breakdown and microtubule organization (Nigg et al., 1996). In metaphase, Plk1 localizes to microtubules at the mitotic spindle and to the midbody during cytokinesis (Nigg et al., 1996).

Cdk1 was first discovered in *S. cerevisiae* and is a highly conserved proline-directed serine/threonine kinase phosphorylating preferentially serine/threonine consensus sites (Hartwell et al., 1973; Rhind and Russell, 2012). Cdk1 interacts with cyclins to be activated in prophase/prometaphase and the complex formed with Cyclin-B regulates many mitotic events such as chromosome condensation, nuclear envelope breakdown and spindle formation (Rhind and Russell, 2012; Suzuki et al., 2015).

It has been shown that Ect2 N-terminus is highly phosphorylated during prophase and metaphase and phosphorylation of one site that was identified is the threonine residue 342 in the linker region. Phosphorylation of T342 by Cdk1 prevents the interaction of Ect2 with centralspindlin complex (Yüce, Piekny, and Glotzer 2005). Therefore Yüce et al. speculate that when levels of Cdk1 decline after metaphase-anaphase transition Ect2 gets dephosphorylated and can associate with centralspindlin complex via its N-terminal BRCT domains. In addition, T342 was shown to be important for the catalytic activity of Ect2 and mutation of T342 (= T341 in Hara et al., 2009) was shown to decrease interaction of N-terminal fragments with C-terminal fragments of Ect2. However, mutations of T341 did not interfere with cytokinesis, which questions the importance of this phosphorylation (Hara et al., 2006). In addition the mitotic kinase Plk1 phosphorylates the subunit of centralspindlin, MgcRacGAP and thereby generates a binding site for the BRCT domains of Ect2 (Burkard et al., 2009; Petronczki et al., 2007; Wolfe et al., 2009).

Also it has been shown that Plk1 directly interacts with Ect2 in a phosphorylation dependent manner *in-vitro* (Niiya et al., 2006). A specific site in the linker region (T412) was shown to be phosphorylated by Cdk1 and prevention of phosphorylation by a phosphodeficient mutation (T412A) prevented Ect2 association with Plk1. Overexpression of Ect2<sup>WT</sup> and phosphomimetic Ect2<sup>T412D</sup>, but not phosphodeficient Ect2<sup>T412A</sup>, resulted in excessive membrane blebbing suggesting the phosphorylation of T412 promotes Ect2 activation (Niiya et al., 2006). Both kinases have been suggested to play an important role

for the correct temporal activation of Ect2 during mitosis. It has been proposed that Cdk1 primes Ect2 for subsequent Plk1 phosphorylation in order to regulate Ect2 function (Niiya et al., 2006).

Moreover, Ect2 linker region was shown to include a nuclear localization signal and phosphorylation of the NLS in a Cdk1 dependent manner promotes export of Ect2 from the nucleus in prophase (Saito et al., 2004; Suzuki et al., 2015). Deletion of the linker region or mutations of the NLS site in the linker region were shown to be causing strong transforming activity of Ect2 (Saito et al., 2004) which hints at an important role of mitotic kinases phosphorylating the linker region and thereby regulating Ect2.

Furthermore, not only the N-terminus has been shown to be phosphorylated by mitotic kinases but also the C-terminus of HsEct2 and T815 has been identified as a major site being phosphorylated by Cdk1 *in-vitro* and *in-vivo* (Dephoure et al., 2008; Niiya et al., 2006). Moreover, it has been shown that phosphorylation of T815 in the PBS domain controls Ect2 membrane localization since the mutation of T815A targets Ect2 prematurely to the plasma membrane in metaphase (Su et al., 2011).

## **1.9. Aims of the thesis**

The goal of my thesis is to understand the distinct roles of the three BRCT domains of Ect2 during cytokinesis. I focused in particular on the function of the three BRCT domains in the temporal and spatial regulation of Ect2 using *in-vivo* structure-function studies in human tissue culture cells and the one-cell embryo of the small nematode *C. elegans*. Many studies have already been performed investigating the regulation of Ect2 (writing of Ect2 here as a simplification for many different model organisms). So why was it important to study the function of the different BRCT domains?

It has been shown by Kotýnková et al., that targeting only the Ect2 GEF domain to the cell cortex is not sufficient for successful cytokinesis suggesting that the N-terminal BRCT domains have a key role in regulating Ect2 function.

Furthermore, initially only the BRCT1 and BRCT2 domain were identified and they were thought to function together as a classical tandem BRCT repeat. However, Zou et al. in 2014 identified the BRCT0 domain and solved the crystal structure of the N-terminus containing all three BRCT domains. This revealed a very different arrangement of the three BRCT domains in Ect2 compared with classical tandem BRCT repeats (Zou et al., 2014).

Based on the organization of the three BRCT domains it is possible that each BRCT domain has a separate and distinct function during cytokinesis. Moreover, it was proposed that binding of Ect2 BRCT1 domain to MgcRacGAP at the spindle midzone is crucial for cytokinesis (Nishimura and Yonemura, 2006; Yüce et al., 2005; Zhao and Fang, 2005). Kotýnková et al., showed that spindle midzone localization of Ect2 is not crucial for its activity and function during cytokinesis. Since interaction of the BRCT1 domain with MgcRacGAP is not required for cytokinesis it raises the question whether the BRCT1 domain has any role during cell division. To test the function of the BRCT0, BRCT1 and BRCT2 domains of Ect2 I generated several RNAi-resistant transgenes in which individual BRCT domains were deleted or substituted. The resulting cytokinetic phenotypes of the different transgenes were analyzed in the presence and absence of endogenous Ect2 protein in *C. elegans* and human tissue culture cells.

Previous *in-vitro* studies showed that the N-terminal tandem BRCT-domains bind the GEF domain of Ect2 and serve as negative regulator of the Ect2 GEF activity. In early mitosis the BRCT domains bind the GEF domain thereby inhibiting its catalytic activity (Kim et al., 2005; Saito et al., 2003). Moreover, a paper by Chan and Nance 2013 showed in *C. elegans* that overexpression of ECT-2 variants without the BRCT domains results in a phenotype that resembles hyperactivation of RhoA (Chan and Nance, 2013; Zanin et al., 2013).

The findings however are mainly based on *in-vitro* studies and whether Ect2 is regulated by an autoinhibitory mechanism *in-vivo* has not yet been answered. During my studies I tried to answer this question by performing structure-function studies in *C. elegans* and human cells. My first aim was the deletion of all three BRCT domains in *C. elegans* and to test the hypothesis that ECT-2 BRCT domains autoinhibit the GEF domain. Only few experiments have been performed so far in *C. elegans* to answer the question of whether ECT-2 is regulated via an autoinhibition (Chan and Nance, 2013). To this end, a transgenic *C. elegans* strain and a transgenic cell line expressing an CeECT-2/ HsEct2 variant with all three BRCT domains deleted was generated and the cytokinetic phenotype was analyzed using DIC and confocal spinning disk microscopy.

Moreover, it has been proposed that the N-terminal BRCT domains act as one tandem repeat to autoinhibit GEF function. Whether this is true has not yet been addressed. Therefore, I generated transgenic *C. elegans* strains and HeLa cell lines expressing CeECT-

2/ HsEct2 variants with deletions of different BRCT domains and assessed the cytokinetic phenotype by DIC and confocal microscopy. Furthermore, I analyzed cytokinetic function by lethality assays and multinucleation assays and assayed cortical contractility in these worm strains and cell lines.

Lastly the linker region between the N-terminal BRCT domains and the C-terminal GEF domain of Ect2 has been shown to be phosphorylated and involved in Ect2 regulation (Niiya et al., 2006; Saito et al., 2004; Suzuki et al., 2015). Therefore, I aimed to test whether the linker region is involved in regulating the activity of Ect2 during mitosis by exchanging all the serines/ threonines to alanines, blocking phosphorylation in this region.

## **2. Methods and materials**

### **2.1. Methods**

#### **2.1.1. *C. elegans* techniques**

##### **2.1.1.1. Maintenance of *C. elegans* worm strains**

*C. elegans* strains were maintained on agar plates containing nematode growth medium (NGM). A thin layer of the bacterial *E. coli* strain OP50 was seeded on NGM plates as a feeder host for the worms. The strain OP50 grows slower than normally *E. coli* because of an Uracil auxotrophy. A slow growth is desirable since it allows easier observation and handling of the worms under the microscope (Sulston and Brenner, 1974). Plates were kept at RT or at 4°C for longer storage. OP50 was seeded onto the NGM plates and kept at either room temperature (RT) or at 4°C for longer storage. Worms were passaged with a worm-pick consisting of a metal holder fixed to a platinum wire. First the platinum wire was disinfected with a flame of an ethanol-burner. Next, a small drop of OP50 was picked up with the tip of the platinum wire and the worms were sucked into the drop of OP50 at the tip of the wire. The wire was flamed in between different passaging rounds in order to avoid cross-contaminations with other worm strains and infections with environmental bacteria or fungi. Worms were incubated at 15°C, 20°C or 25°C depending of the desired growth rate. A stereo-microscope was used to visualize the worms (Table 2).

##### **2.1.1.2. Freezing of *C. elegans* worm strains**

Every newly generated *C. elegans* strain was immediately frozen in order to avoid genome changes during maintenance of the worms and to exclude the risk that strains get lost due to unexpected threats by infections. Four non-contaminated medium NGM plates with starved worms containing mainly L1 larvae were washed off the plate with 3.5 ml M9 buffer per plate and transferred to a 15 ml Falcon. Then the volume of the M9 buffer inside of the Falcon tube was measured and equal volume of 2x freezing medium was added. Worms were resuspended, equally distributed into 5 cryotubes and directly frozen at -80°C. The next day, one of the tubes was thawed and added onto 2 medium NGM plates and worms were tested for survival after the thawing process using a Stereo Microscope (Leica) to observe the movement of the worms with transmission light.

### **2.1.1.3. Generation of transgenic worm strains by MosSCI insertion**

The Mos1-mediated single-copy insertion (MosSCI) is a technique to stably introduce a gene of interest into the *C. elegans* genome at specifically flanked regions (Frøkjaer-Jensen et al., 2008). When microinjecting DNA into the *C. elegans* gonad, the DNA fragments mostly form extrachromosomal arrays and are not integrated into the genome. Extrachromosomal arrays are passed onto the next generation; however, the copy-number and expression of genes is highly variable and quantitative analysis requires a stable and equal gene expression (Mello et al., 1991).

With the MosSCI method a Mos1 transposon is mobilized from its original site by excision through a transposase provided together with the injected plasmid. Excision of the Mos1 transposon causes a double-strand break in the DNA and the gap is filled by the integration of the desired transgene. When injecting the plasmid containing the gene of interest (GOI) together with the transposase and other co-injection markers, extrachromosomal DNA arrays are formed that act as a template for the repair procedure of the double-strand break caused by the Mos1 transposon excision. The arrays contain chromosomal sequences homologous to each flanked region next to the Mos1 element and by homologous recombination the gene of interest is then inserted into the genome.

### **2.1.1.4. Insertion of transgenes and validation of integration in *C. elegans***

Plasmids containing the gene of interest were injected into the worm gonad by microinjection using an injection set-up consisting of a microscope (Nikon Eclipse Ti) coupled to a Micro-Injector (Femtojet Eppendorf). An injection mix containing the target plasmid at a concentration of 50 ng/μl, the transposase and several co-injection markers provided in a 3x pre-mixed “MosSCI mix” were prepared (Table 14). Before injection, the transfection mix was centrifuged at RT at maximum speed for 10 min. Young hermaphrodite worms were immobilized on injection-pads covered with mineral oil. The injection mix was loaded into a micro-needle mounted onto the injector and injection mix was injected into the gonad of the worms. Injected worms were singled onto medium size NGM plates and cultured at 25°C. After 7-10 days worms were starved, and progenies were analyzed for wild-type movers. Worms on different plates were checked for a potential integration by observing movement of the progenies of injected EG6699. First, worms that were moving fast and sigmoidal were easily distinguished from worms with the *unc-119*

phenotype. To check whether the GOI was stably integrated or wild-type phenotype was only caused by extrachromosomal arrays, worms were further analyzed under a fluorescence microscope (Leica, M205 FA) to check for co-injection markers that indicate presence of extrachromosomal arrays. Here, expression of mCherry, especially in the pharynx region, was checked. Per original plate showing wild-type movers, 10 worms without mCherry fluorescence were picked and singled onto small NGM plates. Worms were incubated at 25°C for fast growth. Adult offspring were then further analyzed to distinguish between heterozygous and homozygous integration of the transgene.

#### **2.1.1.5. Verification of homozygous insertion events in *C. elegans***

When the transgene is integrated into the genome it can happen as a homozygous or a heterozygous event. However homozygous integrations are rare and mostly heterozygous worms are generated and homozygous worms occur in the subsequent generation (F1). For all experiments a homozygous integration of the transgene was required to guarantee similar expression levels for quantitative analysis. The *unc-119* phenotype can be leveraged as a reporter for heterozygous integration. The GOI is stably inserted together with the *unc-119* transgene that rescues the uncoordinated movement of the worms lacking a part of the *unc-119* gene (EG6699). If the integration is heterozygous, according to Mendelian segregation, 25% of the progeny loses the *unc-119* transgene and therefore will show uncoordinated movement. From the original plate of the injected worm (F0), after testing for the absence of extrachromosomal arrays, 10 worms (F1) were picked and singled onto small NGM plates. If all F1 progeny shows the wild-type movement phenotype, these were cultured further. Subsequently, two plates were chosen, and 20 worms of each plate were singled and tested for GFP expression of the transgene by Fluorescence-microscopy using the Axioscope A1 (Zeiss). All of the 20 plates were screened for GFP expression and 10 adult worms (F3) of each of the 20 different F2 plates were added into 5µl of M9 buffer within a multi-well plate that was covered with a glass cover-slip. GFP expression in the embryos and in the gonad was analyzed. When all F3 progeny of the 20 singled F2 generation expressed GFP then worms were determined as homozygous and propagated as a new transgenic strain for freezing and analysis of the different transgenes.

#### **2.1.1.6. Verification of GOI insertion by genotyping**

In addition, worms were tested for stable integration of the transgene using a PCR-based approach. Here, specifically designed primers were used that only work if the transgene is stably inserted into the genome (Table 7). Primers (AD325 and AD326, Froekjer-Jensen, 2008) were designed to anneal in the genomic locus of chromosome II and within the *unc-119* transgene inserted together with the gene of interest. The PCR product can thus only be amplified if the transgene is stably integrated into chromosome II. Worms were lysed by a digest reaction where a single worm was put into 5 µl of digestion mix (Table 15). The digest was incubated at 65 °C for 1h. Afterwards, the lysate was used as a PCR template and a PCR with the specific primers was run with the worm lysate in a total volume of 25 µl (Table 16). The PCR reaction was assembled on ice and run at specific thermocycling conditions (Table 16). Afterwards, PCR products were analyzed by agarose-gel electrophoresis (not shown). Expected size for stable integration was 1500bp. The correct size of integration was verified for all generated, transgenic *C. elegans* strains.

#### **2.1.1.7. Worm crosses**

For crossbreeding *C. elegans* strains in order to obtain a strain containing two desired genotypes from two genotypical different parents, a worm cross was set-up between hermaphrodites (young adults) and male individuals. Since males normally occur at low frequency, a common technique to obtain male individuals of the desired strain is to deplete HIM-8 by RNAi which causes defects in X-chromosome segregation (X0 and XX genotypes) and therefore results in high frequency of males. Hermaphrodites were injected with *him-8* double stranded RNA. Young hermaphrodite worms were immobilized on injection-pads covered with mineral oil. The injection mix was loaded into a micro-needle mounted onto the injector and injection mix was injected into the gut of the worms. Around 10 hermaphrodites were injected and put onto one medium NGM plate and cultured at 25°C. After 7-10 days worms were starved, and progenies were analyzed for males under the stereomicroscope. Male worms can be easily distinguished from hermaphrodites by their thin body and a special tail that harbors a copulating apparatus. Once males are visible on the plate, young individuals were picked onto a new small NGM plate for clean-up from other small larvae that might be attached. After 10 minutes, 8 males of the desired strain were put together with 3 hermaphrodites of the other desired strain and cultures at 25°C over night (O/N). The next day, hermaphrodites were singled onto small NGM plates and

offspring (F1) was analyzed either with a fluorescence microscope (in case a fluorescent protein was used as a marker) or by PCR. In case F1 progeny successfully carries both desired alleles, 20x F1 individuals were singles onto small NGM plates and F2 generation was then analyzed as depicted in the chapters “Verification of homozygous insertion events in *C. elegans*” and “Verification of GOI insertion by genotyping” (in case of genotyping with the appropriate primers). Once a homozygous strain was obtained, it was right away frozen for long-term storage at -80°C (see “3.1.1.2. Freezing of *C. elegans* worm strains”).

#### **2.1.1.8. dsRNA production for the depletion of endogenous ECT-2 in *C. elegans***

To deplete endogenous ECT-2 I generated dsRNA (#27) targeting specific region of the 3' UTR of endogenous ECT-2. A region within the 3' UTR of endogenous ECT-2 gene was amplified by PCR using the primers EZ589/EZ590 (Table 7). The primers EZ589/EZ590 contain a T7 overhang that is required as a start point for transcription by the RNA polymerase. The amplified fragment was then later used for *in-vitro* transcription of the RNA targeting the 3'UTR of endogenous ECT-2. Expected size of the fragment was 547 bp and both PCR amplification as well as dsRNA transcription were verified by agarose gel electrophoresis for correct fragment size. Next, I generated dsRNA by using the Ambion® MEGAscript® T7 *In Vitro* Transcription Kit. Every step was performed after cleaning the work-surfaces and pipettes with RNase ZAP (Ambion) in order to remove potential RNases that easily can degrade the generated dsRNA. Additionally, all steps were performed on ice, filter-tips and gloves were used all the time. In order to obtain sufficiently concentrated dsRNA, a larger PCR volume than usual was set-up (total 900 µl). DNA concentration was increased by purification of the whole PCR via one single spin-column. The DNA was then added together with the required reagents for the *in-vitro* transcription in one tube (Table 20). The transcription-mix was incubated at 37°C for 6h. A subsequent DNase digestion step to remove the template DNA was performed, by adding 8 µl DNase Turbo to the mix. The RNA was precipitated by a LiCl-precipitation step. 60µl of RNase free H<sub>2</sub>O and 60µl of LiCl was added to the mix, inverted several times and incubated at -20°C for 1h. The dsRNA was then centrifuged at 4°C, max speed for 15 min. to pellet it. The pellet was washed with 70% ethanol and centrifuged under the same conditions. Pellet was air-dried for 20 min at RT and taken up in 120 µl 1x soaking buffer. Finally, the correct size of the dsRNA was determined by gel electrophoresis its concentration was measured

and determined as 150 ng/μl. The dsRNA was subsequently used for microinjections of *C. elegans* worms in order to deplete endogenous ECT-2.

#### **2.1.1.9. *ect-2(RNAi)*, lethality tests and measurement of brood size in *C. elegans* strains**

Before performing lethality tests, both generated *ect-2* dsRNA and the RNAi-resistant GFP-ECT-2 transgenes in transgenic worm strains were tested for functionality. DsRNA targeting endogenous ECT-2 was injected into young adult worms. Before injection, the dsRNA against endogenous 3'UTR of *ect-2* was centrifuged at 4°C at maximum speed for 10 min. Young hermaphrodite worms were immobilized on injection-pads covered with mineral oil. 0.5 μl of the RNA was loaded into a micro-needle attached to the injector and injected into the worms targeting the region right after the pharynx. Injected worms were transferred onto medium size NGM plates and cultured at 20°C. Worms were grown at 20°C and singled 16-20h post injections, mother worms were sacrificed approximately 40-48h post injections. Embryonic lethality and total brood size (counted all embryos and larvae) after *ect-2(RNAi)* was assayed approximately 72h post injections.

#### **2.1.1.10. *gfp(RNAi)* feeding approach to deplete the *gfp::ect-2<sup>ΔBRCT0+1+2</sup>* transgene during strain generation**

In order to obtain a expressing GFP::ECT-2<sup>ΔBRCT0+1+2</sup> strain more than 72 worms of MoSCI strain EG6699 were injected and only one transgenic strain with an integration of the transgene could be obtained. Normally, one integration per 20 injected worms is obtained and 1 integration per 72 worms represents a low frequency of integration. Since the number of positive integrations of the construct *gfp::ect-2<sup>ΔBRCT0+1+2</sup>* resulted in this very low integration number we hypothesized that the expression of the transgene might lead to embryonic lethality and therefore no strains can be generated when the transgene is expresses. Therefore, the GFP-ceECT-2<sup>ΔBRCT0+1+2</sup> transgene was silenced during strain generation by feeding injected worms with *gfp(RNAi)*. Worms were directly put on *gfp(RNAi)* feeding plates after injection and grown until almost starved and then passaged onto new *gfp(RNAi)* feeding plates to constantly deplete the GFP-ECT-2 transgene in case it induces embryonic lethality. Then L4 worms were transferred from the *gfp(RNAi)* plate to normal plates and to allow expression of GFP-ceECT-2<sup>ΔBRCT0+1+2</sup> was After 24h-72h expression was monitored by fluorescence-microscopy (Axioscope, Zeiss).

#### **2.1.1.11. Live imaging of embryos in *C. elegans* by confocal spinning disk microscopy**

Imaging of *C. elegans* 1-cell stage embryos was performed using spinning-disk microscopy. Adult hermaphrodite worms were put into 5  $\mu$ l M9 buffer drop on a glass cover-slip with the help of a stereo-microscope. The adults were cut with a needle to extrude the embryos and the glass cover-slip was put upside-down onto an agarose-pad prepared from 2% agarose in H<sub>2</sub>O on a glass slide. Spinning disk confocal images of 1-cell stage embryos were acquired at 488 nm and 561 nm excitation on an Axio Observer D1 (Zeiss) coupled to an UltraViewVoX spinning disk unit (PerkinElmer) and 63x/1.4 plan-apochromat oil objective. Image-stacks were acquired at a step-size of 2  $\mu$ m and 3-5 z-planes were acquired. Images were taken in the TRANS channel, with the 488nm laser at 10% laser-power (200ms exposure, 2x binning) for imaging the GFP-signal and with 561nm laser at 30% laser power for imaging mkate2 signal (200ms of exposure, 2x binning). The microscope was controlled by the Volocity software (PerkinElmer).

### **2.1.2. Tissue culture techniques**

#### **2.1.2.1. Maintenance of HeLa FRT cell lines**

All procedures were performed under a sterile hood. Cells were grown in Dulbecco's growth medium (DMEM) containing 10% FBS and 1% Penicillin/Streptomycin (P/S). Every 2-3 days when cells became 90% confluent cells were passaged to a new culture flask (T25). Cells were once washed with 5 ml sterile 1xPBS and PBS was quickly removed from the cells. Then 1ml 1x Trypsin/PBS was added to the cells and immediately removed. Cells were incubated at RT for 5 min, then resuspended in fresh medium and split in 1:8 ratio to a new T25 flask.

#### **2.1.2.2. Freezing of HeLa FRT cell lines**

Cells were grown in a T75 cell culture flask until almost confluent. Cells were washed, trypsinized (see above) and resuspended with 10 ml of fresh medium. Cells were centrifuged at 700 x g for 5 minutes. In the mean-time, a 2x freezing media was prepared containing 20% DMSO, 50% FBS and 30% DMEM. After centrifugation, cells were resuspended with 2.5 ml of culture medium and 2.5 ml of freezing medium was added to

achieve a final concentration of 1x freezing medium. Cells were immediately frozen at -80°C using a cryo-container ensuring gradual cooldown of the cell suspension.

### **2.1.2.3. Generation of transgenic HeLa cell lines**

Transgenic HeLa FRT cell lines containing different hEct2 transgenes were generated by co-transfection of the GOI in a pcDNA5 vector together with the recombinase pOG44 that mediates the integration of the GOI. 150 000 cells/well were seeded in a 6-well plate one day prior to transfection and cultured at 5% CO<sub>2</sub>/37°C during the whole experiment. Cells were transfected with X-tremeGene9 transfection reagent according to the manufacturer's protocol. Briefly, 1 µg total DNA (900 ng pOG44 and 100ng GOI) was transfected together with 3 µl or 6 µl transfection reagent/ well. Cells were incubated for 48h with transfection mix, then all wells were transferred and combined in a big cell culture flask (T75). The next day selection media (DMEM + 10% FBS + 1% Pen/Strep + 300 µg/ml Hygromycin) was applied to the transfected cells and a control of non-transfected cells was included. Every 2-3 days selection media was changed. In a successful experiment, after 1.5-2 weeks all the control cells were dead and cell colonies that have emerged in the transfected lines were trypsinized and pooled into a small T25 flask. Cells were grown until almost confluent, then frozen and used for analysis of the transgenes with various assays.

### **2.1.2.4. Depletion of endogenous Ect2 by RNAi in human cells**

One day prior to the experiment FRT HeLa cells were trypsinized, resuspended in full medium and counted. In a 12-well plate, a total number of 70 000 cells/ well were plated on glass coverslips. Cells were incubated at 37°C, 5% CO<sub>2</sub> O/N. Transfection of siRNA targeting BRCT2 domain of endogenous Ect2 (ThermoFisher, silencer Select, 20 µM stock concentration) was performed using RNAi Max Transfection reagent. RNA was slowly thawed on ice; RNase ZAP spray was used to decontaminate surfaces and pipettes from RNase. Filter tips and gloves were used all the time, all steps to set-up the transfection mix were performed on ice. Media was aspirated from cells and replaced with pre-warmed fresh full medium containing 0.01 µg/ml tetracycline (1ml of medium+tetracycline was added to the well). Total volume per well at the end of transfection was 1200 µl (1ml of media+ 200 µl of RNA containing transfection mix). The transfection mix containing siRNA and transfection reagent RNAi Max was set-up up by preparing two Eppendorf tubes A and B. In tube A, the stock solution of RNA was diluted to a final concentration of 30 nM/ well in

100  $\mu$ l Opti-MEM serum-free medium. In tube B RNAi Max transfection reagent was diluted in Opti-MEM (5  $\mu$ l RNAi Max/100  $\mu$ l Opti-MEM/well). The tubes A and B were gently mixed by softly tapping with a finger. Then the content of tube A (diluted RNA) was added into tube B by carefully pipetting and slowly resuspending 1-2 times. The mix was incubated at RT for 5 min and 200  $\mu$ l of mix was added to each well in a drop-wise manner. The transfection mix was incubated at 37°C, 5% CO<sub>2</sub> for 48 h and subsequent analysis of Ect2 depleted cells was performed.

#### **2.1.2.5. Live Imaging in cells**

Localization of Ect2 mutants were assessed by live-cell imaging using spinning disk confocal microscopy. For live cell imaging experiments 50,000 cells were seeded in a 4-well ibidi  $\mu$ -Slide, at the same time induced with Tetracycline and incubated for 24-48 h at 5% CO<sub>2</sub>, 37°C. Spinning disk confocal images were acquired at 488 nm (30% laser power, 500ms exposure) on a Nikon TiE microscope equipped with a Yokogawa CSU-W1 spinning disk unit (50  $\mu$ m pinhole size, 405/488/561/640 LD Quad dichroic mirror) and laser illumination by an Andor ALC600 laser-beam combiner (405nm/488 nm/561 nm/640 nm). During imaging, cells were grown in CO<sub>2</sub> – independent medium at 37°C supplemented with 10% FCS and 1% P/S. Images were captured with an Andor IXON 888 Ultra EMCCD camera using a Nikon CFI Plan Apo Lambda 40X air and 100x oil-objective. The microscope was controlled via NIS-Elements (version 4.51.01). Over 1h, 3-5 z-planes with 2  $\mu$ m step-size were acquired every 2 minutes.

#### **2.1.2.6. Analysis of expression levels of Ect2 transgenes by Live Imaging**

The expression levels of Ect2 transgenes in the different cell lines were determined in Fiji ImageJ on the acquired time-lapse images. For this purpose, the cytoplasmic value in metaphase in the first time-frame acquired was measured. Background signal outside the cell was measured and subtracted from the cytoplasmic value.

#### **2.1.2.7. Quantification methods of HsEct2 fluorescence intensities at the cell periphery and at the spindle midzone by Live Imaging**

Confocal images were acquired by live-cell imaging as described in 2.1.2.5. Z-stacks were acquired with 100x objective and a midplane image at the first furrow indentation was used for quantification. To measure HsEct2 fluorescence intensities in human cells a line

(width= 6 pixel) was drawn around the cell periphery in ImageJ starting and ending at the left pole and fluorescent intensities were recorded. Cytoplasmic values were measured in a box drawn in the cytoplasm and values were subtracted from the cortex and pole values. After the cytoplasmic HsEct2 fluorescence intensity was subtracted from each value, the mean polar fluorescent intensity (0-10%, 40-60%, 90-100% of the cell length) and the mean equatorial fluorescent intensity (20-30%, 70-80% of cell length) was calculated for each cell. Mean fluorescent intensities at the equatorial and polar cortex were then calculated using the data analysis software KNIME.

To quantify the signal at the spindle midzone, a line scan was drawn underneath the upper equatorial membrane over the spindle midzone down to the lower equatorial membrane (length = 12 pixel) and the mean fluorescent intensity was calculated. Cytoplasmic background was measured in a box drawn in the cytoplasm and calculating the mean pixel intensity. The intensity values for spindle midzone were calculated as a ratio of spindle midzone/cytoplasmic values in Excel.

#### **2.1.2.8. Immunostainings in cells**

Sterile cover-slips (kept in 100% EtOH) were used and placed into 12-well plate, air-dried by putting them vertically at the wall of the well and left for 15 minutes until all the EtOH evaporated. After processing the cells in the according experiment (siRNA transfection, induction of transgenes, C3 application to inactivate RhoGTPases), cells were washed 2x with 1ml 1x PBS/ well and PBS was immediately aspirated to avoid detachment of the cells. Cells were fixed with ice-cold 100% MeOH at room temperature for 20 minutes. Methanol was removed and trashed in a correct container. Cells were washed 2x with 1x PBS at RT for 5 min/wash. Cells were permeabilized with 0.1% TritonX-1xPBS (1xPBST) at RT for 5 minutes. Cells were block with 4% BSA/PBST at RT for 1h. Then cover-slips were transferred into a moist chamber for the subsequent staining. 50µl/ cover-slip of diluted 1st Antibody was added on top of the cover-slip; anillin/tubulin antibody was diluted (1:2000/1:1000) in 4%BSA/PBST and incubated at 4°C O/N. First antibody was washed off by 3 wash steps with 1x PBS at RT for 5 minutes/wash. 2nd antibody was diluted 1:500 in 4%BSA/PBST and added with 50µl/reaction; here anti-rabbit (Anillin) or anti-mouse (Tubulin) labelled to different fluophores (FITC, TexasRed, Cy5, Cy3) was used and incubated at RT for 1h. 2<sup>nd</sup> antibody was washed 3x with PBST at RT for 5 minutes/wash. The cover-slips were mounted upside down onto glass slides using mounting

medium+ Hoechst dye (1:100) was used (1 $\mu$ g/ml stock of Hoechst diluted 1:100 in mounting medium to achieve a working dilution of 0.1 $\mu$ g/ml). Mounted cover-slips were sealed with clear nail polish and stored at -20°C after drying (dry for 1h at RT).

#### **2.1.2.9. C3 Rho inhibitor experiments**

To inactivate RhoA in different cell lines, 150 000 cells were plated one day prior to experiment on glass cover-slips and induced with Tetracycline. Then C3 inhibitor at a concentration of 0.5  $\mu$ g/ml was added to the cells for 6h and cells were fixed and stained for anillin and tubulin by immunohistochemistry (see protocol above for immunostainings). Images were captured with an Andor IXON 888 Ultra EMCCD camera using a Nikon CFI Plan Apo Lambda 100x oil-objective (laser 561nm, laser power 40%, 200ms exposure). The microscope was controlled via NIS-Elements (version 4.51.01).

### **2.1.3. Molecular biology techniques**

#### **2.1.3.1. Polymerase chain reaction for cloning by Gibson Assembly**

In order to generate desired DNA fragments that can be used for the cloning of a prospective plasmid, polymerase chain reaction (PCR) was used to amplify DNA from plasmid, cDNA and genomic DNA. Specific primers designed for Gibson assembly were used harboring a 3' end annealing to the template and 5' overhang that is complementary to the prospective sequence. The used forward and reverse primers were designed to amplify fragments that have a 22 base pair overlap for later annealing and ligation during the Gibson reaction (see 3.1.3.6). The PCR reaction was assembled on ice and run at specific thermocycling conditions (Table 18). Afterwards, PCR products were analyzed by agarose-gel electrophoresis.

#### **2.1.3.2. Agarose gel electrophoresis for PCR products**

The correct size of PCR products was analyzed by agarose gel electrophoresis. Agarose gels of 0,8% agarose/1xTAE were poured and used for the separation of size with an electrophoresis system from Biorad. Gels were run at 120V for 20 min and subsequently analyzed by imaging with the ChemiDoc imaging station from Biorad.

### **2.1.3.3. Dpn1 digest of PCRs amplified from bacterial templates**

PCRs were digested with Dpn1 enzyme in case the template for amplification was from a bacterial origin (plasmid). Dpn1 only digests methylated DNA, so the original template will be digested, whereas the amplified fragments that are not methylated will be not affected by the enzyme. This ensures less background when using the fragments for cloning and subsequent transformation. 1 µl of Dpn1 enzyme was added per 50 µl PCR reaction. The PCR-Dpn1 Mix was well resuspended and incubated at 37°C for 1h. Afterwards PCR was cleaned-up by either gel purification or spin-column centrifugation.

### **2.1.3.4. Purification of PCR products by spin-column**

In case the PCR products showed a single, specific band at the expected size, 200 µl of NTI buffer was added per 100 µl of PCR product (Macherey& Nagel, NucleoSpin Extraction kit). DNA was bound to a spin column by centrifugation of the gel suspension at 11 000g for 30s. Spin column was washed with 700 µl by centrifugation at 11 000g for 30s. The silica membrane of the spin column was dried by centrifuging at 11 000g for 2 min. DNA was eluted with 15-30 µl EB buffer by centrifugation at 11 000g for 1 min.

### **2.1.3.5. Purification of PCR products by gel excision**

In case PCR products had several amplified fragments of different sizes, the band with the correct size was cut out from the gel and subsequently purified over a spin-column (Macherey& Nagel, NucleoSpin Extraction kit). After cutting the band by visualization by UV light (hands, eyes and skin protected by gloves, protection helmet and lab-coat), the gel piece was measured and per 100 µg gel 200 µl of NTI buffer was added. The gel piece was melted in a heating-block at 50°C for 5 min (vortexing several times in between). DNA was bound to a spin column by centrifugation of the gel suspension at 11 000g for 30s. Spin column was washed with 700 µl by centrifugation at 11 000g for 30s. The silica membrane of the spin column was dried by centrifuging at 11 000g for 2 min. DNA was eluted with 15-30µl EB buffer by centrifugation at 11 000g for 1 min.

### **2.1.3.6. Cloning by Gibson Assembly**

After cleaning the amplified, correct PCR fragments from salts and other components the PCR fragments were used for Gibson Assembly to clone a plasmid containing the desired

sequence. Gibson Assembly is a PCR-based approach to assemble multiple fragments of DNA into a single fragment. The technique uses sets of primers that are designed with 22bp overlapping ends in the mutated region. Amplified DNA fragments with blunt ends are added into a 100  $\mu$ l Eppendorf tube together with a 2x Gibson Assembly Master Mix (NEB). The 2x Gibson Mix contains three different enzymes that facilitate the correct fusion of the different fragments. An exonuclease creates 3' overhangs that are causing complimentary sites of the fragments to be combined and which can then anneal together. A DNA polymerase fills the gaps within the annealed fragments. The DNA ligase seals the created nicks in the assembled DNA (Gibson et al., 2009).

First, PCRs were run with the specifically designed primers in order to generate the desired fragments for the Gibson Assembly (table 17). The correct sizes of the bands were checked on an agarose gel and afterwards eventually digested by Dpn1 and subsequently purified by either gel-extraction or spin-column purification (Macherey& Nagel, see protocol above). Then, the concentration of the purified DNA fragments was measured with a Nanodrop device and the right volumes for the Gibson Assembly were calculated (table 18). The optimal reaction to successfully fuse different DNA fragments together is highly dependent on the equal molarities of the DNA fragments. In most cases, a 2-fragment Gibson Assembly was performed. The Gibson Mix containing all required enzymes, dNTPs and buffer was added to the DNA fragments on ice and the reaction was incubated at 50°C for 1h. Afterwards, 10  $\mu$ l of the Gibson-Assembly mix was transformed into 100  $\mu$ l competent DH5alpha bacteria.

#### **2.1.3.7. Transformation in the competent *E. coli* strain DH5alpha**

After Gibson-Assembly reaction was performed, the Gibson Mix containing the desired, newly assembled plasmid, was transformed into competent DH5 $\alpha$  cells. Cells were thawed on ice for 10 min, then 10  $\mu$ l of the Gibson-Assembly Mix was added to 100  $\mu$ l competent cells. The cells and Gibson-Mix was carefully mixed and incubated on ice for 20 min. Afterwards, a heat-shock was performed at 42°C for 45 seconds. The tube was put back to ice for 2 min. Afterwards 1 ml of LB medium was added to the cells and the cells were incubated at 37°C for 45 min. Cells were centrifuged at 4000g for 5 min and cells were resuspended in around 100 $\mu$ l of left-over supernatant of the LB medium. Cells were plated onto LB plates with carbenicillin and the plates were incubated at 37°C O/N. Grown colonies were then screened for correct plasmid.

### **2.1.3.8. DNA preparations by alkaline lysis**

After transformation, colonies on the LB-Agar plates containing carbenicillin which only allows growth of bacteria that successfully took up the mutated plasmid containing a carbenicillin resistance. Colonies were inoculated into 5ml of LB medium with 0.1 mg/ml carbenicillin and incubated at 200 rpm, 37°C/ON. The next morning, DNA was prepared by either alkaline lysis method. The O/N culture was equally distributed into two 2 ml Eppendorf tubes and bacteria were spun down at 4000 rpm for 10 min. Afterwards, one pellet was frozen for eventual DNA preparation with a “clean” method, e.g. by column preparation with a Qiagen Mini/Midi Kit to achieve high purity of the plasmids and subsequent usage. For screening, DNA preparations were performed with the alkaline lysis method since high purity of the DNA for screening purposes is not required. After centrifugation of the bacterial cells, 100 µl of Solution 1 was added to the cells and thoroughly mixed. 200 µl of Solution II was added and thoroughly mixed and incubated for 4 min at RT (do not exceed 5 min). 300 µl of solution III was added to the lysate and after inverting the tube several times, incubation step on ice was performed for 10 min. Afterwards, the content of the tubes was centrifuged at 4°C at max. speed for 10 min. Supernatant containing the DNA was transferred from the old tube to a new tube on ice containing ice-cold 100% ethanol. DNA was precipitated by ethanol and subsequently centrifuged at 4°C, max. speed for 10 min. After centrifugation, the supernatant with 100% ethanol was removed and the pellet was again washed with 70% ethanol as in the step before with 100% ethanol. The 70% ethanol was removed, pellet was air-dried for approx. 15 min under a fume hood. The pellet was resolved in 50 µl TE buffer and DNA was used for genotyping of sequencing.

### **2.1.3.9. DNA preparations by plasmid Mini Kit**

After successful identification of a clone carrying the target sequence the second pellet from the DNA preparation by alkaline lysis was used to prepare DNA with high purity. The high purity DNA was the subsequently used for Gibson Cloning, microinjection of *C. elegans* or transfection of FRT HeLa cells in order to generate stable worm strains or cell lines. For mini prep 250 µl of P1 1 was added to the cells and thoroughly mixed. 250 µl of P2 was added and thoroughly mixed and incubated for 4 min at RT (do not exceed 5 min). 300 µl of P3 was added to the lysate and after inverting the tube several times, the content was centrifuged at 4°C at max. speed for 10 min. Supernatant containing the DNA was

transferred from the old tube to Qiagen spin column and subsequently centrifuged at RT, max. speed for 2 min. After centrifugation, the column was washed with 500  $\mu$ L PB by centrifugation at max. speed for 2 min. After removing the wash-through, the column was air-dried by centrifugation at RT, max. speed for 3 min. 15-30  $\mu$ l of Elution buffer was added to the spin column and incubated for 3-5 min. DNA was eluted into a new 1.5 ml Eppendorf tube by centrifuging at RT, max. speed for 3 min. DNA concentration was determined using a Nanodrop device.

#### **2.1.3.10. Sequencing of positive clones**

Generated plasmids were sequenced to ensure that the ORF of the different transgenes did not have any errors introduced by the cloning procedure. For this purpose, the in-house sequencing service of the faculty of biology was used. The protocol (Cycle, Clean and Run, BigDye v.3.1.) from the sequencing service was chosen and the pipetting scheme originates from the suggestions found on the website of the sequencing service. In brief, a reaction of 7  $\mu$ l total was set-up, containing the plasmid, a sequencing-primer and TE buffer (Table 19). Primers were chosen around 100bp upstream of the location to be sequenced.

#### **2.1.3.11. Western Blot analysis in cells**

To evaluate the expression levels of transgenic HeLa cell lines and to estimate the depletion level after *ect2(RNAi)*, 150 000 cells were seeded into 6-well plates 1 day prior to experiment. Cells were induced with Tetracycline (0.01  $\mu$ g/ml) and eventually transfected with siRNA targeting endogenous Ect2. After 48h, cells were washed with PBS on ice and 200  $\mu$ l of 2x Lämmli buffer was added to the well. Lämmli buffer was moved around with a pipette-tip while cells were forming a viscous substance. The viscous cell suspension was transferred into a 1.5 ml Eppendorf tube stored on ice. Cells were boiled at 95°C for 5 min and lysates were cooled down to RT and centrifugated at max. speed for 5 min before loading onto the SDS gel.

5-10  $\mu$ l of the lysate was loaded onto an SDS gel containing 10.5 % acrylamide. Gel was run at 100V for 1h inside of a Running buffer within in plastic chamber of the Biorad Western Blot system in the lab. The SDS-gel was blotted onto a PVDF membrane, which was activated by 100% ethanol incubation for 1 minute, at 200mA/ membrane in blotting buffer containing 10% ethanol. Membranes were blocked with 5% milk/TBST and incubated with Ect2 antibody (SantaCruz, 1:1000 in 5% milk/TBST) at 4°C O/N.

Membranes were washed with TBST at RT 3x/5minutes wash. Secondary antibody was added (mouse-HRP 1:10000 in 5% milk/TBST) and incubated at RT for 1h. Subsequently membranes were washed 3x with TBST as before. Proteins on membranes were detected (ECL Prime solution, GE Healthcare) and visualized using the ChemiDoc device (Biorad).

## 2.2. Materials

**Table 1. Buffers and solutions**

Buffer/Solution	Composition
1x TAE buffer	0.4 l 50x TAE buffer 19.6 l ddH <sub>2</sub> O
50x TAE buffer *	484 g Tris base 200 ml EDTA (0.5 M, pH 8.0) 114.2 ml glacial acetic acid bring volume to 2000 ml with MilliQ H <sub>2</sub> O
2x freezing buffer *	5.58 g NaCl 6.8 g KH <sub>2</sub> PO <sub>4</sub> 300 ml Glycerol 0.56 ml NaOH to pH 6.0 MilliQ H <sub>2</sub> O to 1 L Add 60 µL of 1M MgSO <sub>4</sub> to each 200 ml volume before use
B broth *	10 g Tryptone 5 g NaCl 1 L MilliQ H <sub>2</sub> O
EB buffer *	10 mM Tris-HCl, pH 8.5
LB Broth *	10 g Tryptone 5 g Yeast extract 10 g NaCl 800 ml MilliQ H <sub>2</sub> O
LB Agar	10 g Tryptone 5 g Yeast extract 10 g NaCl 800 ml MilliQ H <sub>2</sub> O 460 µl 10M NaOH 15 g Agar
M9 *	5.8 g Na <sub>2</sub> HPO <sub>4</sub> 3.0 g KH <sub>2</sub> PO <sub>4</sub> 0.5 g NaCl 1.0g NH <sub>4</sub> Cl MilliQ H <sub>2</sub> O to 1 liter
NGM Agar *	3 g NaCl 2.5 g Bacto-Peptone 20 g Agar

	<p>975 ml ddH<sub>2</sub>O  1 ml CaCl<sub>2</sub> (1M)  1 ml MgSO<sub>4</sub> (1M)  1 ml Cholesterol in EtOH (5 mg/ml)  25 ml KH<sub>2</sub>PO<sub>4</sub> (1M, pH 6.0)</p>
NGM Agar plates *	<p>Plate size NGM volume [ml]  Large 25-30  Medium 15  Small 5</p>
NGM Agar + IPTG	NGM + 1 mM IPTG
P1 *	<p>6.1g Tris  3.7g EDTA-2H<sub>2</sub>O (pH 8.0)  adjust volume to 1 l with HCl  take 50 ml aliquot and add 50 µl RNase A (100 mg/µl)</p>
P2 *	<p>dissolve 8.0 g NaOH in 900 ml MilliQ H<sub>2</sub>O  100 ml 10% SDS</p>
P3 *	<p>dissolve 294g CH<sub>3</sub>CO<sub>2</sub>K in 500ml MilliQ H<sub>2</sub>O  bring pH to 5,5 with Acetic Acid  adjust volume to 1 liter with MilliQ H<sub>2</sub>O</p>
Solution I *	<p>9 ml 20% Glucose  5 ml 1M Tris-HCl  8 ml 0.25M EDTA  adjust volume to 1 l with ddH<sub>2</sub>O  take 100 µL aliquot and add 0.1µL RNase A</p>
Solution III *	<p>29.5ml glacial acetic acid  KOH pellets to pH 4.8  MilliQ H<sub>2</sub>O to 100 ml  TE buffer 10 mM Tris-HCl  1 mM EDTA  adjust pH to 8.0 with HCl  adjust volume to 1 L with ddH<sub>2</sub>O</p>
TE buffer *	<p>10 mM Tris-HCL  1 mM EDTA  adjust pH to 8.0 with HCl  adjust volume to 1 L with ddH<sub>2</sub>O</p>
10x PBS	<p>25.6 g Na<sub>2</sub>HPO<sub>4</sub>·7H<sub>2</sub>O  80 g NaCl  2 g KCl  2 g KH<sub>2</sub>PO<sub>4</sub>.  Adjust to 1 liter with ddH<sub>2</sub>O</p>
1x PBS	<p>100 ml 10x PBS  900 ml ddH<sub>2</sub>O</p>
1x PBST	PBS + 0.1% Tween
10x TBS	<p>2 g KCl  80 g NaCl  30 g Tris-Base  Adjust the pH to 7.4 with HCl</p>

	Adjust to 1 liter with ddH <sub>2</sub> O
1x TBS	100 ml 10x TBS 900 ml ddH <sub>2</sub> O
1x TBST	1x TBS + 0.1% Tween
4% Bovine Serum Albumin in PBS/0.1% Tween	4 g BSA (dried) Adjust to 100 ml with 1x PBST
5% Milk in TBS/0.1% Tween	5 g Milk powder Adjust to 100 ml with 1x TBST
4x Resolving buffer	18.17 g Tris 24 ml 1M HCl Adjust to 100 ml with ddH <sub>2</sub> O
4x Stacking buffer	6 g Tris 38.5 ml 1M HCl 0.4 g SDS Adjust to pH 6.8 with HCl Adjust to 100 ml with ddH <sub>2</sub> O
10% APS	1 g APS Adjust to 10 ml with ddH <sub>2</sub> O
10x Running buffer	30.3 g Tris 144 g Glycine Adjust to 1 liter with ddH <sub>2</sub> O
1x Running buffer	100 ml 10x Running buffer 10 ml 10% SDS Adjust to 1 liter with ddH <sub>2</sub> O
Transfer buffer	100 ml 100% EtOH 100 ml Running buffer Adjust to 1 liter with ddH <sub>2</sub> O
50% Glycerol	50 ml 100% Glycerol Adjust to 100 ml with ddH <sub>2</sub> O
Coomassie Staining Solution	100 ml 100% MeOH 50 ml Glacial Acetic Acid 0.5g Brilliant Blue Adjust to 500 ml with ddH <sub>2</sub> O
Coomassie Destaining Solution	250 ml 100% Ethanol 50 ml Glacial Acetic Acid Adjust to 500 ml with ddH <sub>2</sub> O
2x Lämmli buffer 2x	2 ml 4x stacking buffer 4 ml 10% SDS 140 µl Beta-Mercaptoethanol 4 ml 50% Glycerol 100 µl Saturated Bromophenol blue solution
10% SDS	10 g SDS Adjust to 100 ml with ddH <sub>2</sub> O

\* = generated by lab technicians

## Table 2. Technical equipment

Devices	Supplier
1.5 ml centrifuge tubes	Sarstedt
2 ml microcentrifuge tubes	Sarstedt
Cryo-tubes	Thermo Scientific
15 ml Falcon tubes	Nerbe plus
50 ml Falcon tubes	Nerbe plus
PCR tubes	Nerbe plus
PCR-tube 8 strips	Nerbe plus
Plastic petri dish, 35x10 mm	Greiner Bio One
Plastic petri dish, 60x105 mm	Sarstedt
Cell culture flask T25	Greiner Bio One
Cell culture flask T75	Greiner Bio One
Cell culture multi-well plate 12-Well	Greiner Bio One
Cell culture multi-well plate 6-Well	Greiner Bio One
Serological Pipettes 5 ml	Sarstedt
Serological Pipettes 10 ml	Sarstedt
Pipette tips	Nerbe plus
Filter pipette tips	Nerbe plus
Ethanol burner	n.a.
Cover slides 24x50mm/ 50x 50 mm	Roth
Centrifuge 5424R	Eppendorf
Centrifuge 5424D	Eppendorf
-80 °C freezer	Thermo Scientific/ HFU T-series, Hera Freeze
8 well slide	Medco
4 °C refrigerator	Bosch
37 °C shaker incubator	New Brunswick
Worm incubators	Binder
37 °C incubator	Heraeus
250 ml Erlenmeyer flask	Kimax
-20 °C freezer	Comfort
Gel PowerPac HC, gel tray, lid and comb owl separation systems	Biorad
Glass pick with platinum wire	Self-made
Glass pipettes	Brand
Heating block	Labnet
Gel/ Western Blot detection machine	ChemiDoc™ XRS+ Biorad
Immersion oil	Zeiss
Nikon Eclipse Ti (Injection station)	Nikon
Microinjector, FemtoJet (Injection station)	Eppendorf
Microwave	LG
Photometer	Implen
Thermal cycler, T100TM	Biorad
P1000 pipette	Gilson
P200 pipette	Gilson
P20 pipette	Gilson
P2 pipette	Gilson
Pipette boy	Integra

Neubauer Chamber Improved	Carl Roth
Nitrile gloves	Meditrade
Stereo Microscope SMZ745	Nikon
Microscope Leica M80	Leica
Microscope M55	Leica
Microscope Axioscope A1	Zeiss
Microscope (4D), Imager M2	Zeiss
Microscope, M205 FA	Leica
Confocal spinning disk microscope, UltraviewVOX	Perkin Elmer
Camera UltraviewVOX, EMCCD	Hamamatsu
Confocal spinning disk, Nikon TiE microscope	Nikon
Camera (Spinning disk Nikon), Andor IXON 888 Ultra EMCCD	Andor

**Table 3. Kits**

Kit name	Supplier	Ref. Number
MAXIscript® T7 In Vitro Transcription Kit	Ambion	AM1322
MEGAscript® T7 Transcription Kit	Ambion	AM1334
NucleoSpin® Gel and PCR Clean-up Kit	Macherey-Nagel	740609.250
PureLink® Quick Plasmid Miniprep Kit	Invitrogen	K2100-01
Qiagen Plasmid Midi Kit	Qiagen	12145
Qiagen Plasmid Mini Kit	Qiagen	12125
QiaQuick Gel extraction Kit	Qiagen	28706
QiaPrep Spin Miniprep Kit	Qiagen	27104

**Table 4. Drugs, Chemicals and Reagents**

Chemical, drugs and reagents	Supplier
10x Standard Taq buffer	New England Biolabs
5x HF buffer	New England Biolabs
6x EZ-Vision	Amresco
Gelred	Biotium
10kb DNA ladder	Invitrogen
Acetic Acid	Carl Roth
Bacto-Peptone	BD
Bacto-Tryptone	BD
Yeast Extract	Serva
Blue loading dye	Home-made
Agar	Carl Roth
Agarose	Carl Roth
CaCl <sub>2</sub>	Carl Roth
Carbenicillin (100 mg/ml)	Applichem

Kanamycin	Applichem
CH <sub>3</sub> CO <sub>2</sub> K	Carl Roth
Cholesterol	Sigma-Aldrich
dNTPs	Metabion
DpnI	NEB
EDTA	Carl Roth
Ethanol	Carl Roth
Isopropanol	Carl Roth
Beta-Mercaptoethanol	Carl Roth
Glacial acetic acid	Carl Roth
Gelatin	Carl Roth
Glucose	Carl Roth
Glycerol	Carl Roth
SDS	Carl Roth
NaOH Pellets	Carl Roth
NaCl	Carl Roth
KCl	Carl Roth
Tris Base	Carl Roth
Tris-HCl	Carl Roth
HCl	Carl Roth
MgSO <sub>4</sub>	Carl Roth
KH <sub>2</sub> PO <sub>4</sub>	Carl Roth
Tween	Carl Roth
Triton-X100	Carl Roth
Meliseptol	Carl Roth
Korsolex Basic	MeinNutri
Fetal bovine Serum	Biochrom
Bovine Serum Albumin	Sigma-Aldrich
Milk powder	ShopApotheke
Penicillin/Streptomycin	Biochrom
Opti-MEM Reduced Serum Albumin	Thermofisher Scientific
Thymidine	Sigma-Aldrich
Tetracycline Hydrochloride	Sigma-Aldrich
MG-132	Merck Millipore
Interferrin siRNA Transfection Reagent	VWR
Lipofectamine RNAi Max siRNA transfection reagent	Thermofisher Scientific
X-treme Gene 9 DNA Transfection Reagent	Sigma-Aldrich

**Table 5. Antibodies**

Antibody	Supplier	Ref. No
HsEct2	Santa Cruz	sc-514750
HsAnillin	Home made by Sriyash Mangal	n.a.
Goat-anti-Rabbit-HRP	Biorad	170-6515
Goat-anti-Rabbit-HRP	Biorad	170-6515

Beta-Tubulin	Sigma-Aldrich	T6199
Actin	Sigma-Aldrich	A1978
Rabbit-Texas Red	Dianova	111-075-114
Mouse-Texas Red	Dianova	115-075-146
Rabbit- FITC	Dianova	111-095-144
Mouse-FITC	Dianova	115-095-146
Rabbit-Cy3	Dianova	111-165-144

**Table 6. Enzymes and Enzyme Mixes**

Enzymes	Supplier
2x Gibson Assembly Mix	New England Biolabs
DpnI	New England Biolabs
Proteinase K	AppliChem
Taq Polymerase	Homemade
Phusion Taq Polymerase	New England Biolabs
RNase A (100 mg/ml)	New England Biolabs
RNase ZAP	Ambion
10x Trypsin/EDTA Solution	Biochrom

**Table 7. DNA Primers**

Name	Sequence (5' -> 3')	Usage
EZ545	tcagacagagaatggtcgacagtaaggagaag	Gibson Cloning of transgenic mex-5:: GFP-CeECT-2 <sup>WT</sup> ::tbb2
EZ546	ctgtcgaccattctctgtctgaaacattcaattg	Gibson Cloning of transgenic mex-5:: GFP-CeECT-2 <sup>WT</sup> ::tbb2
EZ547	ccgatatctgaatgcaagatccttcaagcattc	Gibson Cloning of transgenic mex-5:: GFP-CeECT-2 <sup>WT</sup> ::tbb2
EZ548	ggatcttgcaatcagatatcggtgacacgatatg	Gibson Cloning of transgenic mex-5:: GFP-CeECT-2 <sup>WT</sup> ::tbb2
EZ554	aattcccgggtgcgttcagtaatgctcaactcac	Gibson Cloning of CeECT-2 fragment aa 1-421 into pGEX
EZ555	cgctcgagtcgtcagatatcggtgacacgata	Gibson Cloning of CeECT-2 fragment aa 1-421 into pGEX
EZ556	ccgatatctgacgactcgagcggccgcac	Gibson Cloning of CeECT-2 fragment aa 1-421 into pGEX
EZ557	ttactgaacgcacccgggaattccggggat	Gibson Cloning of CeECT-2 fragment aa 1-421 into pGEX
EZ558	aattcccgggtgctgaaaatagtgtattaacatccac	Gibson Cloning of HsEct2
EZ559	cgctcgagtcgtgctgactgcttgaaggaac	Gibson Cloning of HsEct2
EZ560	ctattttcagcaccgggaattccggggatc	Gibson Cloning of HsEct2
EZ561	ctattttcagcaccgggaattccggggatc	Gibson Cloning of HsEct2

EZ589	taatac gactcactatagg aactccccgcaccctgtaac	Production of dsRNA against endogenous 3' UTR of CeECT-2
EZ590	taatac gactcactatagg aagtaggggtgaatttcatttgaac	Production of small dsRNA against endogenous 3' UTR of CeECT-2
EZ609	GAGGTgtcgacccaactggcaaacctcacag	Gibson Cloning of CeECT-2 $\Delta$ BRCT0+1+2 (AA 292-932)
EZ61	ttgccagttgggtcgacACCTCCACCTCCTTTG	Gibson Cloning of ceECT-2 $\Delta$ BRCT0+1+2 (AA 292-932)
EZ653	tcgcagtagagggtcgacacctccacctcttg	Gibson Cloning of CeECT-2 $\Delta$ BRCT0 (AA 114-932)
EZ654	gaggtgtcgaccttactcgagcttatgaaag	Gibson Cloning of CeECT-2 $\Delta$ BRCT0 (AA 114-932)
EZ655	actttgctcttatgcaagatccttcaagcattc	Gibson Cloning of CeECT-2 <sup>BRCT1+2</sup> without BRCT0 and Rest of CeECT-2 (AA 114-293)
EZ656	ggatcttgcataagagcaagttatcctctatag	Gibson Cloning of CeECT-2 <sup>BRCT1+2</sup> without BRCT0 and Rest of CeECT-2 (AA 114-293)
EZ743	gaggtgtcgaccatagacttggcgtatttgaagg	Gibson Cloning of CeECT-2 $\Delta$ BRCT0+1 without BRCT0+1 domains (AA 187-932)
EZ744	ccaagtctatgggtcgacacctccacctcttg	Gibson Cloning of CeECT-2 $\Delta$ BRCT0+1 without BRCT0+1 domains (AA 187-932)
EZ822	tttgggtgatctgagctctggtaccctaggtg	Gibson Cloning of transgenic GFP-CeECT-2 <sup>WT</sup> ::tbb2 under heat-shock promoter
EZ823	accagagctcagatcaccaaaaacggaacg	Gibson Cloning of transgenic GFP-CeECT-2 <sup>WT</sup> ::tbb2 under heat-shock promoter
EZ824	cccttgagacttctgaagtttttagatgcac	Gibson Cloning of transgenic GFP-CeECT-2 <sup>WT</sup> ::tbb2 under heat-shock promoter
EZ825	aaacttcgaaagtctcaagggagaggaggac	Gibson Cloning of transgenic GFP-CeECT-2 <sup>WT</sup> ::tbb2 under heat-shock promoter
EZ826	ttgagacgtcgtcgacacctccacctccc	Gibson Cloning of transgenic GFP-CeECT-2 <sup>WT</sup> ::tbb2 under heat-shock promoter
EZ827	gaggtgtcgacgacgtctcaatgttgaatc	Gibson Cloning of transgenic GFP-CeECT-2 <sup>WT</sup> ::tbb2 under heat-shock promoter
EZ828	ttgccagttgggtcgacacctccacctcccttg	Gibson Cloning of transgenic GFP-CeECT-2 $\Delta$ BRCT0+1+2::tbb2 under heat-shock promoter

EZ829	agctctacaagggaggtggaggtgtcgacgacg	Gibson Cloning of transgenic GFP-CeECT-2 <sup>ΔBRCT0+1+2</sup> ::tbb2 under heat-shock promoter
EZ830	cctccacctccctttagagctcgccattcc	Gibson Cloning of transgenic GFP-CeECT-2 <sup>ΔBRCT0+1+2</sup> ::tbb2 under heat-shock promoter
EZ831	agctctacaagggaggtggaggtgtcgaccc	Gibson Cloning of transgenic GFP-CeECT-2 <sup>ΔBRCT0+1+2</sup> ::tbb2 under heat-shock promoter
EZ882	aggtagataagccaactggcaaaacttcacag	Gibson Cloning of CeECT-2 <sup>ΔBRCT2</sup> (AA 1-205 and 294-932)
EZ883	tgccagttggcttatctacctgaaaattgg	Gibson Cloning of CeECT-2 <sup>ΔBRCT2</sup> (AA 1-205 and 294-932)
EZ595	cgctcgagtcgtagtactagattcatcatactgtacaatac	Gibson Cloning of HsEct2 Amino Acids 1-150
EZ596	atctagtactacgactcgagcggccgcac	Gibson Cloning of HsEct2 Amino Acids 1-150
EZ597	aattccccggtagcttagtacagcgggtgaaac	Gibson Cloning of HsEct2 Amino Acids 640-790
EZ598	cgctcgagtcgactgtccatattctttgtattacttc	Gibson Cloning of HsEct2 Amino Acids 640-790
EZ599	atatggacagtcgactcgagcggccgcac	Gibson Cloning of HsEct2 Amino Acids 640-790
EZ600	tgtactaagctacccgggaattccggggatc	Gibson Cloning of HsEct2 Amino Acids 640-790
EZ601	aattccccgggtccaacagagcaggcaaatgtg	Gibson Cloning of HsEct2 Amino Acids 730-883
EZ602	cgctcgagtcgcatatcaaatgagttgtagatctactaac	Gibson Cloning of HsEct2 Amino Acids 730-883
EZ603	atttgatagactcgagcggccgcac	Gibson Cloning of HsEct2 Amino Acids 730-883
EZ604	gatccccggaattccccgggtccaacagagca	Gibson Cloning of HsEct2 Amino Acids 730-883
EZ727	aactcattgatagagcggccgcccggccgtttaaac	Gibson Cloning of Neongreen-Backbone
EZ728	ttgctcaccatccgcccggcaggggtc	Gibson Cloning of Neongreen-Backbone
EZ729	ctgccccgcgatggtgagcaagggcgagg	Gibson Cloning of Neongreen-fragment
EZ730	tcagccatgctgccgctgccctgtacagctgtccatgc	Gibson Cloning of Neongreen-fragment
EZ731	agggcagcggcagcatggctgaaaatagtgtattaacac	Gibson Cloning of Neongreen-HsEct2 <sup>WT</sup>
EZ732	acttgccacctgctgactgctttgaaggaac	Amplification of HsEct2 Amino Acids 1-421
EZ733	agcagtcagcaaggtggcaagttgcaaaagag	Amplification of HsEct2 Amino Acids 1-421

EZ734	ggccgctcatatcaaatgagttgtagatctac	Amplification of Amino Acids HsEct2 1-421
EZ735	gggaaaggcggaatgagcaagatttctatgcagcagttgat	Introduction of silent mutations for RNAi resistance in HsEct2 <sup>WT</sup>
EZ736	atcaactgctgcatagaaatcttgctcattccgccttccc	Introduction of silent mutations for RNAi resistance in HsEct2 <sup>WT</sup>
EZ737	ggaaaggaggaacgagcaagatttctatgcagcagttgatg	Introduction of silent mutations for RNAi resistance in HsEct2 <sup>WT</sup>
EZ738	catcaactgctgcatagaaatcttgctgctcctccttccc	Introduction of silent mutations for RNAi resistance in HsEct2 <sup>WT</sup>
EZ743	gaggtgtcgaccatagacttggcgtatttgaagg	Gibson Cloning of HsEct2 <sup>ΔBRCT0+1</sup> (Amino Acids 283-883)
EZ744	ccaagtctatggctgacacctccacctccttgg	Gibson Cloning of HsEct2 <sup>ΔBRCT0+1</sup> (Amino Acids 283-883)
EZ745	gcggcagcccgttgtattgtacaagtatgatgaat	Gibson Cloning of HsEct2 <sup>ΔBRCT0</sup> (Amino Acids 139-883)
EZ746	gtacaatacaacgggctgccgctgcccttgtac	Gibson Cloning of HsEct2 <sup>ΔBRCT0</sup> (AA 139-883)
EZ747	cggcagccctcattcaagattgtattttaag	Gibson Cloning of HsEct2 <sup>ΔBRCT0+1</sup> (AA 238-883)
EZ748	atcttgaaatggagggtgccgctgcccttgtac	Gibson Cloning of HsEct2 <sup>ΔBRCT0+1</sup> (AA 238-883)
EZ749	gcggcagcactcctgagctcaagaaatcagtg	Gibson Cloning of HsEct2 <sup>ΔBRCT0+1+2</sup> (AA 328-883)
EZ750	ttgagctcaggagtgtgccgctgcccttgtac	Gibson Cloning of hsEct2 <sup>ΔBRCT0+1+2</sup> (AA 328-883)
EZ943	agctcaggagtaactttaattcatttctaaag	Gibson Cloning of HsEct2 <sup>ΔBRCT2</sup> (AA 1-237 and 328-883)
EZ944	aatttaaagtactcctgagctcaagaaatc	Gibson Cloning of HsEct2 <sup>ΔBRCT2</sup> (AA 1-237 and 328-883)
EZ971	gaagccagaacggattataaagcttgggaaagg	Gibson Cloning of HsEct2 <sup>W211R</sup>
EZ972	ttataaatccgttctggcttcataattggag	Gibson Cloning of HsEct2 <sup>W211R</sup>
EZ973	tcaagcaagagcggttctggggaagcattcaaatgg	Gibson Cloning of HsEct2 <sup>W305R</sup>
EZ974	ccccagaaccgctcttgccttgacaacataaag	Gibson Cloning of HsEct2 <sup>W305R</sup>

EZ975	ctatgctttgctggatttaggaaaaaagaag	Gibson Cloning of HsEct2 <sup>T153A</sup>
EZ976	tcctaaatccagcaaagcatagtagattc	Gibson Cloning of HsEct2 <sup>T153A</sup>
EZ977	aaggagaaatgttcagggttgctgtgagtc	Gibson Cloning of HsEct2 <sup>K195M</sup>
EZ978	gcaaccctgaacatttctccttggtacaatttc	Gibson Cloning of HsEct2 <sup>K195M</sup>
EZ979	tttcatgtcgcactcctgagctcaagaaatc	Gibson Cloning of HsEct2 <sup>ΔBRCT1+2</sup> (AA 1-138 and 328-883)
EZ980	agctcaggagtgcgacatgaaaatggcaaag	Gibson Cloning of HsEct2 <sup>ΔBRCT1+2</sup> (AA 1-138 and 328-883)
EZ981	tttcatgtcgcctccatttcaagattgtatttaag	Gibson Cloning of HsEct2 <sup>ΔBRCT1</sup> (AA 1-138 and 238-883)
EZ982	tgaaatggagggcgacatgaaaatggcaaag	Gibson Cloning of HsEct2 <sup>ΔBRCT1</sup> (AA 1-138 and 238-883)
EZ1040	ttcaagattgtgactatgctttactggatttag	Gibson Cloning of HsEct2 <sup>BRCT1-BRCT1</sup> (AA 1-243 + 149-220 and 325-883)
EZ1041	aagagaatgctcttgaacctttttgaagtc	Gibson Cloning of HsEct2 <sup>BRCT1-BRCT1</sup> (AA 1-243 + 149-220 and 325-883)
EZ1042	aagcatagtacacaatcttgaaatggaggaac	Gibson Cloning of HsEct2 <sup>BRCT1-BRCT1</sup> (AA 1-243 + 149-220 and 325-883)
EZ1043	aggttacaagagcattctcttttccaaaac	Gibson Cloning of HsEct2 <sup>BRCT1-BRCT1</sup> (AA 1-243 + 149-220 and 325-883)
EZ1044	tgatgaatctaatttaagtttctctggattttcag	Gibson Cloning of HsEct2 <sup>BRCT2-BRCT2</sup> (AA 1-148 + 244-324 and 221-883)
EZ1045	aaacttaaaattagattcatcatactgtacaatac	Gibson Cloning of HsEct2 <sup>BRCT2-BRCT2</sup> (AA 1-148 + 244-324 and 221-883)
EZ1062	gtatttgcttattccgcctttccaagc	Gibson Cloning of HsEct2 <sup>BRCT1-BRCT1</sup> (AA 1-243 + 149-220 and 325-883)
EZ1063	aaaggcgggaataaggcaaatactcctgagctcaagaaatc	Gibson Cloning of HsEct2 <sup>BRCT1-BRCT1</sup> (AA 1-243 + 149-220 and 325-883)
EZ1064	aaatcctgttctcatataaatacatagtttc	Gibson Cloning of HsEct2 <sup>BRCT2-BRCT2</sup> (AA 1-148 + 244-324 and 221-883)
EZ1065	atttatatgaagaacaggatttctatgcagc	Gibson Cloning of HsEct2 <sup>BRCT2-BRCT2</sup> (AA 1-148 + 244-324 and 221-883)

EZ1090	aaaaggcaaatgcacctgagctcaagaaagc	Gibson Cloning of HsEct2 <sup>LinkerAA</sup>
EZ1091	acttgccacctagcagcctgcttgcaggaac	Gibson Cloning of HsEct2 <sup>LinkerAA</sup>
EZ1092	agcaggctgctaggtggcaagttgcaaagagc	Gibson Cloning of HsEct2 <sup>LinkerAA</sup>
EZ1093	agctcaggtgcattgcctttcatataaatac	Gibson Cloning of HsEct2 <sup>LinkerAA</sup>
AD325	gacatttgagaatggcattga	Genotyping of integration of transgene in generated <i>C. elegans</i> strains
AD326	tttacaaggacttgataaattgg	Genotyping of integration of transgene in generated <i>C. elegans</i> strains

**Table 8. Plasmids provided by the laboratory**

Plasmid	Description
pCFJ350	Vector for generating MosSCI of CeECT-2 transgenes into <i>C. elegans</i>
pGEX-4T	Vector for bacterial protein expression of CeECT-2 fragments for antibody production
pcDNA-5	Vector for delivery of hsEct2 transgenes into FRT HeLa cells
pCFJ601	Co-injection marker for generating MosSCI strains in <i>C. elegans</i> ; Encodes <i>Peft-3::transposase</i>
pMA122	Co-injection marker for generating MosSCI strains in <i>C. elegans</i> ; Encodes <i>Phsp::peel-1</i>
pGH8	Co-injection marker for generating MosSCI strains in <i>C. elegans</i> ; Encodes <i>prab-3::mcherry</i> (pan-neuronal)
pCFJ90	Co-injection marker for generating MosSCI strains in <i>C. elegans</i> ; Encodes <i>pmyo-2::mcherry</i> (pharynx-muscle)
pCFJ104	Co-injection marker for generating MosSCI strains in <i>C. elegans</i> ; Encodes <i>pmyo-3::mcherry</i> (body-muscle)
pEX-128	Vector for delivery of HsEct2 mutated linker region (T/S to A) by Eurofins for generating the construct HsEct2 <sup>LinkerAA</sup>

**Table 9. Generated plasmids**

Plasmid	Description
pEZ151	<i>mex-5-GFP-CeECT-2<sup>WT</sup>-tbb-2</i> in pCFJ350
pEZ157	HsEct2 <sup>WT</sup> in pGEX-4T
pEZ158	HsEct2 <sup>1-421</sup> in pGEX-4T
pEZ161	<i>mex-5-GFP-CeECT-2<sup>ΔBRCT0+1+2</sup>-tbb-2</i> in pCFJ350
pEZ163	HsEct2 <sup>1-150</sup> in pGEX-4T
pEZ164	HsEct2 <sup>640-790</sup> in pGEX-4T
pEZ168	<i>mex-5-GFP-CeECT-2<sup>ΔBRCT0</sup>-tbb-2</i> in pCFJ350
pEZ169	<i>mex-5-GFP-CeECT-2<sup>BRCT0+1+2</sup>-tbb-2</i> in pCFJ350
pEZ187	<i>mex-5-GFP-CeECT-2<sup>ΔBRCT0+1</sup>-tbb-2</i> in pCFJ350

pEZ189 **	HsEct2 <sup>WT</sup> in pcDNA5
pEZ190 **	Neogreen-HsEct2 <sup>WT</sup> in pcDNA5
pEZ196 **	Neogreen-HsEct2 <sup>WT</sup> with 2 silent mismatches for RNAi resistance in pcDNA5
pEZ197 **	Neogreen-HsEct2 <sup>WT</sup> with 4 silent mismatches for RNAi resistance in pcDNA5
pEZ203 **	Neogreen-HsEct2 <sup>ΔBRCT0+1</sup> with 4 silent mismatches for RNAi resistance in pcDNA5
pEZ204 **	Neogreen-HsEct2 <sup>ΔBRCT0+1+2</sup> with 4 silent mismatches for RNAi resistance in pcDNA5
pEZ215	<i>Hsp6</i> -GFP-CeECT-2 <sup>WT</sup> - <i>tbb-2</i> in pCFJ350
pEZ216	<i>Hsp6</i> -GFP-CeECT-2 <sup>ΔBRCT0+1+2</sup> - <i>tbb-2</i> in pCFJ350
pEZ227 ***	Neogreen-HsEct2 <sup>ΔBRCT0</sup> with 4 silent mismatches for RNAi resistance in pcDNA5
pEZ232 ***	Neogreen-HsEct2 <sup>ΔBRCT2</sup> with 4 silent mismatches for RNAi resistance in pcDNA5
pEZ237	<i>mex-5</i> -GFP-CeECT-2 <sup>ΔBRCT2</sup> - <i>tbb-2</i> in pCFJ350
pEZ242	Neogreen-HsEct2 <sup>ΔBRCT1</sup> with 4 silent mismatches for RNAi resistance in pcDNA5
pEZ243	Neogreen-HsEct2 <sup>ΔBRCT1+2</sup> with 4 silent mismatches for RNAi resistance in pcDNA5
pEZ244	Neogreen-HsEct2 <sup>W211R</sup> with 4 silent mismatches for RNAi resistance in pcDNA5
pEZ245	Neogreen-HsEct2 <sup>W305R</sup> with 4 silent mismatches for RNAi resistance in pcDNA5
pEZ246	Neogreen-HsEct2 <sup>T153A</sup> with 4 silent mismatches for RNAi resistance in pcDNA5
pEZ247	Neogreen-HsEct2 <sup>T153A, K195M</sup> with 4 silent mismatches for RNAi resistance in pcDNA5
pEZ255	Neogreen-HsEct2 <sup>BRCT1-BRCT1</sup> with 4 silent mismatches for RNAi resistance in pcDNA5
pEZ256	Neogreen-HsEct2 <sup>BRCT2-BRCT2</sup> with 4 silent mismatches for RNAi resistance in pcDNA5
pEZ265	Neogreen-HsEct2 <sup>LinkerAA</sup> with 4 silent mismatches for RNAi resistance in pcDNA5

\*\* Plasmids were cloned by Pedro Barbosa

\*\*\* Plasmids were cloned by Seren Baygun

**Table 10. Bacterial strains provided by the laboratory**

Bacterial strain	Usage
OP50	Uracil auxotroph, growth restricted on NGM plates. Maintenance of <i>C. elegans</i>
DH5 alpha	Transformation of DNA
BL-21	Protein Expression

**Table 11. Received *C. elegans* strains**

Strain	Genotype
--------	----------

EG6699	<i>ttTi5605 II; unc-119(ed3) III</i>
N2	<i>C. elegans</i> wild type ancestral strain
EZ141	<i>Si78 [pAZ211(pCFJ151); mKate2:NMY2] IV</i>

**Table 12. Generated *C. elegans* strains**

Per genotype, several worm strains all resulting from independent integration events were additionally generated as back-up strains frozen at -80°C. The strain used for experiments shown in the results part are indicated with “yes”.

Name	Genotype	Used for the data shown in the results part
EZ84	Si48[pEZ151; <i>pmex-5::gfp:ect-2::tbb-2; cb-unc-119(ed3)(+)</i> ]II	
EZ85	Si49[pEZ151; <i>pmex-5::gfp:ect-2::tbb-2; cb-unc-119(ed3)(+)</i> ]II	Yes
EZ90	Si59[pEZ151; <i>pmex-5::gfp:ect-2::tbb-2; cb-unc-119(ed3)(+)</i> ]II	
EZ91	Si60[pEZ151; <i>pmex-5::gfp:ect-2::tbb-2; cb-unc-119(ed3)(+)</i> ]II	
EZ92	Si61[pEZ151; <i>pmex-5::gfp:ect-2::tbb-2; cb-unc-119(ed3)(+)</i> ]II	
EZ108	Si62[pEZ161; <i>pmex-5::gfp:ect-2ΔBRCT0+1+2::tbb-2; cb-unc-119(ed3)(+)</i> ]II	Yes
EZ125	Si82[pEZ161; <i>pmex-5::gfp:ect-2ΔBRCT0+1+2::tbb-2; cb-unc-119(ed3)(+)</i> ]II	Yes
EZ126	Si83[pEZ161; <i>pmex-5::gfp:ect-2ΔBRCT0+1+2::tbb-2; cb-unc-119(ed3)(+)</i> ]II	
EZ127	Si84[pEZ161; <i>pmex-5::gfp:ect-2ΔBRCT0+1+2::tbb-2; cb-unc-119(ed3)(+)</i> ]II	
EZ128	si85[pEZ168; <i>pmex-5::gfp:ect-2ΔBRCT0::tbb-2; cb-unc-119(ed3)(+)</i> ]II	Yes
EZ129	si86[pEZ168; <i>pmex-5::gfp:ect-2ΔBRCT0::tbb-2; cb-unc-119(ed3)(+)</i> ]II	
EZ130	si87[pEZ168; <i>pmex-5::gfp:ect-2ΔBRCT0::tbb-2; cb-unc-119(ed3)(+)</i> ]II	
EZ172	Si112[pEZ187; <i>pmex-5::gfp:ect-2ΔBRCT0+1::tbb-2; cb-unc-119(ed3)(+)</i> ]II	Yes
EZ173	Si113[pEZ187; <i>pmex-5::gfp:ect-2ΔBRCT0+1::tbb-2; cb-unc-119(ed3)(+)</i> ]II	
EZ210	Si147[pEZ161; <i>pmex-5::gfp:ect-2ΔBRCT0+1+2::tbb-2; cb-unc-119(ed3)(+)</i> ]II	Yes
EZ211	Si148[pEZ161; <i>pmex-5::gfp:ect-2ΔBRCT0+1+2::tbb-2; cb-unc-119(ed3)(+)</i> ]II	
EZ228	Si78[pCFJ151; <i>mKate2:NMY-2] IV; si85[pEZ168; pmex-5::gfp:ect-2ΔBRCT0::tbb-2; cb-unc-119(ed3)(+)</i> ]II	

EZ232	Si78[pCFJ151; <i>mKate2:NMY-2</i> ] IV; <i>si85</i> [pEZ168; <i>pmex-5::gfp:ect-2ΔBRCT0::tbb-2; cb-unc-119(ed3)(+)]II</i>	Yes
EZ241	<i>si127</i> [pEZ216; <i>phsp-5::neongreen:ect-2ΔBRCT0+1+2::tbb-2; cb-unc-119(ed3)(+)]II</i>	
EZ243	<i>si128</i> [pEZ215; <i>phsp-5::neongreen:ect-2-WT::tbb-2; cb-unc-119(ed3)(+)]II</i>	Yes
EZ244	<i>si129</i> [pEZ215; <i>phsp-5::neongreen:ect-2-WT::tbb-2; cb-unc-119(ed3)(+)]II</i>	
EZ245	<i>si130</i> [pEZ216; <i>phsp-5::neongreen:ect-2ΔBRCT0+1+2::tbb-2; cb-unc-119(ed3)(+)]II</i>	Yes
EZ260	Si78[pCFJ151; <i>mKate2:NMY-2</i> ] IV; <i>Si49</i> [pEZ151; <i>pmex-5::gfp:ect-2::tbb-2; cb-unc-119(ed3)(+)]II</i>	Yes
EZ261	Si78 [pCFJ151; <i>mKate2:NMY-2</i> ] IV; <i>Si113</i> [pEZ187; <i>pmex-5::gfp:ect-2-deltaBRCT0+1::tbb-2; cb-unc-119(ed3)(+)]II</i>	

**Table 13. Generated cell lines**

Cell line	Background	Description	Amino acid sequence of Ect2-Transgene
FRT	HeLa Flp-In T-Rex	No transgene insertion (Tighe, 2004)	None
EZ69 ****	HeLa Flp-In T-Rex	Expression of HsEct2WT	1-883
EZ70 ****	HeLa Flp-In T-Rex	Expression of HsEct2 ΔBRCT0	139-883
EZ71 ****	HeLa Flp-In T-Rex	Expression of HsEct2 ΔBRCT0+1	238-883
EZ72 ****	HeLa Flp-In T-Rex	Expression of HsEct2 ΔBRCT0+1+2	328-883
EZ73 ****	HeLa Flp-In T-Rex	Expression of HsEct2 BRCT0+1+2	1-327
EZ74	HeLa Flp-In T-Rex	Expression of HsEct2 ΔBRCT2	1-237 and 328-883
EZ76	HeLa Flp-In T-Rex	Expression of HsEct2 ΔBRCT1	1-138 and 238-883
EZ76.3	HeLa Flp-In T-Rex	Expression of HsEct2 ΔBRCT1 ; subclone obtained by single-cell FACS sorting of EZ76; did not survive freezing/thawing process	1-138 and 238-883
EZ76.5	HeLa Flp-In T-Rex	Expression of HsEct2 ΔBRCT1; subclone obtained by single-cell FACS with Dr. Christoph Ziegenhain (Enard Group) sorting of EZ76; did not survive freezing/thawing process	1-138 and 238-883
EZ77	HeLa Flp-In T-Rex	Expression of HsEct2 ΔBRCT1+2	1-138 and 328-883
EZ78	HeLa Flp-In T-Rex	Expression of HsEct2W211R	1-883, W211R
EZ79	HeLa Flp-In T-Rex	Expression of HsEct2W309R	1-883, W305R

EZ80	HeLa Flp-In T-Rex	Expression of HsEct2T153A, K195M	1-883, T153A, K195M
EZ81	HeLa Flp-In T-Rex	Expression of HsEct2 BRCT1-BRCT1	1-243, 149-220 and 325-883
EZ82	HeLa Flp-In T-Rex	Expression of HsEct2 BRCT2-BRCT2	1-148, 244-324 and 221-883
EZ83	HeLa Flp-In T-Rex	Expression of HsEct2 LinkerAA	1-883, exchange of serines/threonines for alanine in sequence 323-421

\*\*\*\* = Cell lines generated by Seren Baygun

**Table 14. Components of the MosSCI Injection Mix**

Components	Volume
3x MosSCI Mix: pCFJ601; Pef3::transposase: 150 ng/ $\mu$ L pMA122; Phsp::peel21 30 ng/ $\mu$ L pGH8; Prab-3::mCherry (Pan-neuronal): 30 ng/ $\mu$ L pCJF905; Pmyo-2::mCherry (pharynx muscle): 7.5 ng/ $\mu$ L pCJF1045 Pmyo23::mCherry (body5muscle): 15 ng/ $\mu$ L	2 $\mu$ l
Target plasmid: 50 ng/ $\mu$ L	X $\mu$ l
H <sub>2</sub> O	0-4 $\mu$ l
Total volume	6 $\mu$ l

**Table 15. Digestion mix for worm lysis**

Component	Volume
Proteinase K	0.25 $\mu$ l
10x Standard Taq-Buffer	0.5 $\mu$ l
H <sub>2</sub> O	4.25 $\mu$ l
<b>Total volume per reaction</b>	<b>5 <math>\mu</math>l</b>

**Table 16. PCR pipetting scheme and cycler settings for genotyping and RNA generation**

Pipetting scheme	
Component	Volume
2x Taq-Master Mix	12.5 $\mu$ l
H <sub>2</sub> O	7.25 $\mu$ l
Primer 1 (100pmol/ $\mu$ L)	0.125 $\mu$ l
Primer 2 (100pmol/ $\mu$ L)	0.125 $\mu$ l
Worm lysate (table 15)	5 $\mu$ l
<b>Total volume per reaction</b>	<b>25 <math>\mu</math>l</b>

PCR cyclers settings	
Step	Temperature, Time
Pre-heating the lid	105 °C, until lid is heated
Denaturation of DNA	95 °C, 3 min
Denaturation of DNA	95 °C, 30s
Primer Annealing	52-65 °C, 30 s
Elongation	68 °C, 1000 bp/ min, depending on the fragment-size
Loop	Repeat steps 3-5, 34x
Final elongation step	68 °C, 5 min
Cooling down	12 °C, until temperature is reached

**Table 17. Pipetting scheme and cyclers settings of PCR for Gibson assembly**

Pipetting scheme	
Component	Volume
5x HF Phusion buffer (NEB)	10 µl
H <sub>2</sub> O	33 µl
Primer 1 (Xpmol/ µl)	0.25 µl
Primer 2 (Xpmol/ µl)	0.25 µl
dNTPs (2 mM)	5 µl
Phusion (NEB)	0.5 µl
Template (20ng/µl)	1 µl
<b>Total volume per reaction</b>	<b>50 µl</b>
PCR cyclers settings	
Step	Temperature, Time
Pre-heating the lid	105 °C, until lid is heated
Denaturation of DNA	98 °C, 30 s
Denaturation of DNA	95 °C, 10s
Primer Annealing	56 °C, 45 s
Elongation	72 °C, 2000bp/ min, fragment-dependent
Loop	Repeat steps 3-5, 29x
Final elongation step	72 °C, 5 min/ fragment < 5000bp; 10 min/ fragment > 5000bp
Cooling down	12 °C, until temperature is reached

**Table 18. Pipetting scheme of Gibson Reaction**

Component	Volume
DNA fragment 1 (0.02- 0.5 pmol)	X <sub>1</sub> µl
DNA fragment 2 (0.02- 0.5 pmol)	X <sub>2</sub> µl
H <sub>2</sub> O	7.5 µl - (X <sub>1</sub> +X <sub>2</sub> ) µl
Gibson Assembly Master Mix (2x)	7.5 µl
<b>Total volume</b>	<b>15 µl</b>

**Table 19. Pipetting scheme of sequencing reaction according to the protocol “Cycle, Clean and Run BigDye v.3.1. from the LMU sequencing service**

Component	Volume
Plasmids, 150-300 ng total	1 $\mu$ l
Primer (100pmol/ $\mu$ l, 1:20)	1 $\mu$ l
TE buffer	5 $\mu$ l
<b>Total volume</b>	<b>7 <math>\mu</math>l</b>

**Table 20. Pipetting scheme of the transcription mix**

Component	Volume
rNTPs (UTPs, ATPs, GTP, CTPs)	16 $\mu$ l each (total 64 $\mu$ l)
10x T7 buffer	4 $\mu$ l
PCR product (1 $\mu$ g total DNA)	10 $\mu$ l
Enzyme Mix	4 $\mu$ l
<b>Total</b>	<b>40 <math>\mu</math>l</b>

### 3. Results

During cytokinesis contractile ring formation depends on the activation of RhoA via the GEF Ect2. How Ect2 activity is controlled *in-vivo* to achieve orderly RhoA activation is not completely understood. To analyze Ect2 regulation *in-vivo* I performed structure-function studies in *C. elegans* and human HeLa cells to study whether 1.) Ect2 is regulated by an autoinhibitory mechanism through the interaction of its N-terminal BRCT domains with the GEF domain and 2.) whether Ect2 BRCT domains have distinct roles in Ect2 regulation.

I started my work in the *C. elegans* system where I tested the function of the BRCT domains by deleting specific domains. First a genetic replacement system of endogenous and transgenic CeECT-2 transgenes was established which allowed me study CeECT-2 transgenes in absence of endogenous CeECT-2. Then I analyzed the cytokinetic phenotype by transmission microscopy and the function of different CeECT-2 mutants in the presence and absence of endogenous CeECT-2 by measuring embryonic lethality and brood size. Moreover, CeECT-2 transgenes were tagged with a GFP for localization studies during cell division by confocal spinning disk microscopy. First, I deleted all three BRCT domains and analyzed the cytokinetic phenotype by transmission microscopy and the localization of CeECT-2 without the N-terminus by confocal microscopy. I also deleted BRCT0 and BRCT0+1 domain and studied the localization, function and cytokinetic phenotype in these mutants. Moreover, I used the contractility marker CeNMY-2 (non-muscle myosin II) and analyzed whether deletion of BRCT0 and BRCT0+1 lead to an increase in contractility.

In *C. elegans* CeECT-2 exclusively localizes to the plasma membrane (Jenkins, 2006; Motegi and Sugimoto, 2006). In human cells HsEct2 localizes to the cell equator and additionally to the spindle midzone and specifically spindle midzone localization was thought to be important for activation of Ect2 at the cell equator (Nishimura and Yonemura, 2006; Tatsumoto et al., 1999; Wolfe et al., 2009; Yüce et al., 2005). To study whether the different localizations are connected to differences in the regulation of CeECT-2 / HsEct2 I also wanted to study HsEct2 structure function in human cells. Moreover, some of the important *C. elegans* mutants I could not test since the transgenes were silenced during strain generation, probably due to cytotoxicity. Therefore, I decided to continue my work entirely in the human system since some of the important transgenes I could not express in the *C. elegans* system, I could successfully express in human cells.

First, a similar molecular replacement system of HsEct2 was established in the human HeLa cell line which allowed me to study the HsEct2 transgenes in absence of endogenous HsEct2.

Then I deleted or replaced specific BRCT domains alone or in combination to test the cytokinetic phenotype by transmission light microscopy, the function of the BRCT domains by estimating multinucleation and the localization of the different transgenes tagged with neongreen using confocal microscopy.

Moreover, I measured contractility in the cell lines by quantifying membrane protrusions and analyzed whether anillin, a contractility marker in a highly contractile mutant is elevated.

### **3.1. CeECT-2 BRCT0 and BRCT1 domains are not inhibiting GEF activity but are required for cytokinesis and viability**

#### **3.1.1. Establishing a molecular replacement system for CeECT-2 in *C. elegans***

To study CeECT-2 regulation *in-vivo* I established a genetic replacement system of endogenous and transgenic CeECT-2. CeECT-2 transgenes were integrated into a single, specific locus in the *C. elegans* genome and designed to be RNAi resistant against siRNA targeting endogenous CeECT-2.

To establish the molecular replacement system, I used the Mos1-mediated Single Copy Insertion (MosSCI) technique to generate transgenic worm strains stably expressing different mutant CeECT-2 versions (Frøkjær-Jensen et al., 2008). With the MosSCI system a gene of interest can be stably integrated into the genome of *C. elegans* as a single-copy. This allows quantitative analysis of transgenes using different read-outs, e.g. live-cell imaging.

The MosSCI system uses the presence of a Mos1 transposon originating from *D. melanogaster* within the *C. elegans* genome in the strain EG6699. By micro-injection into the germline of this worm strain, a gene of interest can be stably integrated into a specific locus of the *C. elegans* genome and this insertion is mediated by the excision of the Mos1 transposon. The Mos1 transposon is excised with the help of a transposase that causes a

double-strand break in the DNA that in turn is repaired by the gene of interest (Fig. 6A). Additionally, to the Mos1 transposon, the worm strain EG6699 carries the *unc-119* allele *ed3* that causes low brood size, immobility of the worms and defects in dauer larvae formation after starvation (Maduro and Pilgrim, 1995). The desired transgene to be inserted carries a functional *unc-119* allele that can complement the defective *unc-119* allele of EG6699. In case the transgene is stably integrated into the *C. elegans* genome the typical phenotypical defects are rescued and the worms can normally breed, crawl and form dauer larvae after starvation.

The first goal was to generate a *C. elegans* strain that stably expressed transgenic, RNAi resistant CeECT-2<sup>WT</sup> that can rescue embryonic lethality, reduction of brood size and cytokinetic failure caused by depletion of endogenous CeECT-2 (Fig. 6A). RNAi resistance was achieved by exchange of the endogenous 3'UTR of CeECT-2 locus with the 3'UTR from the *tbb-2* gene (Beta-Tubulin). It was previously shown that *tbb-2* 3'UTR and the *mex-5* 5'UTR drive constant and stable gene expression in the germline and early embryo (Merritt et al., 2008; Zeiser et al., 2011). Therefore, I replaced the endogenous UTRs with the *tbb-2* 3' UTR and the *mex-5* 5'UTR and used the endogenous open reading frame (ORF) containing all exons and introns for constructing the rest of the CeECT-2<sup>WT</sup> transgene.

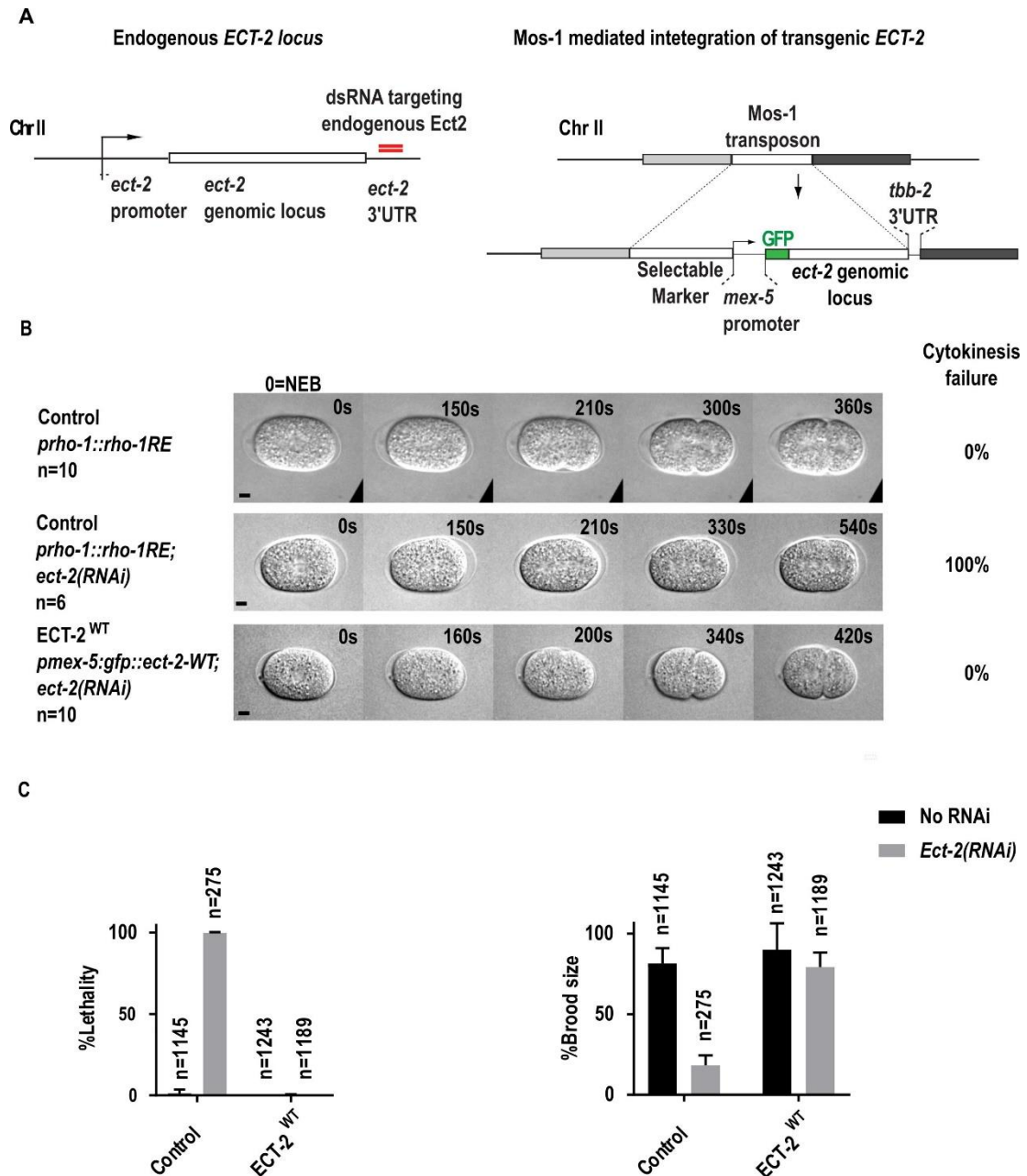


**Fig. 6. RNAi resistant, transgenic GFP-CeECT-2<sup>WT</sup> rescues cytokinetic failure, lethality and brood size.** (A) MosSCI method to obtain homozygous worm strains. Transgenic GFP-CeECT-2<sup>WT</sup> comprises a *tbb-2* 3'UTR that generates RNAi resistance to dsRNA targeting the endogenous 3'UTR of endogenous CeECT-2. (B) Transmission images of time-lapse movies showing the 1st cell division of control and transgenic CeECT-2<sup>WT</sup> *C. elegans* strains. Depletion of endogenous CeECT-2 leads to 100% cytokinetic failure in the control strain expressing only endogenous CeECT-2. The strain expressing transgenic CeECT-2<sup>WT</sup> can rescue cytokinetic failure. n= number of filmed embryos. (C) Depletion of endogenous CeECT-2 leads to 99% embryonic lethality and a strong reduction in brood size in the control strain. The strain expressing transgenic CeECT-2<sup>WT</sup> rescues embryonic lethality and brood size. n= number of total offspring analyzed (embryos+hatched larvae). Error bars represent standard deviation of the mean (SDM). Micrographs acquired with a spinning disk confocal microscope (UltraView VoX). Scale bars = 10µm.

CeECT-2 depletion by RNAi results in 100% cytokinesis failure, 99% embryonic lethality and a strong reduction of brood size as previously shown (Morita et al., 2005). Expression of RNAi resistant CeECT-2<sup>WT</sup> completely rescues cytokinesis failure, embryonic lethality and the reduction of brood size caused by depleting endogenous CeECT-2 (Fig. 6B and C). This suggests that the CeECT-2<sup>WT</sup> transgene is completely functional.

### 3.1.2. Absence of CeECT-2 BRCT domains cause high sterility in *C. elegans*

It has been previously shown by *in-vitro* studies that the N-terminus of HsEct2 binds the GEF domain and thereby inhibits the GEF activity of HsEct2 (Kim et al. 2005, Saito et al., 2004). To test whether the BRCT domains inhibit GEF activity *in-vivo* I deleted all three BRCT domains (CeECT-2<sup>ΔBRCT0+1+2</sup>, Fig. 7). I generated several strains that integrated the CeECT-2<sup>ΔBRCT0+1+2</sup> into the genome (verified by PCR analysis, not shown) but that did not express CeECT-2<sup>ΔBRCT0+1+2</sup> presumably due to gene silencing (approach 1, Fig. 7A). Expression of CeECT-2<sup>ΔBRCT0+1+2</sup> might be lethal since constitutive active CeECT-2 might cause cortical hypercontractility and cytokinesis failure. To overcome this problem, I followed 2 more approaches (approach 2 and 3, Fig. 7A) to generate a strain expressing CeECT-2<sup>ΔBRCT0+1+2</sup> described in the following.

With the second approach I depleted the gene product of GFP-CeECT-2<sup>ΔBRCT0+1+2</sup> during strain generation. Depletion of the GFP-CeECT-2<sup>ΔBRCT0+1+2</sup> protein was achieved by feeding bacteria producing dsRNA targeting GFP in the transgenic mRNA of GFP-CeECT-2<sup>ΔBRCT0+1+2</sup>. Injected worms were maintained on feeding plates with bacteria producing dsRNA against GFP. After approximately 1.5-2 weeks when the worms started to starve, normally crawling offspring were screened for integration of the transgene and further kept on *gfp(RNAi)* plates. L4/ young adult worms were transferred onto normal feeder plates and after 20-24h offspring were analyzed for contractility of the cell cortex and were used for localization studies of GFP-CeECT-2<sup>ΔBRCT0+1+2</sup> by confocal spinning disk microscopy. First, I studied whether expression of CeECT-2<sup>ΔBRCT0+1+2</sup> leads to increased contractility in embryos (Fig. 7C). Inactivation of the major RHO-1 inhibitor RGA-3/4 leads to hyperactivation of RHO-1 which results in hypercontractility of the cell cortex (Schmutz et al., 2007; Schonegg et al., 2007). If the BRCT domains inhibit GEF activity of CeECT-2 *in-vivo*, deletion of the BRCT domains should lead to a hyperactivation of CeECT-2 and subsequently RHO-1 and therefore to an increased contractility similar to embryos where RGA-3/4 is depleted (Fig. 7C). Expression of CeECT-2<sup>ΔBRCT0+1+2</sup> does not cause

hypercontractility or cytokinesis failure in the presence of endogenous CeECT-2 (Fig. 7A). This data is based on the observation of one 1-cell stage embryo where I was able to film the first cell division, and which successfully completed the first division (Fig. 7C). Moreover, I was able to film two more embryos in later embryonic stages that obviously had successfully completed the first cell division (not shown), however whether these embryos did or did not show any contractility in the first cell division could not be analyzed. Then I analyzed the localization of CeECT-2<sup>ΔBRCT0+1+2</sup> by confocal microscopy and I found that CeECT-2<sup>ΔBRCT0+1+2</sup> localizes to the plasma membrane in one one-cell embryo (n=1, Fig. 7D), in two two-cell embryos (n=2, data not shown) and in two multicellular embryos (n=2, not shown). However due to high sterility of the worms when expressing CeECT-2<sup>ΔBRCT0+1+2</sup> the embryonic phenotype of this mutant could not be monitored in detail.

Therefore, I followed a third approach with the goal to induce expression of CeECT-2<sup>ΔBRCT0+1+2</sup> with the heat shock promoter *hsp-16.2* (Fig. 7A). A former paper showed that single-copy transgenes expression can be induced in the germline after heat shock at 33°C for 1h (Zeiser et al., 2011). I exchanged the *mex-5* promoter of the transgenes CeECT-2<sup>WT</sup> and CeECT-2<sup>ΔBRCT0+1+2</sup> for the heat shock promoter *hsp-16.2* and stably integrated the transgenes into the genome using the MosSCI technique. I subjected adult hermaphrodites to 15-90 min of heat shock at 33°C to define the right time frame for inducing gene expression. Worms were directly analyzed for expression by fluorescence microscopy at 20°C since high sterility of the worms was observed 2h after heat-shock. Both CeECT-2<sup>WT</sup> and CeECT-2<sup>ΔBRCT0+1+2</sup> were successfully expressed in somatic cells and late stage embryos (Fig. 7E). However, expression in the gonad and in early embryos was not observed. One possibility could be that induced expression of CeECT-2<sup>ΔBRCT0+1+2</sup> in early embryos and the gonad was below the detection level. Also, in the paper of Zeiser et al., 2011 they reported that germ line expression was very weak in comparison to somatic expression. Monitoring the expressing of CeECT-2<sup>ΔBRCT0+1+2</sup> in late embryos confirmed the results I obtained using the *gfp(RNAi)* feeding approach. Heat-shock induced CeECT-2<sup>ΔBRCT0+1+2</sup> localized to the plasma membrane in late-stage embryos as observed before (Chan and Nance, 2013, Fig. 7E).

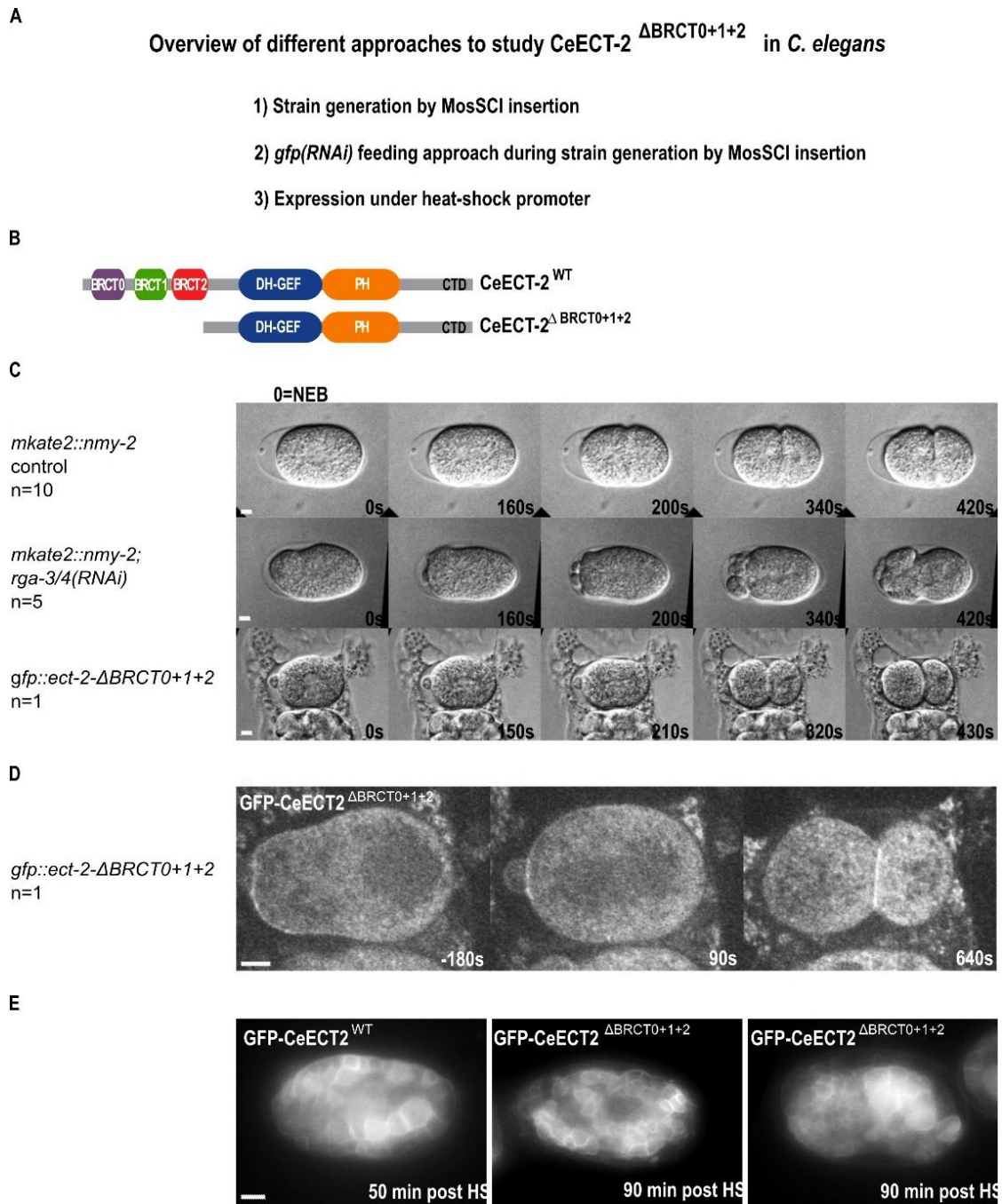


**Fig. 7. Different experimental strategies to express GFP-CeECT-2<sup>ΔBRCT0+1+2</sup> in the one-cell *C. elegans* embryo.** (A) Overview of 3 different, independent approaches to study CeECT-2<sup>ΔBRCT0+1+2</sup> in *C. elegans*. (B) Protein organization of CeECT-2<sup>WT</sup> and CeECT-2<sup>ΔBRCT0+1+2</sup>. (C) Transmission light micrographs of dividing 1-cell stage embryos of the control strain with and without depletion of the RHO-1 GAP RGA-3/4 and the strain expressing CeECT-2<sup>ΔBRCT0+1+2</sup> (approach 2). Depletion of the RGA-3/4 induces hypercontractility of the cortex since RHO-1 is not inactivated. One 1-cell embryo expressing CeECT-2<sup>ΔBRCT0+1+2</sup> could be filmed during cytokinesis. Hypercontractility of the cell cortex was not observed and the embryo divided normally, however the embryo showed an enlarged polar body at the anterior. (D) Confocal spinning disk micrographs of an embryo expressing GFP-CeECT-2<sup>ΔBRCT0+1+2</sup> (approach 2). CeECT-2<sup>ΔBRCT0+1+2</sup> localizes to the plasma membrane in presence of endogenous CeECT-2. Micrographs acquired with

a spinning disk confocal microscope (UltraView VoX). **(E)** Wide-field fluorescence images of multi-stage embryos expressing CeECT-2<sup>WT</sup> and CeECT-2<sup>ΔBRCT0+1+2</sup> under a heat-shock promoter (approach 3). CeECT-2<sup>WT</sup> and CeECT-2<sup>ΔBRCT0+1+2</sup> both localize to the plasma membrane in multi-stage embryos. Micrographs acquired with an AxioScope A1 Imager (Zeiss). n= number of imaged embryos. Scale bars= 10μm.

Following three independent approaches (Fig. 7) to study whether CeECT-2<sup>WT</sup> is regulated by an inhibitory mechanism I could only monitor expression and localization of CeECT-2<sup>ΔBRCT0+1+2</sup> in a low number of early embryos in presence of endogenous CeECT-2. However, a pre-requisite for solid conclusions is a sufficient number of analyzed embryos. The difficulty to express and analyze CeECT-2<sup>ΔBRCT0+1+2</sup> hints that CeECT-2 BRCT domains are important for embryogenesis and germ line function. Since the system did not allow studies in higher offspring numbers, I continued my work in the human HeLa FRT system to study whether Ect2 is regulated by an autoinhibitory mechanism *in-vivo* (see part 3.2.).

### **3.1.3. CeECT-2 BRCT0 and BRCT1 domains are required for embryonic viability and cytokinesis**

For a long time, it was thought that the BRCT1 and BRCT2 domains are a classical tandem BRCT domain, however it was shown that they have a very different structural configuration. Moreover, BRCT0 domain was only discovered by a study that analyzed the crystal structure of HsEct2 BRCT domains (Zou et al., 2014). Although it was shown that the deletion of all three BRCT domains increases CeECT-2 GEF activity *in-vitro* and prevents cleavage furrow ingression *in-vivo* when expressed transiently, the function of the individual BRCT domains has not been addressed (Kim et al., 2005; Su et al., 2011). To test the individual function of each BRCT domain in regulating CeECT-2 activity and localization *in-vivo* I generated transgenic strains where I deleted BRCT0 and BRCT0+1. In contrast to the CeECT-2<sup>ΔBRCT0+1+2</sup>, I was able to generate transgenic strains that express CeECT-2<sup>ΔBRCT0</sup> and CeECT-2<sup>ΔBRCT0+1</sup> and that produce normal number of offspring (Fig. 8). After receiving the strains expressing CeECT-2<sup>ΔBRCT0</sup> and CeECT-2<sup>ΔBRCT0+1</sup> I analyzed the localization by confocal microscopy, cytokinetic failure by transmission microscopy and lethality by measuring embryonic lethality and brood size in these mutants. Transgenic CeECT-2<sup>WT</sup> localizes to the plasma membrane during cell division (Fig. 8B). CeECT-2<sup>ΔBRCT0</sup> and CeECT-2<sup>ΔBRCT0+1</sup> localize to the plasma membrane similar as transgenic

CeECT-2<sup>WT</sup> (Fig. 8B). However, CeECT-2<sup>ΔBRCT0</sup> signal was very low in the imaged embryos.

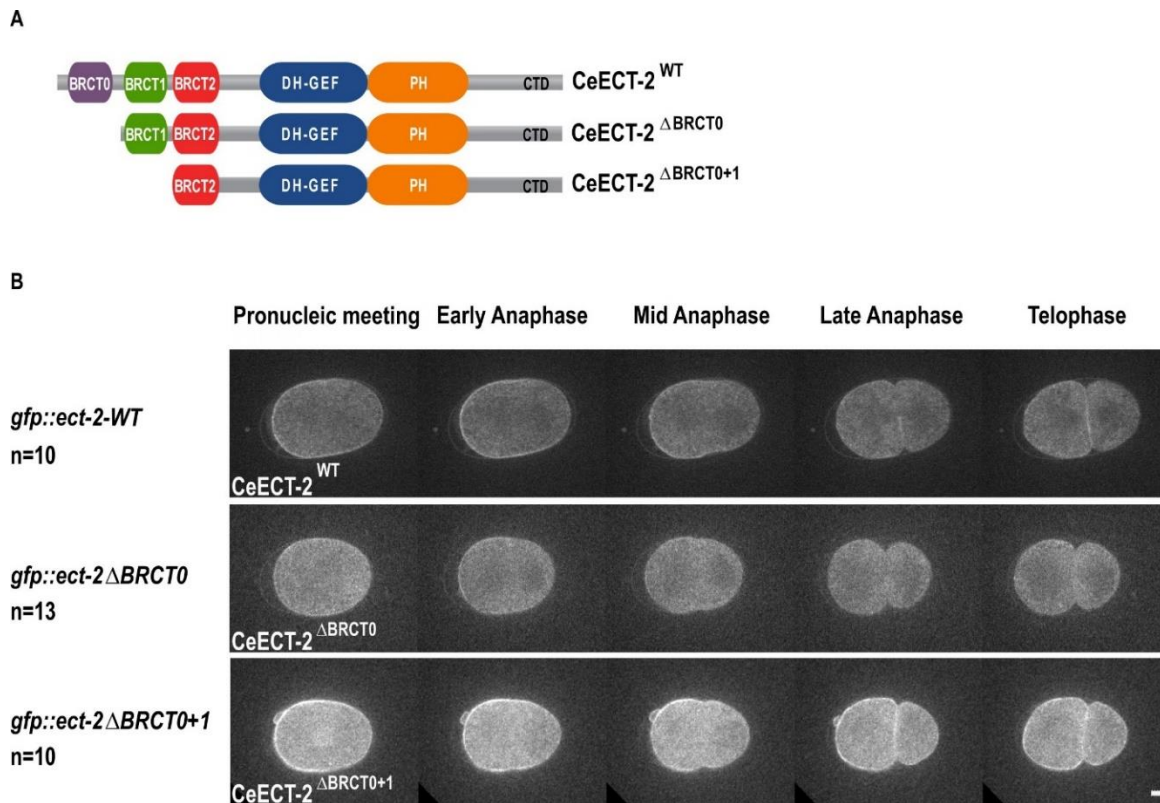


**Fig. 8. CeECT-2 BRCT0 and BRCT1 are not required for membrane localization.** (A) Schematic representation of the protein domain organization of CeECT-2<sup>WT</sup> and the deletion constructs CeECT-2<sup>ΔBRCT0</sup> and CeECT-2<sup>ΔBRCT0+1</sup>. (B) Confocal micrographs showing a time lapse series of 1-cell stage embryos expressing CeECT-2<sup>WT</sup>, CeECT-2<sup>ΔBRCT0</sup> and CeECT-2<sup>ΔBRCT0+1</sup> transgenes and localization of GFP-CeECT-2 transgenes in the presence of endogenous CeECT-2. n= number of imaged 1-cell stage embryos. CeECT-2<sup>ΔBRCT0</sup> and CeECT-2<sup>ΔBRCT0+1</sup> both localize to the cell cortex, however the localization of CeECT-2<sup>ΔBRCT0</sup> is quite low compared to CeECT-2<sup>ΔBRCT0+1</sup>. Images acquired with Ultra View VoX microscope. Scale bar= 10 μm.

Next, I tested whether the BRCT0 and BRCT1 are required for cytokinesis during embryonic development. The expression of CeECT-2<sup>ΔBRCT0</sup> leads to 16% (n=13) cytokinesis failure in absence of endogenous CeECT-2 when cytokinesis is monitored after 16-20h after the dsRNA was injected. The time frame of 16-20h of RNAi was chosen since the depletion levels were sufficient to induce an *ect-2* phenotype in all control embryos (no furrow formation) and a decent number of offspring was still available to analyze since CeECT-2 depletion leads to high sterility in the worms. Deletion of BRCT0+1 leads to 0% (n=10) cytokinesis failure after 16-20h RNAi (Fig. 9A). However, when monitoring first

cytokinesis after longer RNAi (30-38h), 63% (n=11) cytokinesis failure in the 1-cell embryo was observed (Fig. 9B and Fig. 11B+C). These results suggest that BRCT0 and BRCT1 domain are required for cytokinesis. Moreover, I quantified the type of cytokinetic failure in embryos expressing CeECT-2<sup>ΔBRCT0</sup> and CeECT-2<sup>ΔBRCT0+1</sup> in the absence of endogenous CeECT-2. Whereas *ect-2(RNAi)* in control embryos abolished cleavage furrow formation, embryos expressing CeECT-2<sup>ΔBRCT0+1</sup> formed a cleavage furrow which later regressed (Fig. 9B; regressing furrows in CeECT-2<sup>ΔBRCT0+1</sup>, n=5/11). Embryos expressing CeECT-2<sup>ΔBRCT0</sup> showed 16% of regressing furrows after 16-20h of RNAi (Fig. 9A, regressing furrows in CeECT-2<sup>ΔBRCT0</sup>, n= 2/13). This indicates that CeECT-2<sup>ΔBRCT0</sup> and CeECT-2<sup>ΔBRCT0+1</sup> are still partially active and that BRCT0 and BRCT1 domains are rather required for later stages of cytokinesis, e.g. for the stability of the cleavage furrow or abscission.

Next, I tested whether the BRCT0 and BRCT1 are required during embryonic development. Depletion of endogenous CeECT-2 leads to over 99% embryonic lethality in the control strain that only expressed endogenous CeECT-2 (n=275) (Fig. 9C). The expression of transgenic CeECT-2<sup>WT</sup> rescues embryonic lethality (0%, n= 1189). Deletion of BRCT0 leads to 91% of embryonic lethality in absence of endogenous CeECT-2 (n=236). Expression of CeECT-2<sup>ΔBRCT0+1</sup> cannot rescue the phenotype caused by depletion of endogenous CeECT-2 and absence of BRCT0 and BRCT1 domains leads to 85% embryonic lethality in absence of endogenous CeECT-2 (n=138). Moreover, absence of BRCT0 and BRCT1 domains lead to a drastic decrease of total brood size after depletion of endogenous CeECT-2 (Fig. 9C). These findings show that BRCT0 domain is required for embryonic viability and germ line function.

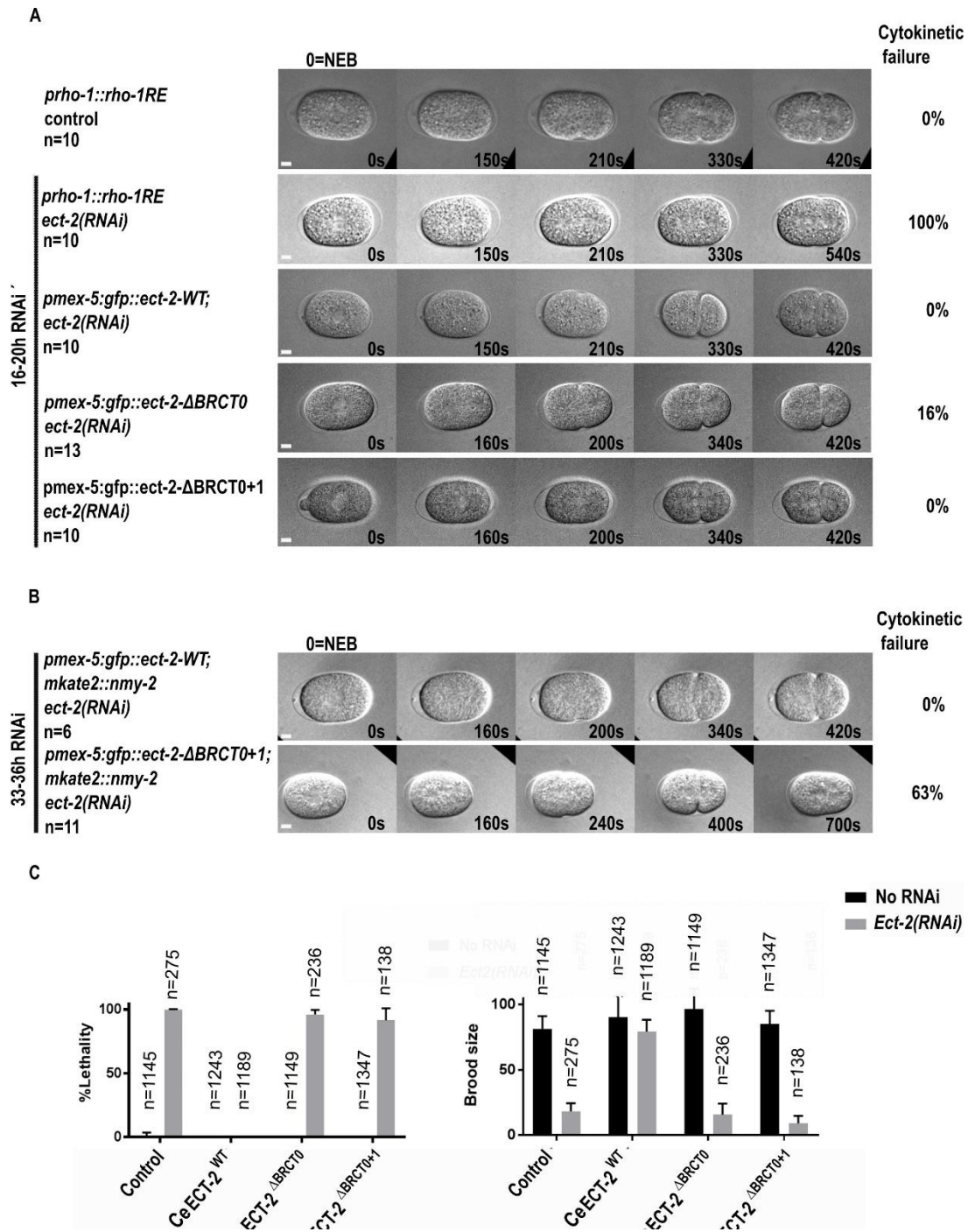


**Fig. 9. CeECT-2 BRCT0 and BRCT1 domains are required for embryonic viability and cytokinesis.** Time-lapse series of 1-cell stage embryos of the control strain and strains expressing different CeECT-2 transgenes. **(A)** Depletion of endogenous CeECT-2 leads to 100% cytokinetic failure in the control, 0% in the strain expressing CeECT-2<sup>WT</sup> and 16% cytokinetic failure in the strain expressing CeECT-2<sup>ΔBRCT0</sup> after 16-20h of RNAi. **(B)** In the strain expressing CeECT-2<sup>ΔBRCT0+1</sup> 63% of cytokinetic failure is observed after 33-36h of RNAi. n= number of imaged embryos. Images acquired with UltraView VOX microscope. Scale bars =10 μm. **(C)** Depletion of endogenous CeECT-2 leads to 99% embryonic lethality and a strong reduction in brood size in the control and the strains expressing CeECT-2<sup>ΔBRCT0</sup> and CeECT-2<sup>ΔBRCT0+1</sup>. n= number of total offspring (embryos+ hatched larvae). Error bars represent SDM.

One aim of my thesis was to study whether BRCT0 and BRCT1 inhibit the GEF domain. In presence and absence of endogenous CeECT-2, I did not observe increased contractility (Fig. 8B and 9A+B). Since I saw partial cytokinesis defects in embryos expressing CeECT-2<sup>ΔBRCT0</sup> and CeECT-2<sup>ΔBRCT0+1</sup> in absence of endogenous CeECT-2 I wanted to analyze whether CeNMY-2 levels are increased in these strains. Therefore, I decided to use a more sensitive read-out to monitor whether deletion of BRCT0 and BRCT0+1 result in changes of CeECT-2 activity. I crossed mKate2-CeNMY-2 into the transgenic CeECT-2 strains and imaged the different mutants by confocal spinning disk microscopy (Fig. 10 and 11). I quantified the signal of mkate2-CeNMY-2 at the furrow tip when the furrow was half ingressed in the different strains in presence and absence of endogenous CeECT-2 (Fig. 10B). In presence of endogenous CeECT-2 CeNMY-2 is significantly decreased in the strain expressing CeECT-2<sup>ΔBRCT0</sup>. Even though CeNMY-2 levels in the strain expressing CeECT-2<sup>ΔBRCT0+1</sup> are not significantly decreased, the levels are lower than in WT.

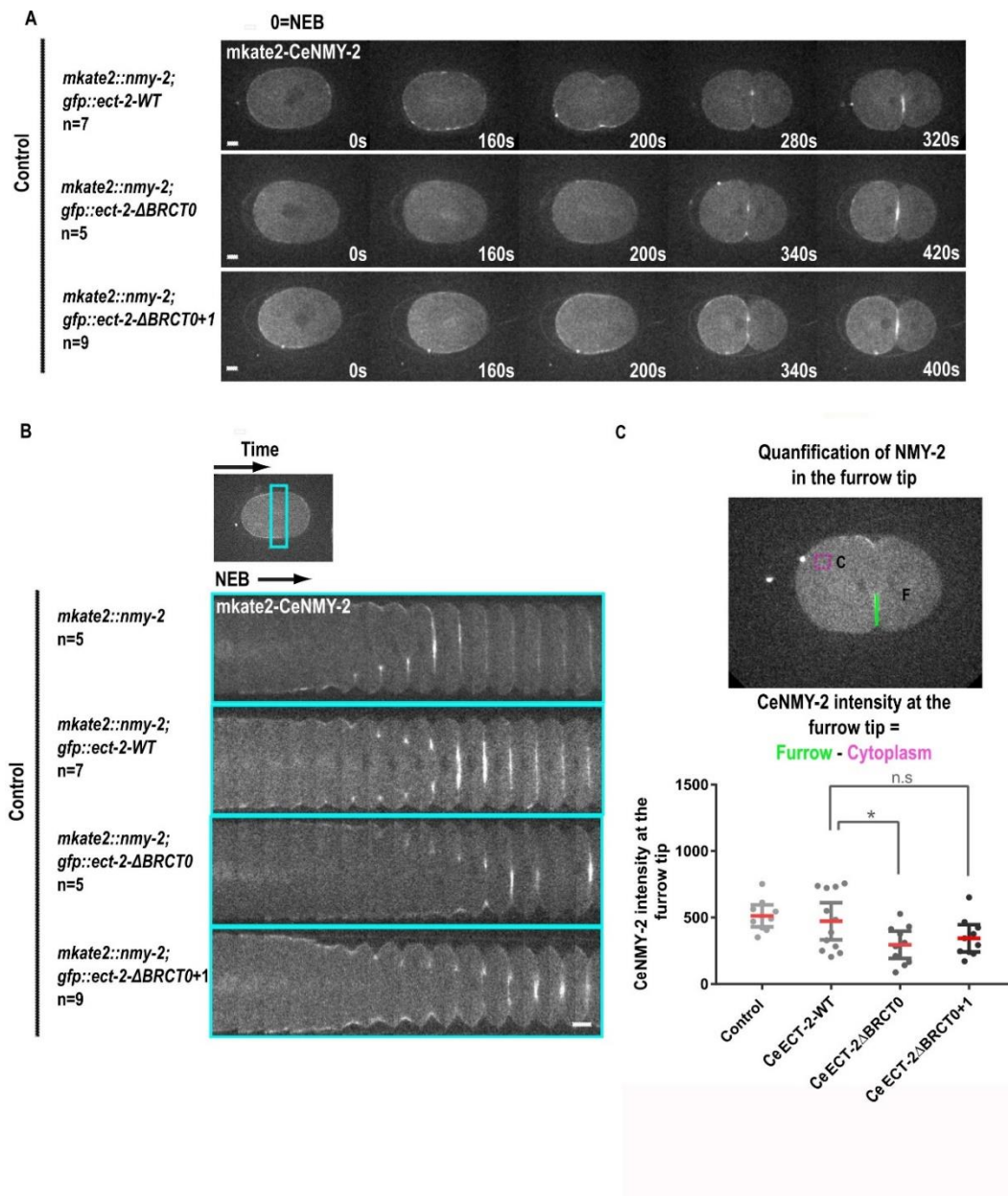


**Fig. 10. CeNMY-2 levels in CeECT-2<sup>ΔBRCT0</sup> transgenic strains are decreased at the furrow tip.** Confocal micrographs of 1-cell stage embryos expressing CeNMY-2 and CeECT-2 transgenes. (A) Time-lapse series of confocal live-cell imaging in control embryos expressing mkate-2-CeNMY-2 and GFP-CeECT-2 transgenes in presence of endogenous CeECT-2. (B) Kymographs of control embryos expressing mkate-2-CeNMY-2 and GFP-CeECT-2 transgenes. Images acquired with a spinning disk confocal microscope (UltraView VoX). n= number of imaged embryos. Scale bars= 10μm. (C) Quantification of CeNMY-2 levels in CeECT-2 transgenic strains in presence of endogenous CeECT-2. At time when the furrow was ingressed by half, a 6px wide line was drawn along starting from the furrow tip to the outside of the embryo and background was measured by a drawing a square box in the cytoplasm. The first ten values measured were averaged and background noise was subtracted from the furrow signal. Images acquired with a spinning disk confocal microscope (UltraView VoX). n= number of imaged embryos. Scale bars= 10μm. Statistical significance tested by ANOVA, p< 0,05. Error bars represent standard error of the mean (SEM).

Next, I depleted endogenous CeECT-2 in embryos expressing CeECT-2<sup>WT</sup>, CeECT-2<sup>ΔBRCT0</sup> and CeECT-2<sup>ΔBRCT0+1</sup> (Fig. 11) and measured CeNMY-2 levels at the furrow tip after 16-20h and 33-38h (Fig. 11C). In absence of endogenous CeECT-2, CeNMY-2 is significantly decreased after 16-20h RNAi. CeNMY-2 levels are also lower after 16-20h and 33-38h in CeECT-2<sup>ΔBRCT0+1</sup> than in CeECT-2<sup>WT</sup> embryos, however the decrease is not statistically significant. This might be due to a lower sample number as compared to the quantification after 16-20h. Another reason could be the high variability of the signal in the embryos expressing CeECT-2<sup>WT</sup> and this variability might be due to technical fluctuations at the microscope since embryos were imaged in a time frame of about 6 months to achieve n=11 after 33-38h for each strain (high sterility of worms after depletion of endogenous CeECT-2 for more than 30h).

In conclusion, these results suggest that deletion of BRCT0 and BRCT0+1 domain rather reduces than enhances the activity of CeECT-2. This finding would be consistent with a model in which BRCT0 and BRCT1 are required for full CeECT-2 activation.

Next, I generated a construct where I deleted only the BRCT2 domain. Like the transgenes where the three BRCT domains were deleted at once, also this transgene successfully integrated into the genome (verified by PCR, not shown) but was silenced. Silencing of CeECT-2<sup>ΔBRCT0+1+2</sup> and CeECT-2<sup>ΔBRCT2</sup> transgenes suggest that the BRCT2 domain has a very important role in regulating CeECT-2 activity and that presumably deletion of BRCT2 results in hyperactive CeECT-2 and therefore is cytotoxic.

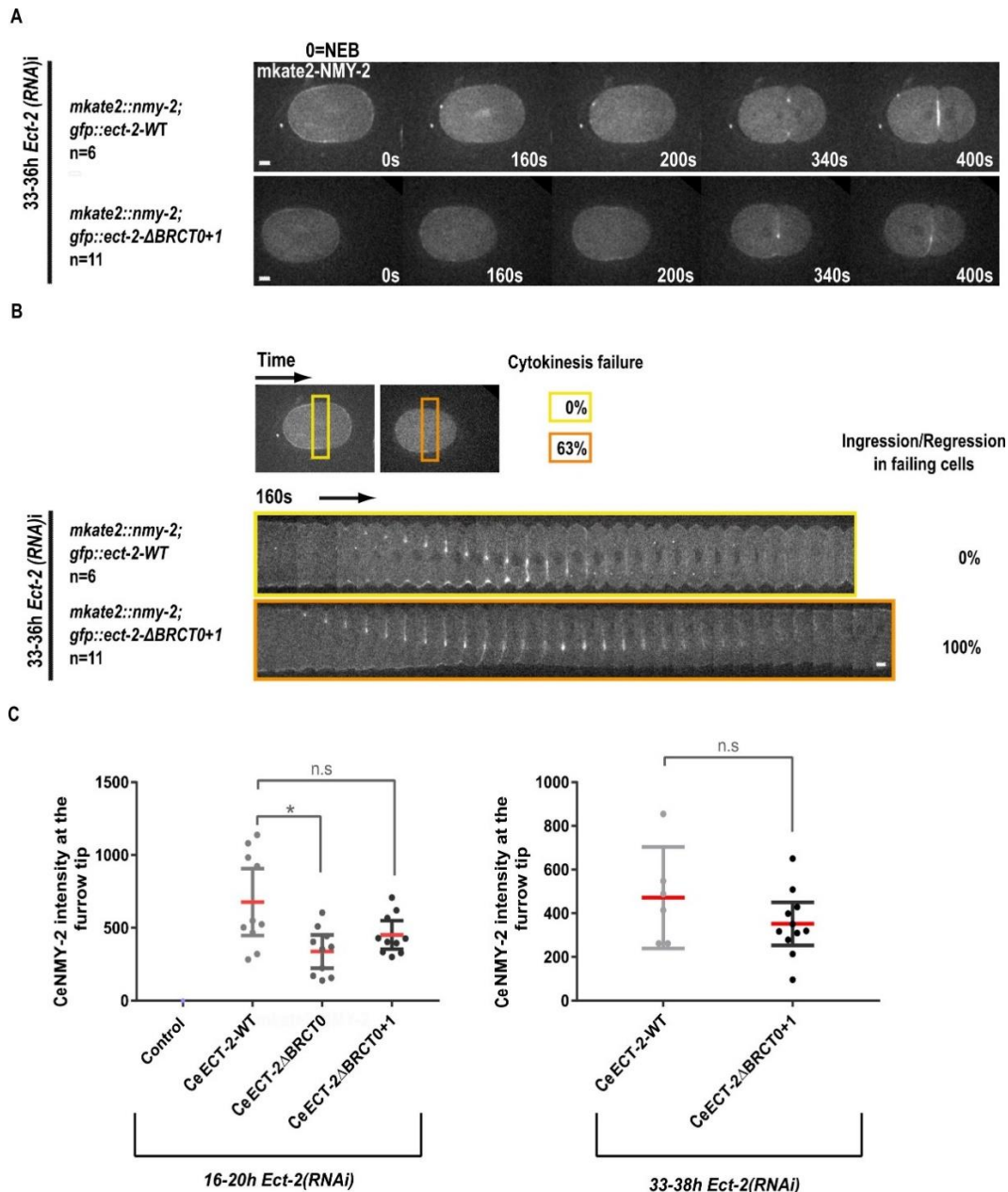


**Fig. 11. The BRCT0 domain promotes CeNMY-2 recruitment to the furrow in the absence of endogenous CeECT-2.** Confocal micrographs of 1-cell stage embryos expressing CeNMY-2 and CeECT-2 transgenes in absence of endogenous CeECT-2. **(A)** Longer depletion (33-38h) of endogenous CeECT-2 in embryos expressing CeECT-2<sup>WT</sup> and CeECT-2<sup>ΔBRCT0+1</sup>. Embryos do not show increase of CeNMY-2 levels. **(B)** Kymographs of embryos expressing CeECT-2<sup>WT</sup> and CeECT-2<sup>ΔBRCT0+1</sup>. Embryos expressing CeECT-2<sup>WT</sup> show normal division but 63% of CeECT-2<sup>ΔBRCT0+1</sup> show furrow ingression followed by regression after 33-38h of RNAi. Images acquired with a spinning disk confocal microscope (UltraView VoX). n= number of imaged embryos. Scale bars= 10μm. **(C)** Quantification of CeNMY-2 levels in CeECT-2 transgenic strains in absence of endogenous CeECT-2. Depletion of endogenous CeECT-2 in embryos expressing CeECT-2<sup>ΔBRCT0</sup> leads to a decrease of CeNMY-2 levels in 16-20h conditions. Control embryos did not form a furrow since endogenous CeECT-2 was depleted. Therefore, no values for CeNMY-2 in the furrow tip could be measured. Statistical significance tested by ANOVA. p< 0,05. Error bars represent SEM.

### **3.1.4. Summary of results obtained in *C. elegans***

In conclusion, my results show that BRCT domains are not required for membrane localization since CeECT-2<sup>ΔBRCT0</sup> and CeECT-2<sup>ΔBRCT0+1</sup> show plasma membrane localization like CeECT-2<sup>WT</sup> in presence and absence of endogenous CeECT-2. Moreover, I could reveal with my study that BRCT0+1 are not inhibiting ECT2 GEF activity since the mutants expressing CeECT-2<sup>ΔBRCT0</sup> and CeECT-2<sup>ΔBRCT0+1</sup> do not show increased levels of CeNMY-2 which suggests that BRCT0 and BRCT1 domains might promote full Ect2 activation. Further I studied whether BRCT0 and BRCT1 domains are required for cytokinesis. My results show that BRCT0 and BRCT1 domain are partially required for cytokinesis since embryos expressing CeECT-2<sup>ΔBRCT0+1</sup> in absence of endogenous CeECT-2 fail cytokinesis. Importantly I could reveal that BRCT0+1+2 are important for embryonic development and germline function since expression of CeECT-2<sup>ΔBRCT0+1+2</sup> causes high sterility of the worms in presence of endogenous CeECT-2. Moreover, deletion of BRCT0 and BRCT1 domain results in high embryonic lethality and dramatic brood size reduction in absence of CeECT-2. Lastly my data suggests that BRCT2 might inhibit Ect2 GEF activity since strains expressing constructs without the BRCT2 domain could not be obtained.

## **3.2 HsEct2 BRCT1 and BRCT2 domains are required for cytokinesis and inhibit GEF function *in-vivo***

### **3.2.1. Establishment of a molecular replacement system for the RhoA GEF HsEct2 in human cells**

For successful cytokinesis, contractile ring formation is essential, and the formation of the contractile ring is dependent on the activation of the small GTPase RhoA by the GEF HsEct2. Other than in *C. elegans*, HsEct2 localizes to the spindle midzone in addition to the plasma membrane during cell division (Tatsumoto et al. 1999). To study whether the different localization of HsEct2 and CeECT-2 are related to different mechanisms of regulation, a similar genetic replacement system of endogenous and transgenic HsEct2 as in *C. elegans* was established in HeLa cells with the help of the students Seren Baygun and Pedro Barbosa Silva. In contrast to the *C. elegans* system, in the human HeLa system HsEct2 transgenes only contained exons and no introns.

In order to study HsEct2 regulation *in-vivo*, my first goal was to establish a molecular replacement system for HsEct2 using the HeLa Flp-In T-Rex system (for simplification, FRT HeLa system). In this molecular replacement system endogenous and transgenic HsEct2 can be exchanged by depleting endogenous HsEct2 by RNAi whereas the transgenic version is RNAi resistant and its expression can be induced by the addition of tetracycline to the culture media (Fig. 12).

In this system different single-copy HsEct2 transgenes were integrated into a specific locus in the *T-REx<sup>TM</sup> HeLa* cell line that harbors FRT sites at a specific locus (Berens, 1994; Yao and Eriksson, 2002). The gene of interest is inserted by homologues recombination mediated by the co-expression of a recombinase that mediates the integration. Transcription of the integrated gene is blocked by a repressor that binds to a TetO2 site adjacent to the transgene. Tetracycline binds the repressor which in turn can no longer bind the TetO2 site and expression of the transgene is activated (Fig. 12).

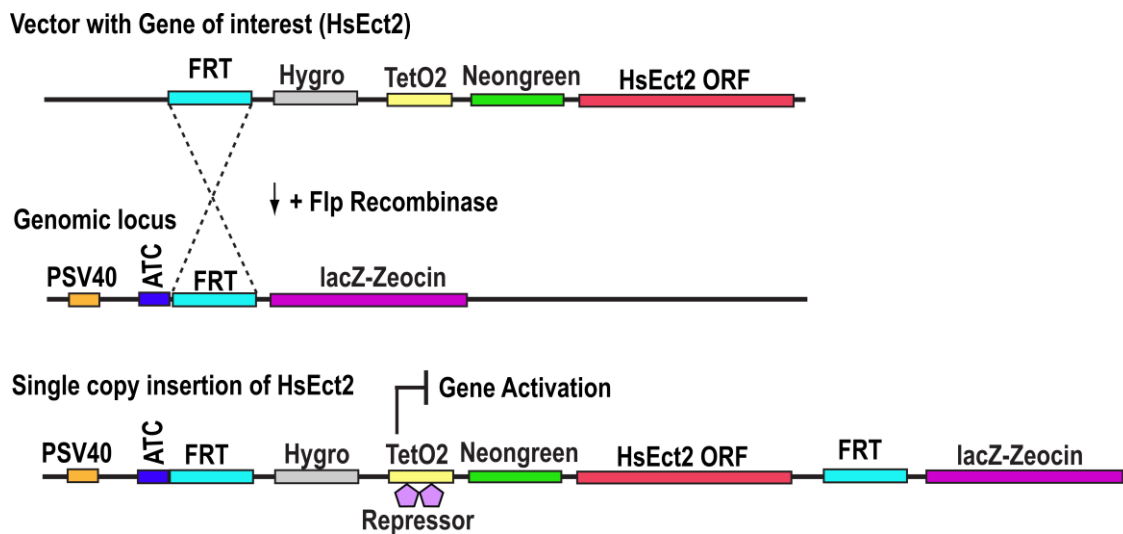


**Fig. 12. Flp-In T-REx<sup>TM</sup> HeLa system to generate transgenic HsEct2 cell lines with single-copy insertions of the transgenes.** The gene of interest (here HsEct2<sup>WT</sup>) is cloned into a vector containing an FRT site. To generate stably expressing cells the vector containing the HsEct2 gene is transfected together with a Flp recombinase that mediates the integration of the transgene into a specific locus. After insertion, gene expression of HsEct2<sup>WT</sup> is inhibited by the binding of a repressor to the TetO2 site near the integrated HsEct2 gene. To induce gene expression tetracycline is added to the culture medium that binds the repressor and thereby activates gene expression.

First, HsEct2 ORF was cloned by the student Pedro Barbosa Silva using human cDNA (donation by Dr. Christoph Ziegenhain from Prof. Enard Laboratory) and 4 point mutations were introduced in the BRCT1 domain that do not alter the amino acid sequence of HsEct2 but lead to RNAi resistance against the siRNA targeting endogenous HsEct2 (Fig. 13B). Then the student Seren Baygun used the FRT HeLa system to generate a cell line that stably expressed HsEct2<sup>WT</sup> and tested whether the transgenic version of HsEct2<sup>WT</sup> is functional. Depletion of HsEct2 leads to high bi- and multinucleation in human cells (Kim et al., 2005, Su, Takaki, and Petronczki 2011). In the control cell line depletion of endogenous HsEct2 leads to a high bi- and multinucleation (Fig. 13A+C). In the generated transgenic cell line expressing HsEct2<sup>WT</sup> bi- and multinucleation is not observed (Fig. 13B+C). This result showed that transgenic HsEct2<sup>WT</sup> is functional and the molecular replacement system of HsEct2<sup>WT</sup> can be used to study HsEct2 function *in-vivo*.

After receiving the cell line stably expressing HsEct2<sup>WT</sup> transgene I analyzed the localization and expression of HsEct2<sup>WT</sup> (Fig. 13B). As previously published HsEct2<sup>WT</sup> (n=40) localizes to the nucleus in interphase and to the cytoplasm in metaphase after NEB. In anaphase, neongreen-HsEct2<sup>WT</sup> (n=40) localizes to the spindle midzone and is enriched at the equatorial plasma membrane (Fig. 13B) (Su, Takaki, and Petronczki 2011; Tatsumoto et al. 1999, Yüce et al., 2005). Depletion of endogenous HsEct2 by RNAi in the control and HsEct2<sup>WT</sup> cell line with and without the addition of tetracycline revealed by western blot analysis that most of endogenous HsEct2, running at ~ 120kDa, is depleted after 48h of RNAi but transgenic, RNAi resistant, neongreen-HsEct2<sup>WT</sup>, running at ~ 150kDa, is still expressed and that levels of endogenous and transgenic HsEct2<sup>WT</sup> are similar (Fig. 13D). In conclusion these results show that transgenic RNAi resistant HsEct2<sup>WT</sup> is functional and expressed at similar levels as endogenous HsEct2 and thus can be used for structure-function studies.

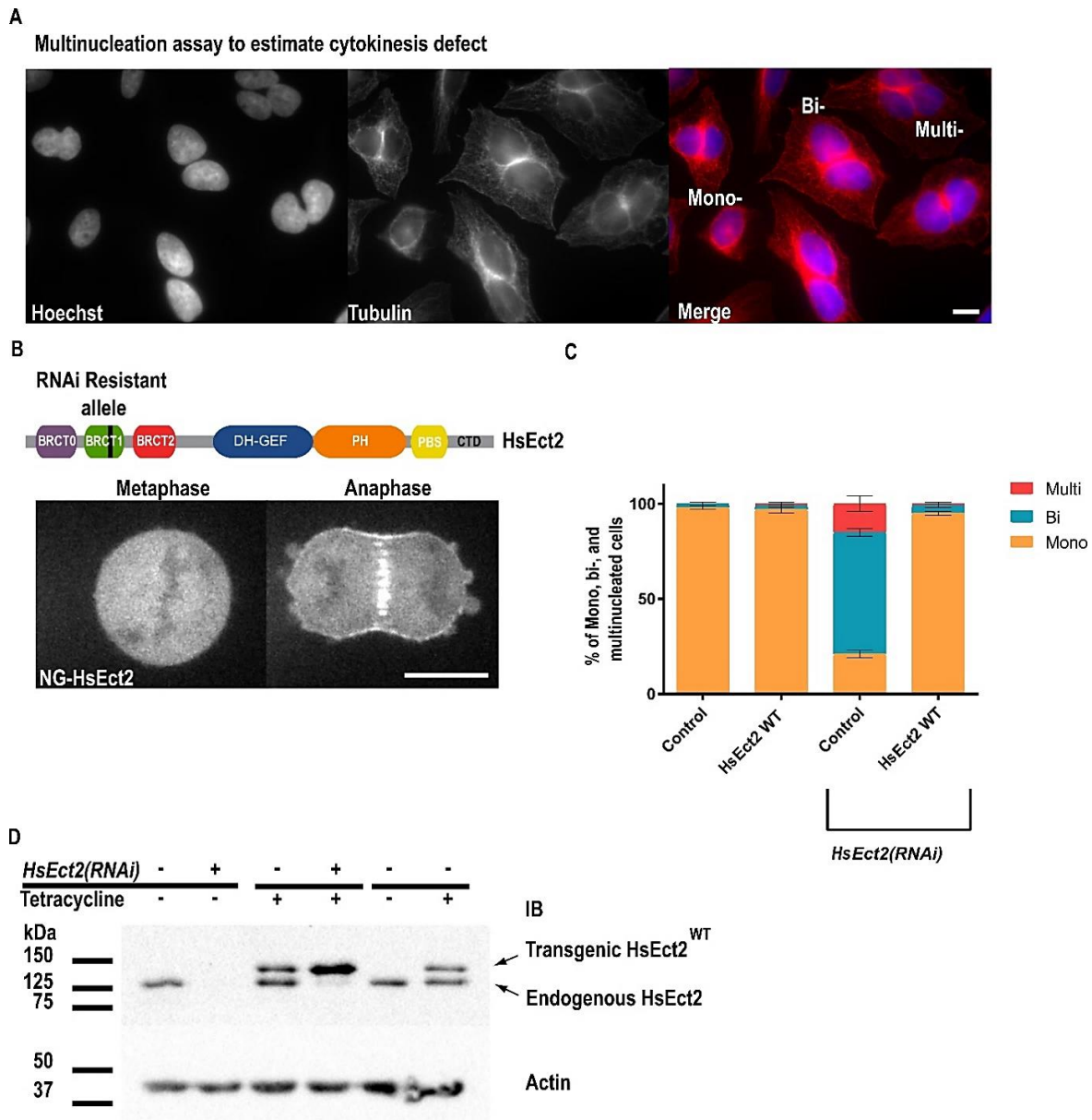


**Fig. 13. Transgenic, RNAi resistant HsEct2<sup>WT</sup> rescues cytokinesis defect after depletion of endogenous HsEct2.** (A) Principle of the multinucleation assay to estimate cytokinesis failure in the different cell lines. Fluorescence micrographs of cells after fixation and immunostaining of tubulin and staining of DNA with Hoechst solution. Mono-, bi- and multinucleated cells were counted. N= 2-3 independent experiments; n> 150 cells counted in total. Error bars are standard deviation of the mean. (B) Domain organization of HsEct2<sup>WT</sup> with 3 N-terminal BRCT domains, a DH-GEF domain and C-terminal domain comprising a PH, PBS and a CTD domain. The BRCT1 domain contains 4 point mutations that do not alter the amino-acid sequence but makes the HsEct2 transgenes RNAi resistant. During anaphase, neogreen-HsEct2<sup>WT</sup> localizes to the spindle midzone and to the equatorial plasma membrane and during metaphase to the cytoplasm. Scale bar = 10µm. (C) Percentage of mono-, bi-, and multinucleated control and HsEct2<sup>WT</sup> expressing cells with and without Ect2 RNAi. Depletion of endogenous HsEct2<sup>WT</sup> leads to a high bi- and multinucleation in the control but not in the cell line expressing transgenic, RNAi resistant neogreen-HsEct2<sup>WT</sup>. n> 150 cells counted in total. Error bars are standard deviation of the mean. (D) Western blot analysis of endogenous and transgenic neogreen-HsEct2<sup>WT</sup> with

and without depletion of endogenous HsEct2. Transgenic neogreen-HsEct2<sup>WT</sup> (~150kDa) is expressed upon tetracycline addition in presence and absence of endogenous HsEct2. Actin was plotted as a loading control.

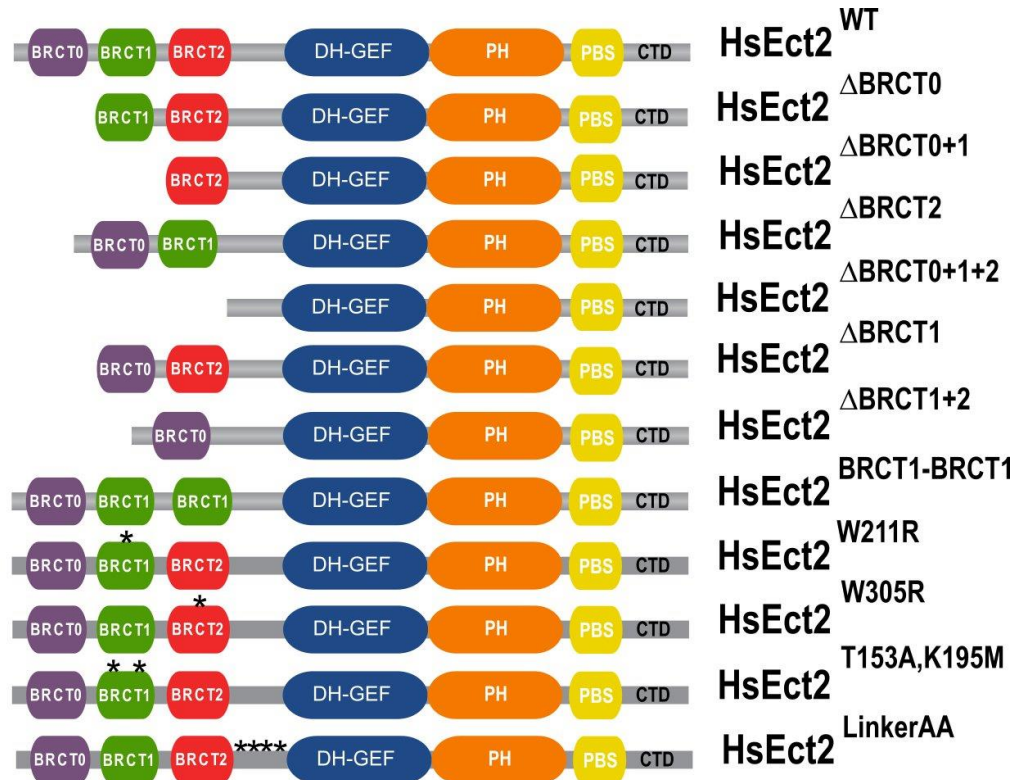


**Fig. 14. Overview of generated transgenic HsEct2 cell lines.** Transgenic cell lines harbor either N-terminal deletions, substitutions of different BRCT domains or single point mutations in the BRCT domains or linker region (indicated with black asterisks). All HsEct2 transgenes are single-copy insertions, RNAi resistant and can be induced by tetracycline.

### 3.2.2. The BRCT0 domain contributes to spindle midzone localization and is not required for cytokinesis

The BRCT0 domain of HsEct2 was first discovered when the crystal structure of HsEct2 N-terminus was resolved in 2014 (Zou et al., 2014). The BRCT0 domain is the least conserved BRCT domain of HsEct2 and the most variable one among different species in evolution which also explains why there are different views on whether HsEct2 contains a tandem or a triple BRCT domain in the N-terminus (Zou et al. 2014). To test if BRCT0 is required for HsEct2 function and localization I deleted BRCT0 domain (Fig. 15). To make sure that the expression levels of HsEct2<sup>ΔBRCT0</sup> were similar to HsEct2<sup>WT</sup>, protein

expression was analyzed by western blot analysis and quantified on confocal spinning disk images (Fig. 16). Western blot analysis showed that endogenous HsEct2<sup>WT</sup> and transgenic HsEct2<sup>ΔBRCT0</sup> are expressed at similar levels (Fig. 16A). Cytoplasmic and background pixel intensities were measured by drawing a box in the cytoplasm and outside of the cell. Background signal was then subtracted from the cytoplasmic values (Fig. 16B). Western Blot analysis and imaging analysis revealed that the cell line expressing HsEct2<sup>ΔBRCT0</sup> comprises similar percentages of low, medium and high expressing cells (Fig. 16A+C).

Then I analyzed the function of the HsEct2<sup>ΔBRCT0</sup> in presence and absence of endogenous HsEct2 by measuring cytokinesis failure with multinucleation assays. Endogenous HsEct2 was depleted by RNAi and cells were fixed and stained for tubulin and DNA, then the number of mono-, bi- and multinucleated cells was counted (Fig. 13A). Depletion of endogenous HsEct2 leads to high cytokinesis failure (79% of bi- and multinucleation) and expression of HsEct2<sup>ΔBRCT0</sup>, like HsEct2<sup>WT</sup>, fully rescues cytokinesis defects (Fig. 15C).

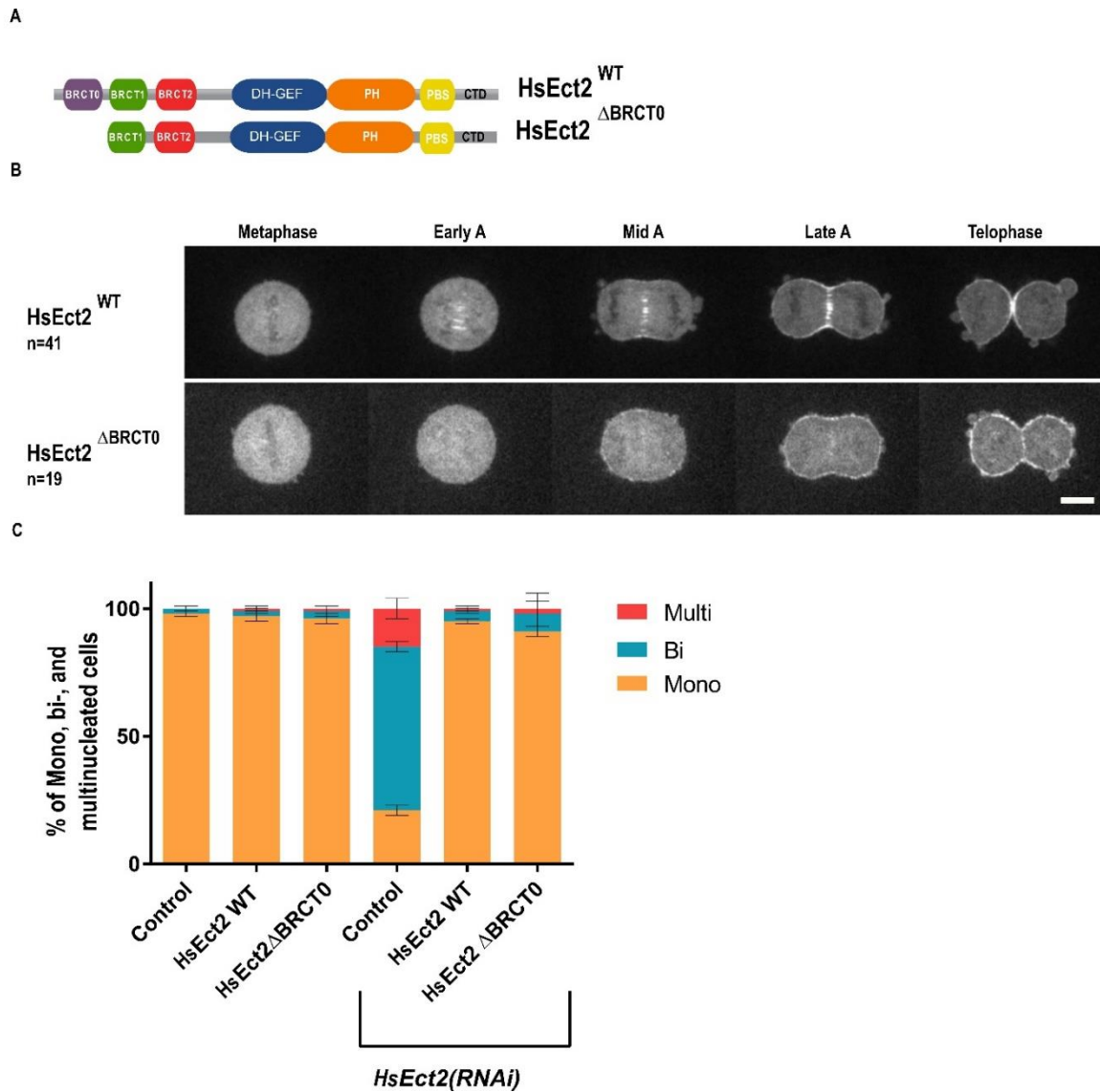


**Fig. 15. BRCT0 domain is not required for cytokinesis.** (A) Domain structure of HsEct2<sup>WT</sup> and HsEct2<sup>ΔBRCT0</sup> transgenes. (B) Micrographs of live-cell imaging of dividing cells expressing neogreen-HsEct2<sup>WT</sup> and neogreen-HsEct2<sup>ΔBRCT0</sup>. HsEct2<sup>WT</sup> localizes to the spindle midzone and to the equatorial plasma membrane. Cells expressing Ect2<sup>ΔBRCT0</sup> show plasma membrane and reduced spindle midzone localization. (C) Depletion of endogenous HsEct2 in control cell line induces bi- and multinucleation (>79%). Transgenic, RNAi-resistant HsEct2<sup>WT</sup> and HsEct2<sup>ΔBRCT0</sup> rescue cytokinesis failure in absence of endogenous HsEct2. n>150 cells of 2-3 independent experiments. Scale bar = 10 μm. Error bars represent SDM.

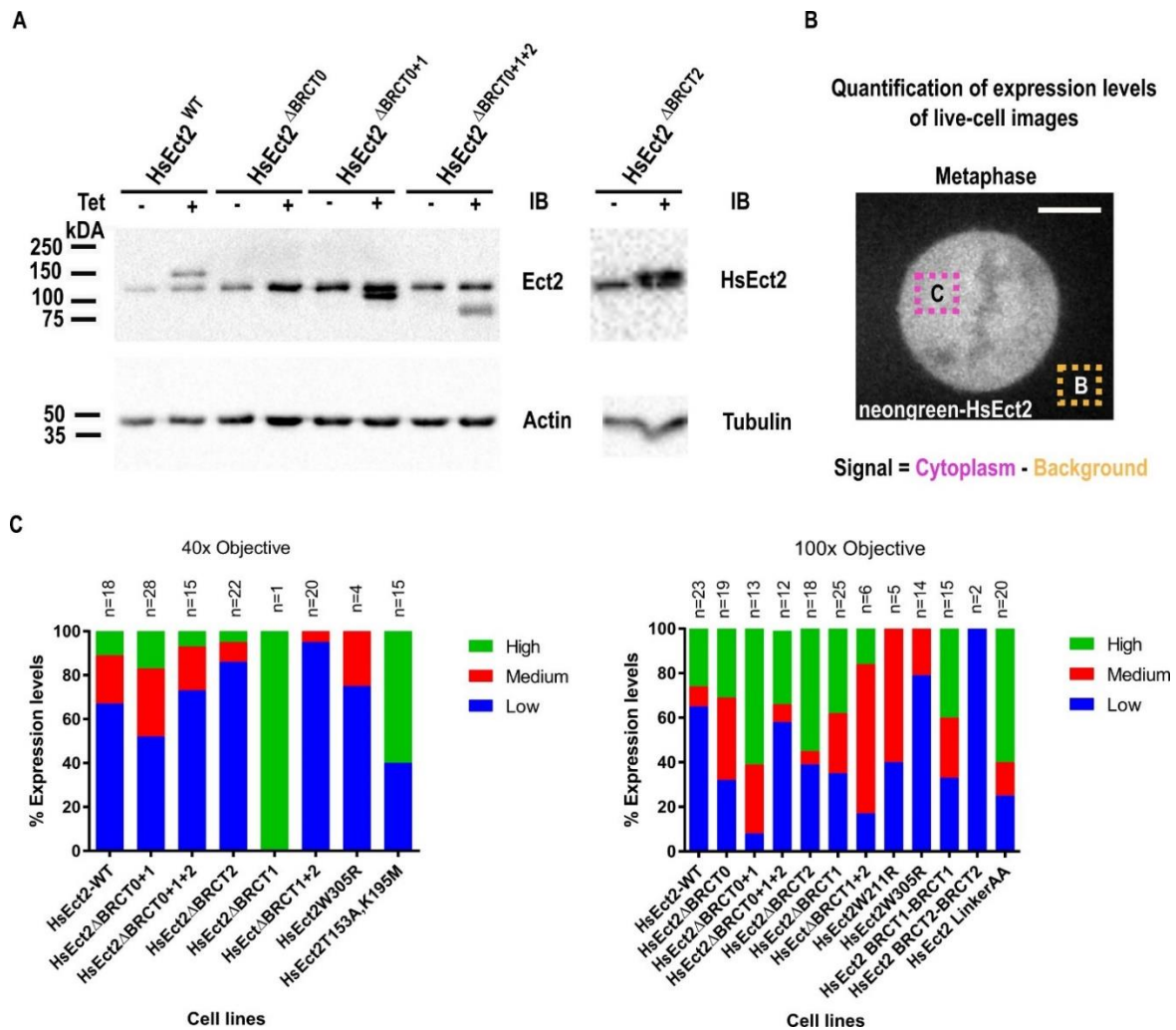


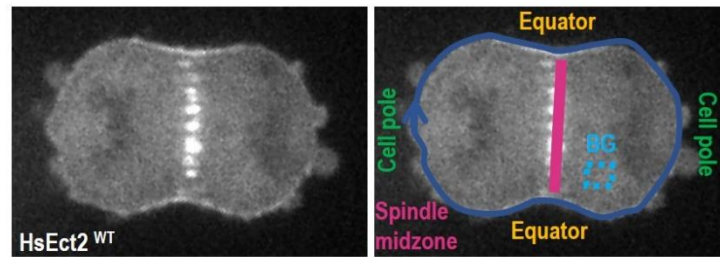
**Fig. 16. HsEct2 transgenes are expressed at similar levels.** (A) Western blot analysis of HsEct2 cell lines expressing endogenous and neongreen-HsEct2<sup>WT</sup>, HsEct2<sup>ΔBRCT0</sup>, HsEct2<sup>ΔBRCT2</sup>, HsEct2<sup>ΔBRCT0+1</sup> and HsEct2<sup>ΔBRCT0+1+2</sup>. Transgene expression was induced with tetracycline for 48h and cells were harvested for cell lysates. Proteins were separated by SDS-PAGE and detected by HsEct2, tubulin or actin antibody with western blot. Expected size of endogenous HsEct2 is 120kDa and size of neongreen-tag is 27kDa. Transgenic neongreen-HsEct2<sup>WT</sup> is expected to run at 150kDa, neongreen-HsEct2<sup>ΔBRCT0</sup> and neongreen-HsEct2<sup>ΔBRCT2</sup> are expected at 120kDa, neongreen-HsEct2<sup>ΔBRCT0+1</sup> at 100kDa and HsEct2<sup>ΔBRCT0+1+2</sup> at 80kDa. Tubulin and actin were plotted as a loading control. (B) Method of determining expression levels in images acquired with a 40x and 100x objective during confocal live-cell imaging. Cytoplasmic pixel intensities were measured, and background signal was subtracted from the cytoplasmic values. (C) Expression levels of neongreen-HsEct2 cell lines determined on confocal images obtained by live-cell imaging with a 40x and 100x objective. A threshold for no, low, medium and high expression was set according to the objective used for imaging (Table 21). Numbers above columns indicate number of analyzed cells per cell line. n= number of imaged cells. Scale bar = 10μm

**Table 21. Thresholds of fluorescent intensity levels used for the different categories of HsEct2 transgene expression in cell lines analyzed by confocal microscopy images.**

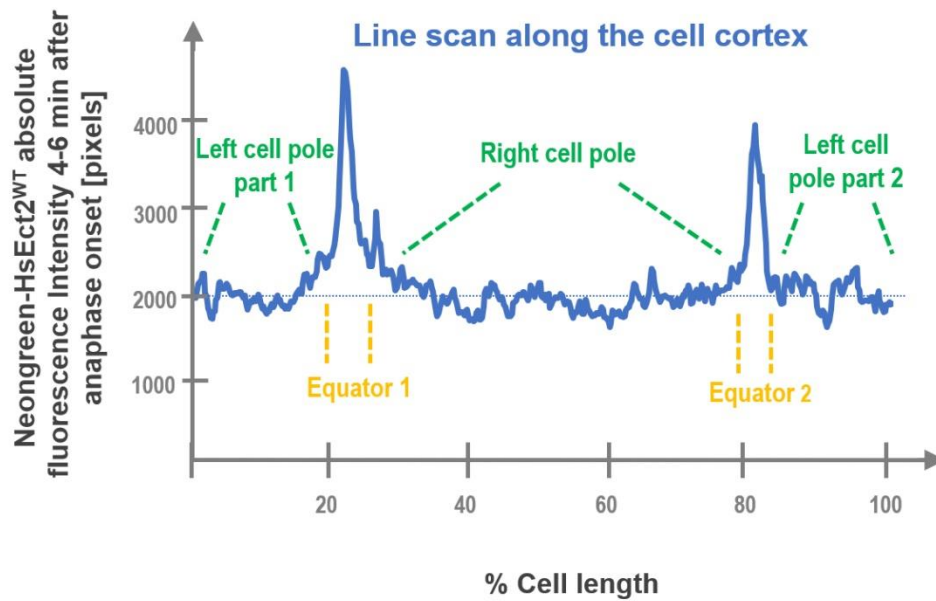
Definition expression levels: 16bit original images	
100x Objective	40x Objective
<b>No expression (-BG): 0-50</b>	<b>No expression (-BG): 0-10</b>
<b>Low expression (-BG): 50- 500</b>	<b>Low expression (-BG): 10-250</b>
<b>Medium expression (-BG): 500-1000</b>	<b>Medium expression (-BG): 250-500</b>
<b>High expression (-BG): &gt;1000</b>	<b>High expression (-BG): &gt;500</b>

Next, I analyzed the localization of HsEct2<sup>ΔBRCT0</sup> during mitosis by performing confocal live-cell imaging. In anaphase HsEct2<sup>ΔBRCT0</sup> (n=19) localizes to the plasma membrane as HsEct2<sup>WT</sup> (Fig. 15B) but shows reduced spindle midzone localization. Since HsEct2<sup>ΔBRCT0</sup> localization differed from HsEct2<sup>WT</sup> I wanted to study in detail how the localization at the cell cortex and the spindle midzone changes when BRCT0 is deleted. Signal intensities at the cell cortex were measured by drawing a line around the cell cortex, starting and ending at the left cell pole in mid anaphase (Fig. 17A+B). I measured the signal at the poles and at the equator and data was further processed by using the program KNIME (analysis done by doctoral student Sriyash Mangal). Moreover, I measured HsEct2 signal intensities at the spindle midzone by drawing a line from underneath the equatorial plasma membrane to the opposite site of the cell equator (Fig. 17A). The signal intensities of cells expressing HsEct2<sup>ΔBRCT0</sup> are strongly reduced at the spindle midzone compared to HsEct2<sup>WT</sup>. Moreover, HsEct2<sup>ΔBRCT0</sup> localizes to the equatorial plasma membrane and also to the cell poles whereas HsEct2<sup>WT</sup> only localizes to the cell equator (Fig. 17C). These results suggest that BRCT0 domain contributes to spindle midzone localization and, is required to enrich HsEct2 at the cell equator.

A



B



C

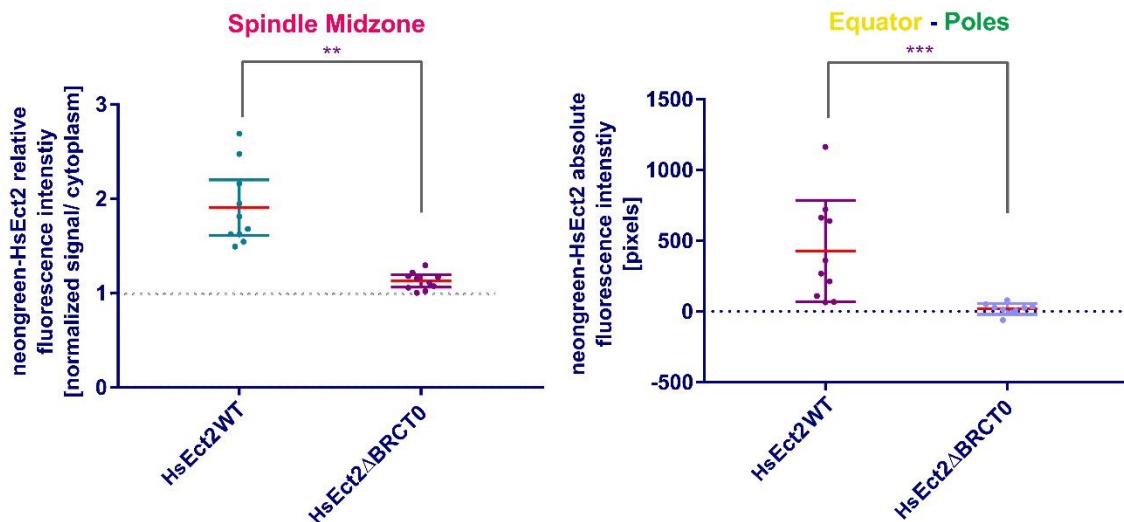
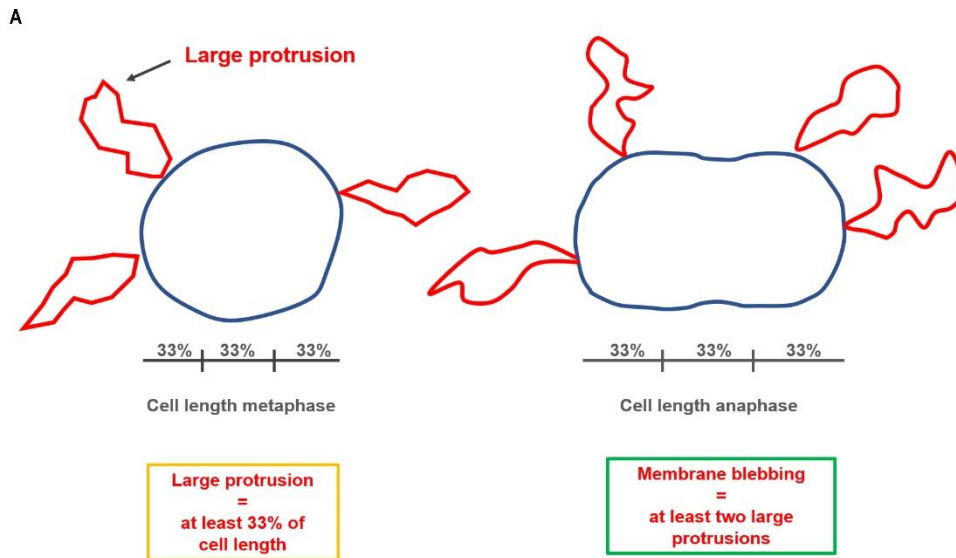


**Fig. 17. BRCT0 domain contributes to spindle midzone localization, and is required to enrich HsEct2 at the cell equator.** (A) Schematic of quantification methods of HsEct2 fluorescence intensities at the cell equator, around the cell periphery and at the spindle midzone on confocal images acquired by live-cell imaging. Z-stacks were acquired with 100x objective and a midplane image at the first furrow indentation was used for

quantification. A line (width= 6 pixel) was drawn around the cell periphery in ImageJ starting and ending at the left pole and fluorescent intensities were measured. Fluorescent intensities of HsEct2 were further analyzed at the cell poles and at the cell equator using the program KNIME. Cytoplasmic values were measured in a box drawn in the cytoplasm and values were subtracted from the cortex and pole values (dashed line in the plot). To quantify the signal at the spindle midzone, a line was drawn underneath the upper equatorial membrane over the spindle midzone down to the lower equatorial membrane and cytoplasmic background was measured in a box drawn in the cytoplasm. Mean intensity values for spindle midzone and cytoplasm were calculated (length = 12 pixel). **(B)** Representative line-scan of the HsEct2<sup>WT</sup> fluorescent intensity around the cell periphery in anaphase. **(C)** HsEct2<sup>ΔBRCT0</sup> is reduced on the spindle midzone and not enriched at the cell equator compared to HsEct2<sup>WT</sup>. Left panel: Fluorescence signal of HsEct2<sup>WT</sup> and HsEct2<sup>ΔBRCT0</sup> at the spindle midzone (normalized ratio = midzone signal/ cytoplasmic signal). Right panel: Absolute fluorescence signal intensities of cell equator minus poles of HsEct2<sup>WT</sup> and HsEct2<sup>ΔBRCT0</sup>. Equatorial and polar fluorescent intensity was calculated for each cell. Dots are quantified cells. Dotted line = background signal. Statistics performed with student's t-test. Error bars are Error bars are SDM. P-values are from student's t-test, p< 0,001(\*\*), and p< 0,0001(\*\*\*)).

Next, I wanted to know whether BRCT0 domain inhibits HsEct2 GEF activity that leads to hyperactivation of HsEct2 that in turn leads to hyperactivation of RhoA. In the past it has been shown that hyperactive RhoA results in huge membrane protrusions (here called membrane blebbing) of the cell during mitosis (Zanin et al., 2013). An increase in GEF activity should result in hyper membrane blebbing as observed before (Zanin et al., 2013). I analyzed cortex contractility by measuring membrane blebbing of the different HsEct2 transgenic cells lines by confocal live-imaging in presence of endogenous HsEct2 (Fig. 18A). I quantified the percentage of membrane protrusions in all generated cell lines during metaphase and anaphase during live-imaging of the cells. If the protrusions of the cells were at least 1/3 of the size of the metaphase or anaphase cell, the protrusions were scored as strong blebbing and counted as “blebby” for the quantification (Fig. 18C). In cells expressing HsEct2<sup>ΔBRCT0</sup> in metaphase no blebbing is observed (0%) as in HsEct2<sup>WT</sup> (0%). In anaphase membrane blebbing of HsEct2<sup>ΔBRCT0</sup> is slightly reduced (5%) when compared to HsEct2<sup>WT</sup> (17%) (Fig. 18C). These results suggest that the BRCT0 domain does not inhibit Ect2 GEF activity.



Representative images of cells with and without membrane protrusions

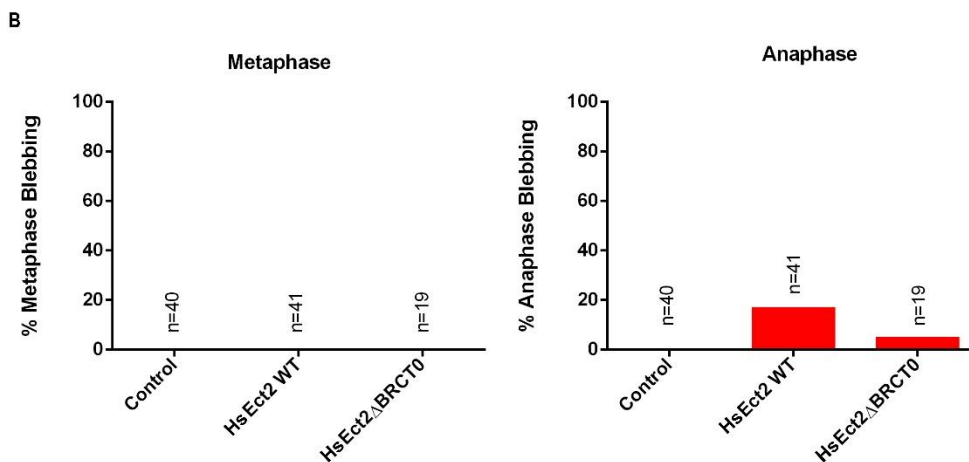
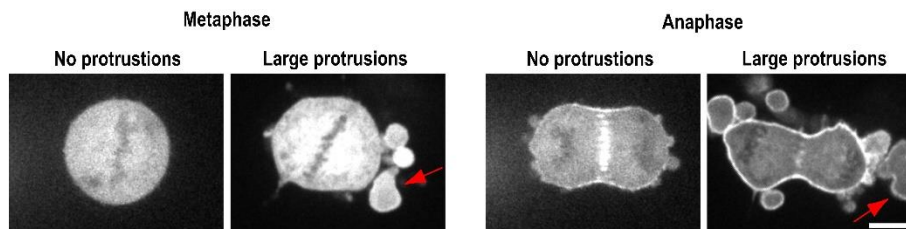


**Fig. 18. Absence of BRCT0 domain does not increase membrane blebbing during mitosis.** (A) Schematic of the quantification of membrane protrusions and blebbing used in different cell lines. Confocal live-cell imaging was performed, and cells were analyzed for membrane protrusions in metaphase and anaphase using ImageJ. If the length of the membrane protrusions were at least 33% of the length of the cell, protrusions were classified as “membrane blebbing”. (B) Membrane blebbing during metaphase and anaphase in presence of endogenous HsEct2 in transgenic cell lines expressing HsEct2<sup>WT</sup> and HsEct2<sup>ΔBRCT0</sup>. Blebbing was determined by confocal live-cell imaging. In anaphase membrane blebbing is slightly reduced in cells expressing HsEct2<sup>ΔBRCT0</sup>. n= number of analyzed cells per cell line that expressed the HsEct2 transgenes. Red arrows indicating membrane blebbing in metaphase and anaphase. Scale bar = 10 μM.

In summary, these data suggest that BRCT0 is not inhibiting HsEct2 GEF activity and is not required for successfully cytokinesis. However, my data indicates that the BRCT0 domain contributes to spindle midzone binding of Ect2 and is required to enrich HsEct2 at the cell equator.

### **3.2.3. The BRCT1 domain is the major spindle midzone binding domain and is required for cytokinesis**

Previous studies have shown that HsEct2 and centralspindlin are required for RhoA accumulation at the cell equator and HsEct2 BRCT1 domain interacts with MgcRacGAP in a phospho-dependent manner (Nishimura and Yonemura, 2006; Yüce et al., 2005). This suggested that the interaction of MgcRacGAP and HsEct2 is essential for cytokinesis. Moreover it was previously shown that two point mutations in the BRCT1 (T153A, K195M, HsEct2<sup>T153,K195M</sup>) domain inhibit the interaction with MgcRacGAP and completely abolished HsEct2 localization to the spindle midzone (Kotýnková et al., 2016). Moreover Kotýnková et al. showed that HsEct2<sup>T153,K195M</sup> transgene rescues cytokinesis defects after depletion of endogenous HsEct2 suggesting that spindle midzone localization and MgcRacGAP binding is not essential for cytokinesis. To investigate whether the BRCT1 domain has any role during cytokinesis, I generated two transgenes where I deleted BRCT0+1 and BRCT1 domain (Fig. 19A). Expression of transgenic HsEct2<sup>ΔBRCT0+1</sup> was analyzed by western blot analysis and image quantification on confocal spinning disk images (Fig. 16). Western blot analysis revealed similar expression levels of endogenous and transgenic HsEct2<sup>ΔBRCT0+1</sup> (Fig. 16A). Image quantification of expression levels demonstrated that HsEct2<sup>ΔBRCT0+1</sup> and HsEct2<sup>ΔBRCT1</sup> were expressed at similar levels like HsEct2<sup>WT</sup> (Fig. 16C).

Then I analyzed the localization of HsEct2<sup>ΔBRCT0+1</sup> and HsEct2<sup>ΔBRCT1</sup> transgenes in the presence of endogenous HsEct2. HsEct2<sup>ΔBRCT0+1</sup> (n=41) and HsEct2<sup>ΔBRCT1</sup> (n=27) are absent from the spindle midzone and only present on the plasma membrane (Fig. 19B).

Next, I measured the fluorescence intensity of HsEct2<sup>ΔBRCT0+1</sup> (n=41) at the cell equator and at the poles (Fig. 17 A+B) and cells expressing HsEct2<sup>ΔBRCT0+1</sup> show that the signal at the cell equator and at the cell poles are equal (Fig. 20A). These results are consistent with previous models that interaction between the BRCT1 domain and MgcRacGAP targets HsEct2 to the spindle midzone and enriches HsEct2 at the equatorial membrane during anaphase (Wolfe et al., 2009; Yüce et al., 2005).

Since truncations of entire protein domains can alter the protein folding and lead to artifacts, I introduced a point mutation in BRCT1 domain (W211R) and another point mutation in BRCT2 domain (W305) that should disrupt the function of the BRCT domains. It was previously shown that mutating a highly conserved tryptophan in the BRCT2 domain (W305R) abolishes the intramolecular interaction of HsEct2 N-terminus with its C-terminus (Kim et al., 2005). Dr. Esther Zanin identified the equivalent and conserved tryptophan in BRCT1 domain (W211) and so I generated a cell line expressing HsEct2<sup>W211R</sup> (Fig. 19A) and analyzed whether the exchange of tryptophan 211 (W211R) disrupts the function of the BRCT1 domain. Unfortunately, expression of the HsEct2<sup>W211R</sup> (n=5) transgene was very low and it localized mostly to the cytoplasm and therefore HsEct2<sup>W211R</sup> was not analyzed further (Fig. 19B).

Previously it was shown that two point mutations in the BRCT1 domain (HsEct2<sup>T153A, K195M</sup>) which inhibit the interaction of HsEct2 with the centralspindlin component MgcRacGAP do not abrogate HsEct2 function (Kotýnková et al. 2016). To confirm these observations, I generated a stable cell line expression HsEct2<sup>T153A, K195M</sup> and indeed I found that the phenotype resulting from depletion of endogenous HsEct2 is largely rescued by HsEct2<sup>T153A, K195M</sup> (Fig. 19C). BRCT domains are often phosphopeptide binding motifs that interact with their binding partners upon phosphorylation (Manke, 2009). These point mutations abolish the interaction of HsEct2 and MgcRacGAP and prevent spindle midzone localization (Wolfe et al., 2009). In my hands, expression of HsEct2<sup>T153A, K195M</sup> (n=15) resulted in a reduced spindle midzone localization but did not entirely abolish spindle midzone localization in presence of endogenous HsEct2 (Fig. 19B). However, these results are preliminary and quantification for a solid conclusion is required in the future.

Then I tested the function of HsEct2<sup>ΔBRCT0+1</sup>, HsEct2<sup>ΔBRCT1</sup> and of HsEct2<sup>T153A, K195M</sup> after depleting endogenous HsEct2 in these cell lines. In presence of endogenous HsEct2, cell lines expressing HsEct2<sup>ΔBRCT0+1</sup> (4%), HsEct2<sup>ΔBRCT1</sup> (9%) and HsEct2<sup>T153A, K195M</sup> (4%) show very little bi- and multinucleated cells (Fig. 19C). In absence of endogenous HsEct2 cell lines expressing HsEct2<sup>ΔBRCT0+1</sup> (81%) and HsEct2<sup>ΔBRCT1</sup> (69%), and HsEct2<sup>T153A, K195M</sup> (19%) shows increased bi- and multinucleated cells in absence of endogenous HsEct2. Since the cell line expressing HsEct2<sup>ΔBRCT1</sup> showed little expression levels in interphase and mitotic cells, the cell line was sorted with fluorescence-activated cell scanning (FACS) with the help of Dr. Christoph Ziegenhain from Prof. Enard's laboratory. This was done to exclude that the high percentage of bi- and multinucleation in

HsEct2<sup>ΔBRCT1</sup> (69%) after depletion of endogenous HsEct2 did not result from low expression but from a non-functional HsEct2 version when BRCT1 domain is deleted. To identify a clone that expresses uniformly the HsEct2<sup>ΔBRCT1</sup> transgene, 5x 96-well plates were FACS sorted each well containing one single cell (480 wells in total). I identified 5 clones out of 480 that survived FACS sorting and 2 out of 5 clones expressed HsEct2<sup>ΔBRCT1</sup> in a similar amount than HsEct2<sup>WT</sup>. One of the two cell lines derived from HsEct2<sup>ΔBRCT1</sup> by single-cell FACS sorting (HsEct2<sup>ΔBRCT1 (FACS)</sup>) was used to repeat the assay in presence and absence of endogenous HsEct2 and the assays confirmed the result obtained with the non-FACS sorted HsEct2<sup>ΔBRCT1</sup> cell line. Together these results suggest that the BRCT1 domain is essential for cytokinesis but binding of the BRCT1 domain to MgcRacGAP is not.

Then cortex contractility was monitored by live-cell imaging by quantifying membrane blebbing in metaphase and anaphase. In metaphase, no (0%) blebbing was observed in HsEct2<sup>WT</sup>, HsEct2<sup>ΔBRCT0+1</sup>, HsEct2<sup>ΔBRCT1</sup>, and HsEct2<sup>T153A, K195M</sup>. In anaphase HsEct2<sup>ΔBRCT0+1</sup> (29%), HsEct2<sup>ΔBRCT1</sup> (46%), and HsEct2<sup>T153A, K195M</sup> (47%) showed elevated levels of membrane blebbing compared to HsEct2<sup>WT</sup> (17%). This suggests that BRCT1 domain might be involved in the inhibition of HsEct2. However live-cell imaging experiments in absence of endogenous HsEct2 is required to prove whether BRCT1 domain is involved in HsEct2 inhibition. Unfortunately, RNAi depletion was not as efficient and therefore no live-cell imaging was performed in absence of endogenous HsEct2 (see discussion part).

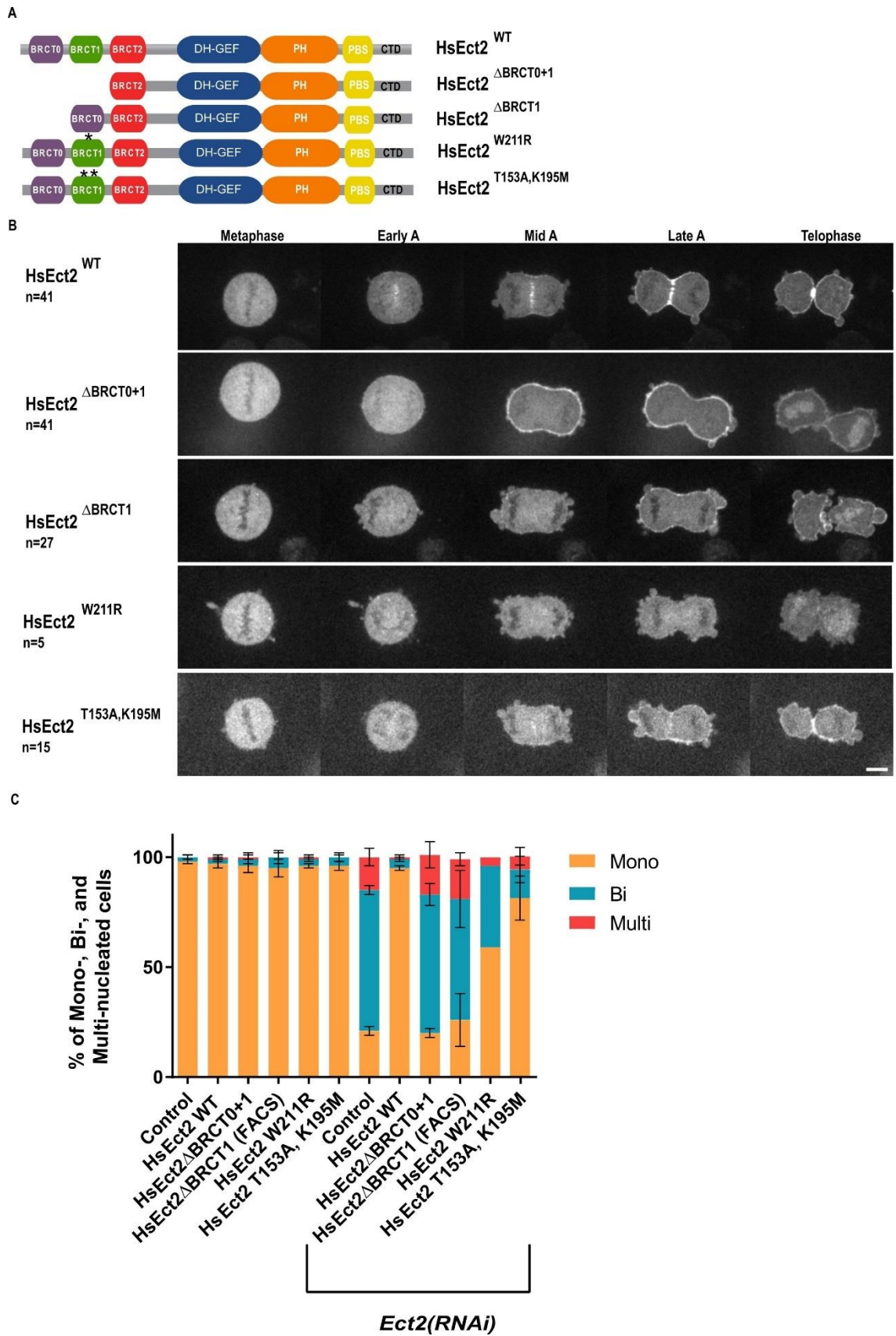


**Fig. 19. The BRCT1 domain is required for cytokinesis and deletion of BRCT1 abolishes spindle midzone localization.** (A) Domain structure of HsEct2<sup>WT</sup>, HsEct2<sup>ΔBRCT0+1</sup>, HsEct2<sup>ΔBRCT1</sup>, HsEct2<sup>W211R</sup> and HsEct2<sup>T153A, K195M</sup> transgenes. (B)

Micrographs of live-cell imaging in dividing cells expressing neogreen-HsEct2<sup>WT</sup>, neogreen-HsEct2<sup>ΔBRCT0+1</sup>, neogreen-HsEct2<sup>ΔBRCT1</sup>, neogreen-HsEct2<sup>W211R</sup> and neogreen-HsEct2<sup>T153A, K195M</sup>. HsEct2<sup>WT</sup> localizes to the spindle midzone and to the equatorial plasma membrane. In the absence of the BRCT1 domain spindle midzone localization is abolished and the protein is present on the plasma membrane but not enriched at the equatorial membrane. Scale bar = 10 μm. n= number of analyzed cells per cell line that expressed the HsEct2 transgenes. (C) Deletion of BRCT1 domain causes severe cytokinesis failure measured by multinucleation assay, n>150 cells of 2-3 independent experiments (except HsEct2<sup>W211R</sup> because of low expression in the cell line).

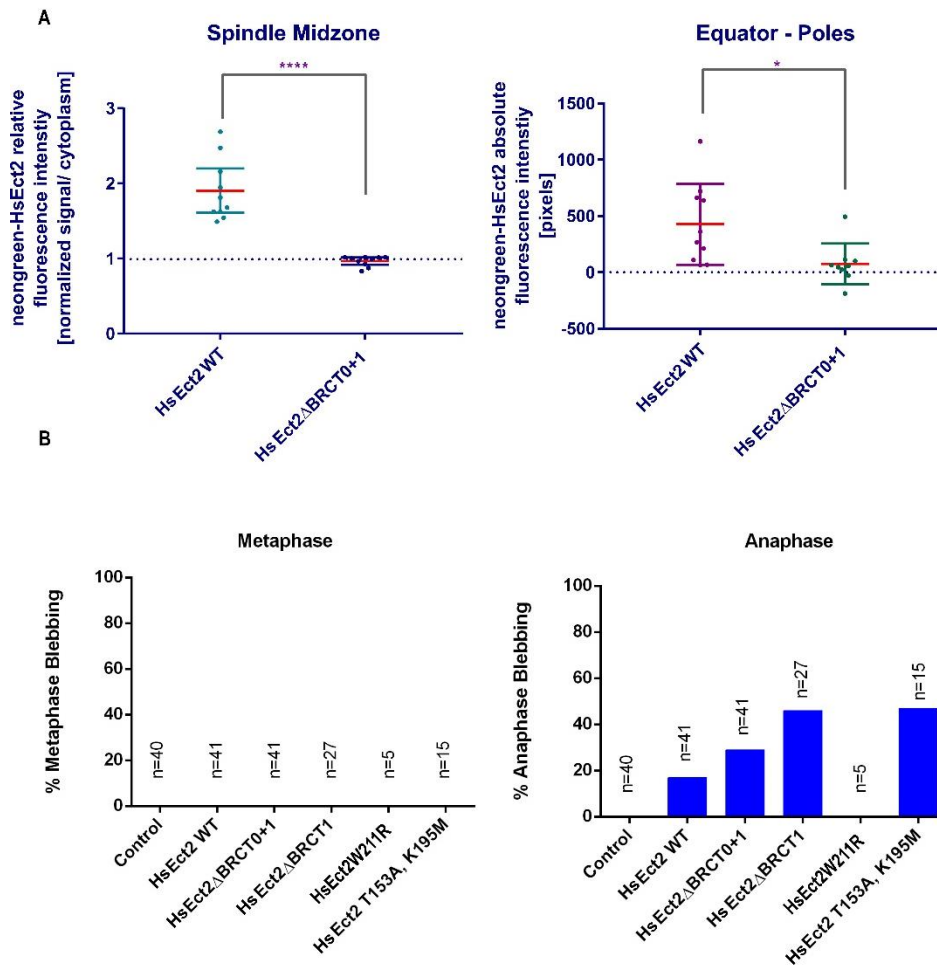


**Fig. 20. BRCT1 domain is required to enrich HsEct2 at the equatorial membrane and deletion of BRCT1 induces mild membrane blebbing in anaphase. (A)** Spindle midzone signal and signal of cell equator minus poles was measured as depicted in Figure 17A+B. HsEct2<sup>ΔBRCT0+1</sup> is absent from the spindle midzone and is not enriched at the cell equator compared to HsEct2<sup>WT</sup>. Dots are quantified cells. Equatorial and polar fluorescent intensity was calculated for each cell. Dotted line = background signal. Statistics performed with student's t-test. Error bars are SDM. P-values are from student's t-test, p< 0,05(\*), and p< 0,0001(\*\*\*\*). **(B)** Membrane blebbing during metaphase and anaphase in presence of endogenous HsEct2 in transgenic cell lines expressing HsEct2<sup>WT</sup>, HsEct2<sup>ΔBRCT0+1</sup>, HsEct2<sup>ΔBRCT1</sup>, HsEct2<sup>W211R</sup> and HsEct2<sup>T153A, K195M</sup> was quantified as described in Fig. 18A. Blebbing was determined by confocal live-cell imaging. In anaphase membrane blebbing is slightly increased in cells expressing HsEct2<sup>ΔBRCT0+1</sup>, HsEct2<sup>ΔBRCT1</sup> and HsEct2<sup>T153A, K195M</sup>. n= number of analyzed cells per cell line that expressed the HsEct2 transgenes.

### 3.2.4. The BRCT2 domain is required for cytokinesis and inhibits GEF activity

Next, I wanted to study whether BRCT2 domain is required for Ect2 activity and function. In the literature, mainly BRCT1 domain was mentioned and characterized, but what the specific role of BRCT2 domain is has not yet been analyzed. Therefore, I generated cell lines where I deleted the BRCT2 domain. To exclude that the observed phenotype is an artifact of deleting the entire BRCT2 domain, I also generated a cell line where I substituted the BRCT2 domain with BRCT1 domain instead of deleting BRCT2 domain. Additionally I introduced a specific point mutation (W305R) which was claimed to prevent folding of the BRCT2 domain and abolish the interaction of HsEct2 N-terminus with its C-terminus (Kim et al., 2005) (Fig. 16A). Moreover, I deleted all the three BRCT domains to analyze whether deletion of all the three BRCT domains results in an increased GEF activity and whether deletion of all three BRCT domains shows similar effects than deleting only BRCT2 domain.

First, I measured expression levels of the different transgenic HsEct2 cell lines by western blot and fluorescent image quantification (Fig. 16). Western blot analysis revealed that HsEct2<sup>ΔBRCT0+1+2</sup> and HsEct2<sup>ΔBRCT2</sup> are expressed at similar levels as endogenous HsEct2. Imaging analysis showed a homogenous expression of low, medium and high expressing cells in the cell lines HsEct2<sup>ΔBRCT0+1+2</sup>, HsEct2<sup>ΔBRCT2</sup> and HsEct2<sup>BRCT1, BRCT1</sup> measured with either 40x or 100x objective. However, in the cell line expressing HsEct2<sup>W305R</sup> and HsEct2<sup>ΔBRCT1+2</sup> expression levels were quite low in the analyzed cells.

Then I analyzed the localization of HsEct2 in transgenic cell lines where BRCT2 domain is absent by confocal live cell imaging (Fig 21B). In cells expressing HsEct2<sup>ΔBRCT0+1+2</sup> (n=27) and HsEct2<sup>ΔBRCT1+2</sup> (n=26) no spindle midzone localization can be observed as expected since BRCT1 domain is also missing (Fig. 21B). The cell line expressing HsEct2<sup>W305R</sup> shows a similar localization like HsEct2<sup>WT</sup> (Fig. 21B). To study whether BRCT2 contributes to spindle midzone localization I deleted or substituted BRCT2 with BRCT1 domain. Then I analyzed HsEct2<sup>ΔBRCT2</sup> (n=40) and HsEct2<sup>BRCT1, BRCT1</sup> (n=15) expressing cells and a weak spindle midzone and strong plasma membrane localization can be observed. Next, I quantified the signal around the cell cortex in cells expressing HsEct2<sup>ΔBRCT2</sup> and at the spindle midzone as depicted in Figure 17A+B. Analysis revealed that indeed spindle midzone signal is reduced in comparison to HsEct2<sup>WT</sup>. Moreover,

HsEct2<sup>ΔBRCT2</sup> is not enriched at the cell equator as in HsEct2<sup>WT</sup> but shows an equal distribution at the cell equator and at the poles (Fig. 22A). These results show that BRCT2 domain contributes to spindle midzone localization and is required to enrich HsEct2 at the cell equator.

Next, I tested the function of HsEct2<sup>ΔBRCT0+1+2</sup>, HsEct2<sup>ΔBRCT1+2</sup>, HsEct2<sup>ΔBRCT2</sup>, HsEct2<sup>W305R</sup> and HsEct2<sup>BRCT1, BRCT1</sup> and measured mono-, bi- and multinucleation before and after depleting endogenous HsEct2 in these cell lines (Fig. 21C). In presence of endogenous HsEct2 cells expressing HsEct2<sup>ΔBRCT0+1+2</sup> (3%), HsEct2<sup>ΔBRCT2</sup> (11%), HsEct2<sup>ΔBRCT1+2</sup> (6%) and HsEct2<sup>W305R</sup> (3%) show low numbers of bi- and multinucleation. After depletion of endogenous HsEct2 cells expressing HsEct2<sup>ΔBRCT0+1+2</sup> (65%), HsEct2<sup>ΔBRCT2</sup> (50%), HsEct2<sup>ΔBRCT1+2</sup> (52%) and HsEct2<sup>W305R</sup> (25%) show an increased number of bi- and multinucleation but partially rescue cytokinesis failure since the controls without any transgene showed in the same experiments between 79-81% bi- and multinucleation. Interestingly HsEct2<sup>BRCT1-BRCT1</sup> (70%) showed a higher percentage of bi- and multinucleation than HsEct2<sup>ΔBRCT2</sup> (52%) suggesting that BRCT1 and BRCT2 domains have separate functions since HsEct2<sup>BRCT1-BRCT1</sup> is not partially functional. The cell line expressing HsEct2<sup>W305R</sup> showed 25% bi- and multinucleation which suggests that HsEct2<sup>W305R</sup> is mainly functional. This is in contrast to previous results from Kim et al., 2005 where it was reported that the mutation W304R in the BRCT2 domain (equivalent to my construct HsEct2<sup>W305R</sup>) abolished the interaction of the BRCT domains with the GEF domain and strongly increased the GEF activity of Ect2<sup>304R</sup> *in-vitro* (GEF assays). My results question the importance of the residue W305 regarding cytokinesis.

Then I analyzed membrane blebbing in these cell lines (Fig. 22A). Deletion of BRCT1+2 domains resulted in strong increase of blebbing in anaphase (62%). Strong blebbing was also observed when all the three BRCT domains were deleted (22% in metaphase and 89% in anaphase) and the same effect was observed when only BRCT2 domain is deleted alone (28% in metaphase and 88% in anaphase). Interestingly metaphase blebbing was only observed in the cell lines expressing HsEct2<sup>ΔBRCT0+1+2</sup> (22%) and HsEct2<sup>ΔBRCT2</sup> (28%) which could be indicative for a premature activation of HsEct2 in metaphase when BRCT2 domain is deleted. Also, in cells expressing HsEct2<sup>BRCT1-BRCT1</sup> strong membrane blebbing occurs during metaphase (62%) and anaphase (80%) (n=15). These results suggest that BRCT2 is the major inhibitory domain that inhibits HsEct2 GEF activity in metaphase and anaphase.

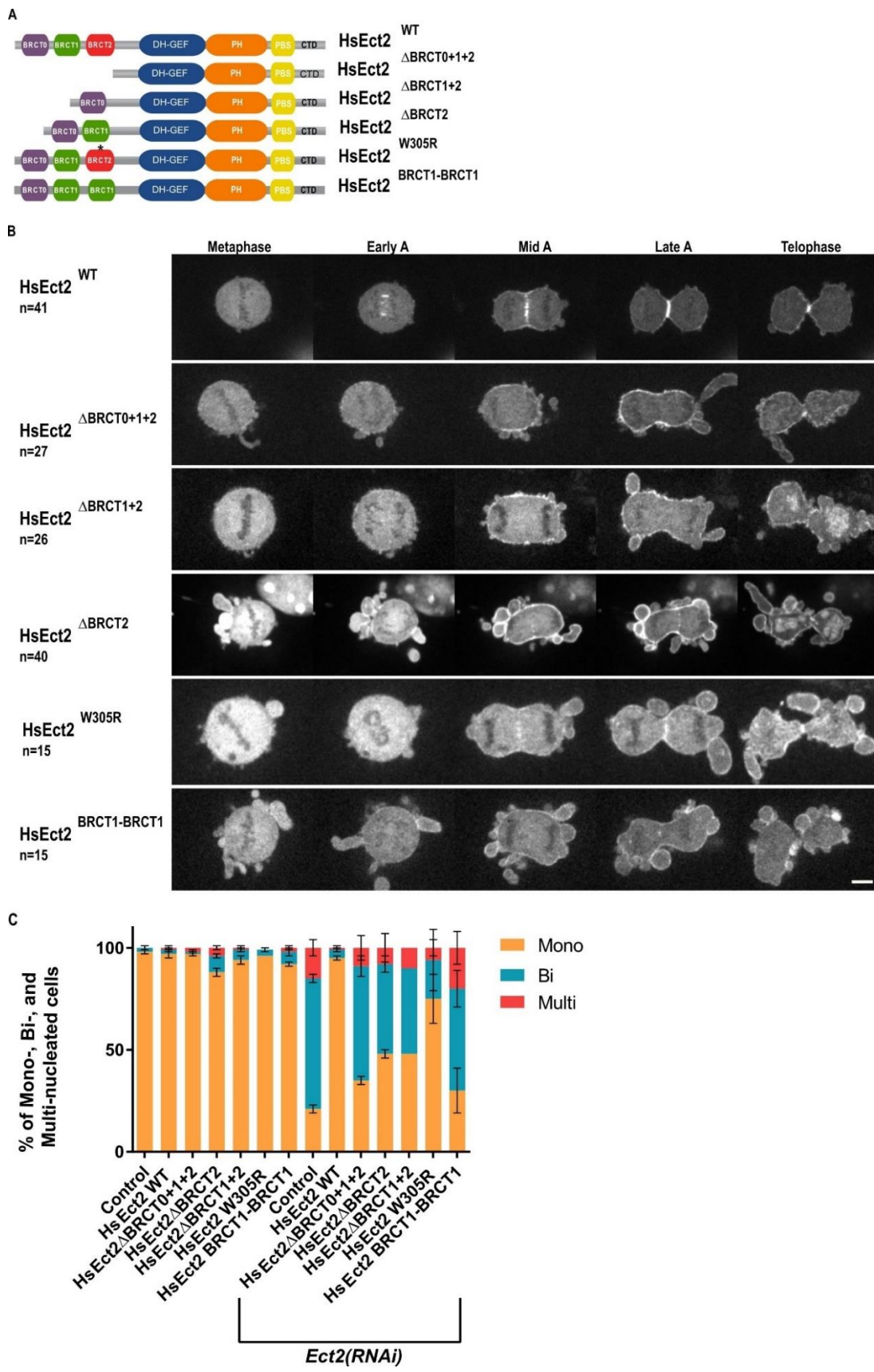


**Fig. 21. BRCT2 domain is required for cytokinesis and contributes to spindle midzone localization.** (A) Domain structure of HsEct2<sup>WT</sup>, HsEct2<sup>ΔBRCT0+1+2</sup>, HsEct2<sup>ΔBRCT1+2</sup>, HsEct2<sup>ΔBRCT2</sup>, HsEct2<sup>W305R</sup> and HsEct2<sup>BRCT1-BRCT1</sup> transgenes. (B) Micrographs of live-cell imaging in dividing cells expressing neogreen-HsEct2<sup>WT</sup>, neogreen-HsEct2<sup>ΔBRCT0+1+2</sup>, neogreen-HsEct2<sup>ΔBRCT1+2</sup>, neogreen-HsEct2<sup>W305R</sup> and neogreen-HsEct2<sup>BRCT1-BRCT1</sup>. Cells lacking BRCT2 domain show plasma membrane and reduced spindle midzone localization. Scale bar = 10 μm, n= number of imaged cells (C) Absence of BRCT2 domain causes increased cytokinesis failure measured by multinucleation assay, n>150 cells of 2-3 independent experiments (except HsEct2<sup>ΔBRCT1+2</sup> because of low expression in the cell line).

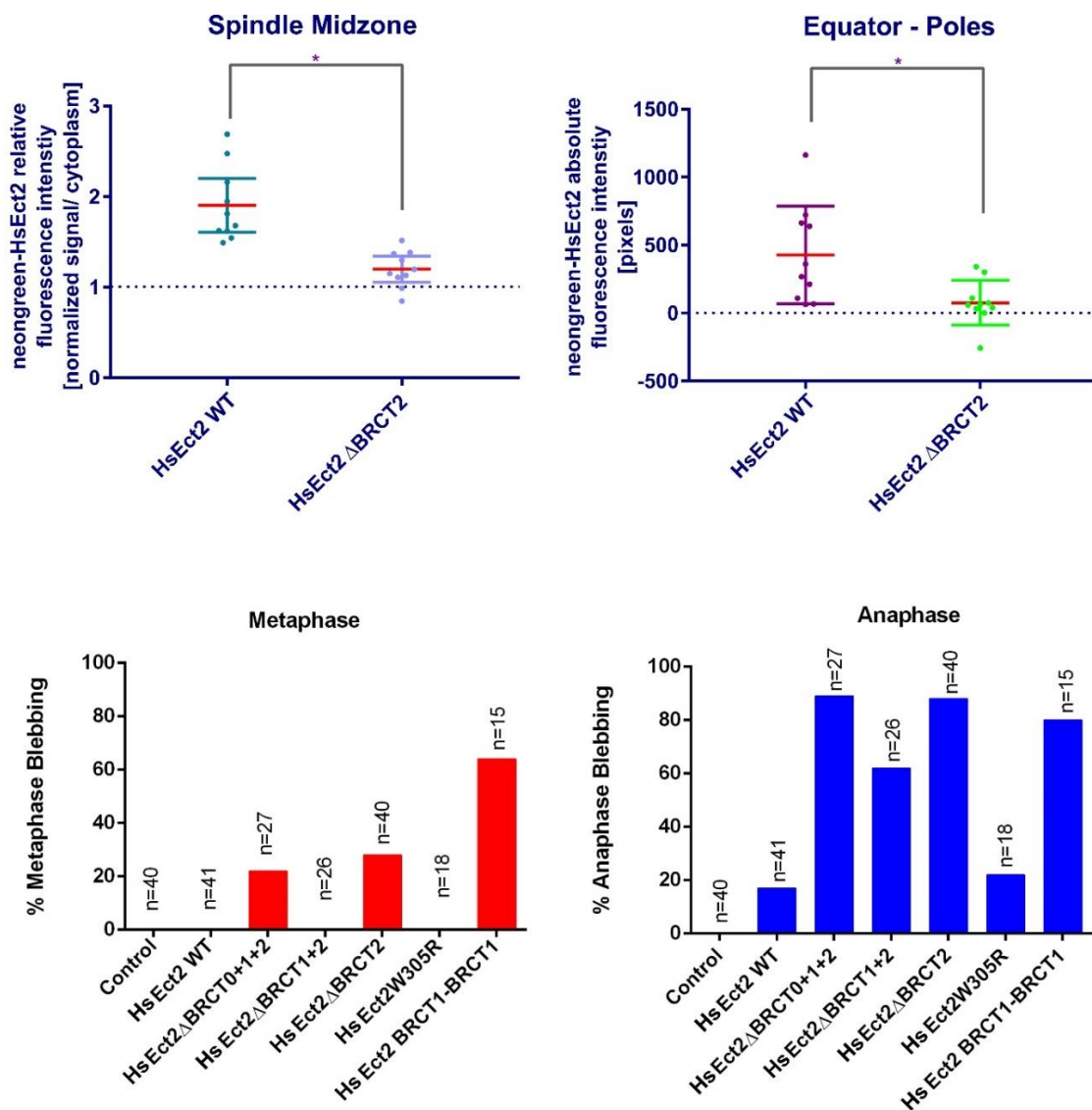


**Fig. 22. BRCT2 domain is required to enrich HsEct2 at the equatorial plasma membrane and absence of BRCT2 causes severe membrane blebbing.** (A) The transgene lacking the BRCT2 domain shows reduced spindle midzone localization and HsEct2<sup>ΔBRCT2</sup> is not enriched at the cell equator. Dots are quantified cells. Dotted line = background signal. Statistics performed with student's t-test. Error bars are SDM. P-values are from student's t-test, p< 0,05(\*). (B) Membrane blebbing during metaphase and

anaphase in transgenic HsEct2 cell lines expressing HsEct2<sup>WT</sup> and HsEct2<sup>ΔBRCT0+1+2</sup>, HsEct2<sup>ΔBRCT1+2</sup>, HsEct2<sup>ΔBRCT2</sup>, HsEct2<sup>W305R</sup> and HsEct2<sup>BRCT1-BRCT1</sup>. In cells lacking BRCT2 domain blebbing is dramatically increased during cell division. During metaphase blebbing is severely increased in cells expressing HsEct2<sup>ΔBRCT0+1+2</sup>, HsEct2<sup>ΔBRCT2</sup> and HsEct2<sup>BRCT1-BRCT1</sup>. Blebbing was determined by confocal live-cell imaging. Scale bar = 10 μm. n= number of analyzed cells per cell line that expressed the HsEct2 transgenes.

### 3.2.5. Membrane blebbing in HsEct2<sup>ΔBRCT2</sup> is caused by hyperactive Rho

Since I saw a dramatic increase in membrane blebbing in the cell line expressing HsEct2<sup>ΔBRCT2</sup> (22% in metaphase and 88% in anaphase, Fig. 21B, Fig. 22B and Fig. 23). I addressed the question whether increased membrane blebbing in the transgenic cell lines is caused by hyperactive RhoA. It has been previously shown that constitutive active RhoA leads to massive membrane protrusions (Zanin et al., 2013). Therefore, I wanted to test whether RhoA inhibition in the cell line expressing HsEct2<sup>ΔBRCT2</sup> can reduce membrane blebbing (Fig. 24).

In order to test this hypothesis, I inhibited Rho activity by applying the highly specific inhibitor for RhoGTPases C3 to the cells after induction of the transgenes with tetracycline. C3 Transferase from the bacterium *Clostridium botulinum* is an exoenzyme and very effectively blocks Rho activity. C3 Transferase is fused to a cell-penetrating component that helps the C3 enzyme to cross the plasma membrane. In the cytoplasm the cell-penetrating moiety is removed, and the C3 Transferase inactivates RhoA, RhoB, and RhoC. The C3 Transferase is specific for RhoA/B/C and it does not inhibit Cdc42 or Rac1 (Aktories et al., 1989; Wilde and Aktories, 2001).

First, I tested whether C3 inhibitor efficiently inhibited RhoA by analyzing whether anillin is strongly reduced in the cleavage furrow in the control cell line during anaphase performing immunostainings in the cells. Anillin levels were drastically reduced which showed that the inhibitor effectively inhibited RhoA (Fig. 23A). Then I quantified membrane blebbing in the cells before and after C3 application by immunostainings (Fig. 23B). As already observed in live-cell imaging in FRT control cells no blebbing was observed in metaphase and anaphase before and after C3 application (0% in metaphase and 0% in anaphase). In HsEct2<sup>WT</sup> little membrane blebbing was observed during metaphase (9%) and anaphase (11%) and C3 application resulted in a slight reduction of membrane blebbing in metaphase (5%) and anaphase (0%). As in live-cell imaging analyzed before,

in the immunohistochemical assays cells expressing HsEct2<sup>ΔBRCT2</sup> still showed strong blebbing during metaphase (32%) and anaphase (30%). Inhibition of RhoA in HsEct2<sup>ΔBRCT2</sup> by C3 resulted in a strong reduction of membrane blebbing in both metaphase (15%) and anaphase (8%). Together these results support the hypothesis that the BRCT2 domain is the major inhibitory domain of HsEct2 and suggest that deletion of BRCT2 domain increases HsEct2 activity and thus of its downstream effector RhoA.

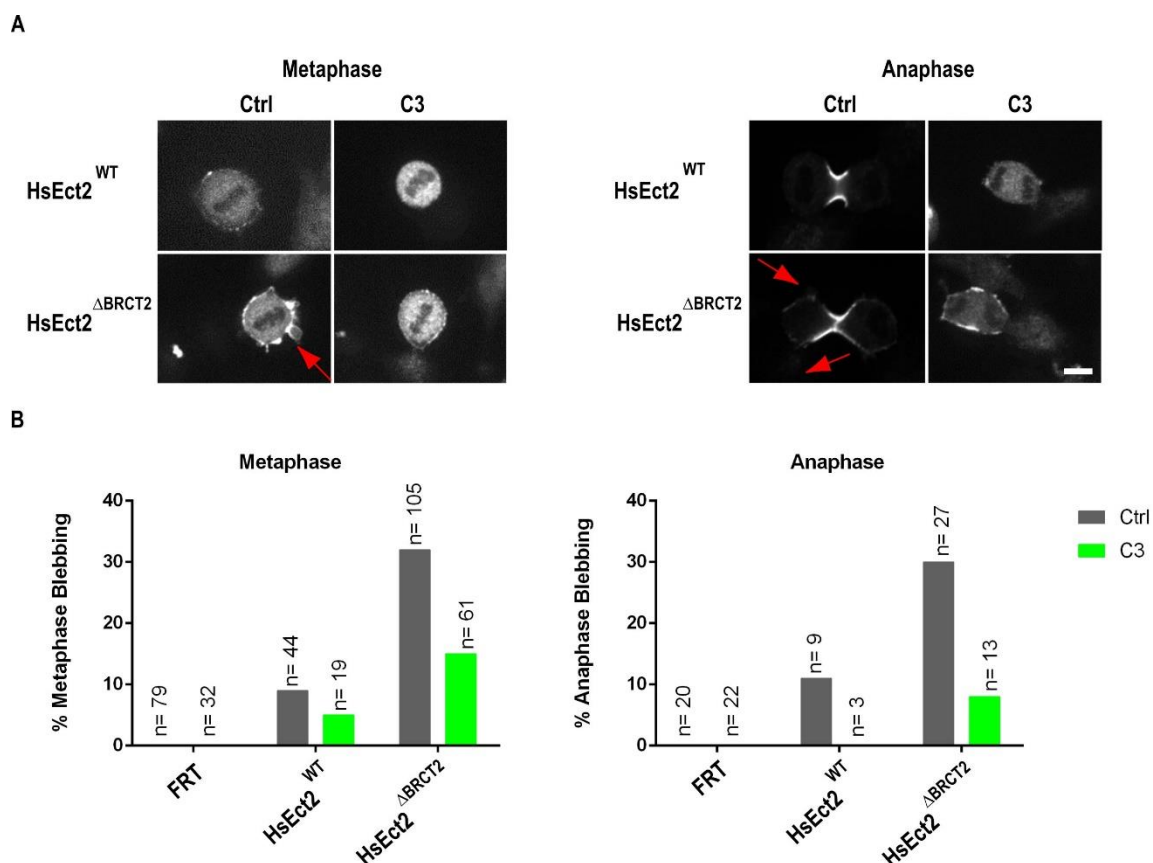


**Fig. 23. Blebbing in HsEct2<sup>ΔBRCT2</sup> expressing cells is reduced upon RhoA inhibition.** (A) Immunostainings of endogenous anillin in FRT control and HsEct2<sup>ΔBRCT2</sup> cell lines before and after C3 application. Red arrows indicating membrane protrusions in cells expressing HsEct2<sup>ΔBRCT2</sup> during metaphase and anaphase. Scale bar = 10μM (B) Membrane blebbing was quantified in all imaged cells of fixed samples and subsequent immunohistochemical stainings of anillin. Images were acquired with a spinning disk microscope. n= number of imaged cells. Number of independent experiments = 2.

### 3.2.6. Deletion of BRCT2 domain results in increased anillin levels

To further investigate whether deletion of BRCT2 domain results in hyperactivation of HsEct2 and its downstream effectors I analyzed anillin levels in HsEct2<sup>ΔBRCT2</sup> cells and compared it to the control cell line. If HsEct2 is hyperactive after deleting the BRCT2

domain then RhoA and its downstream effectors, e.g. the scaffold protein anillin is expected to increase at the cell cortex.

Cells were fixed and stained for anillin and tubulin by immunohistochemistry. Confocal images of cells in metaphase and anaphase were taken and anillin levels were quantified in metaphase cells by drawing a segmented line around the cell cortex and measuring the signal intensity at the cortex. A square box was drawn in the cytoplasm to measure the background signal. Image analysis was performed in Fiji ImageJ by subtracting the background values from the cortex values and summing up the total anillin signal of the cortex for each cell (Fig. 24A).

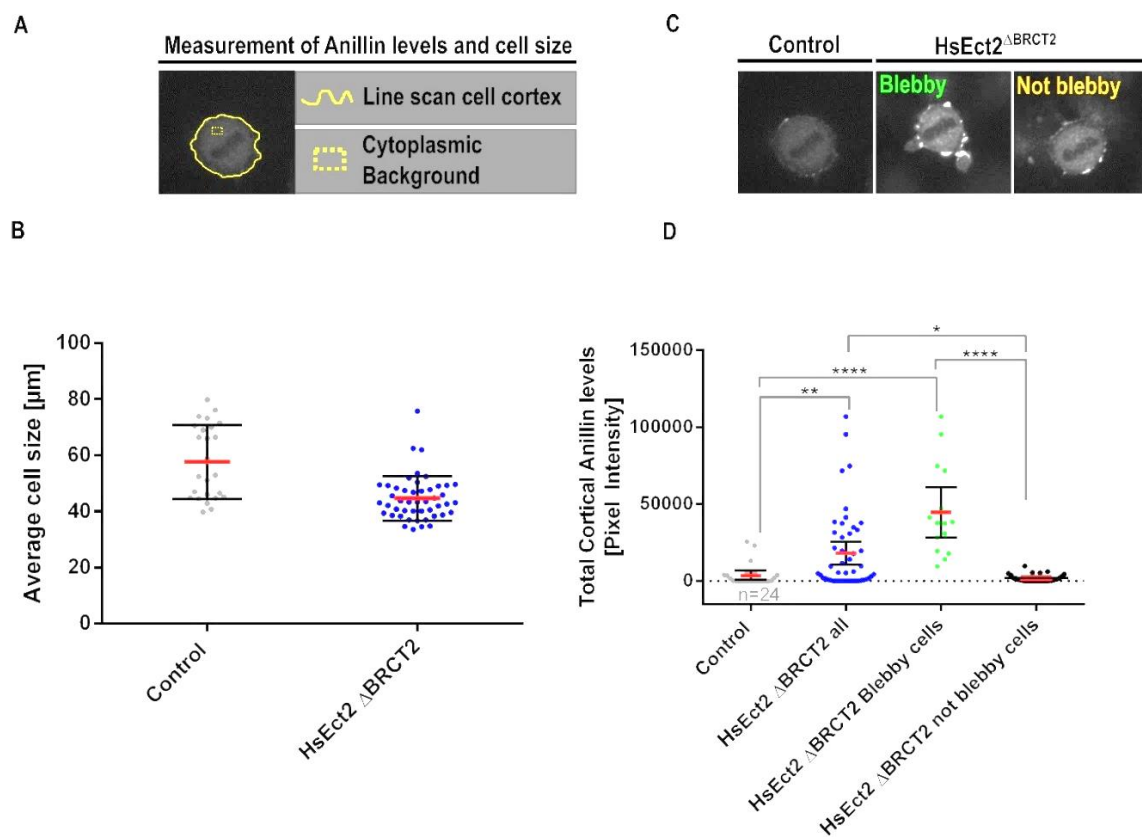


**Fig. 24. Cortical anillin levels are increased in metaphase when cells express HsEct2 $\Delta$ BRCT2.** (A) Method of quantification of cell size and cortical anillin levels. A line scan was drawn around the cell cortex in metaphase cells to measure the circumference of the cells and the pixel intensities of anillin at the cell cortex. (B) Metaphase cell size is reduced when cells express HsEct2 $\Delta$ BRCT2. Dots are quantified cells. Lines and error bars are mean values and 95% confidence interval. Significance was tested by t-test. (C) Cortical anillin levels in metaphase were measured in the control cell line and the cell line expressing HsEct2 $\Delta$ BRCT2. Some cells of HsEct2 $\Delta$ BRCT2 show massive membrane blebbing (“Blebbly”) and some do not show elevated membrane blebbing (“Not blebbly”). (D)

Quantification of anillin levels in metaphase cells. Anillin levels are significantly increased when BRCT2 domain is deleted ( $p < 0,01$ ). Dots are all quantified cells which were obtained from 2 independent experiments. Dotted line = background signal. Lines and error bars are mean values and 95% confidence intervals. Significance was tested using ANOVA.  $n$  = numbers of analyzed cells per cell line. Number of independent experiments=2.  $P < 0,05$  (\*),  $P < 0,001$  (\*\*), and  $p < 0,0001$  (\*\*\*\*).

No or very little anillin was present in FRT control cells ( $n=24$ ) at the cell cortex during metaphase. In HsEct2<sup>ΔBRCT2</sup> cells anillin levels are significantly elevated ( $p < 0,01$ ) when compared to control (Fig. 24C+D). Since only 30% of HsEct2<sup>ΔBRCT2</sup> show membrane blebbing during metaphase (Fig. 24), I additionally compared anillin levels of only the “blebby” cells with the control. In the cells that do show metaphase blebbing there the increase of anillin is highly significant ( $p < 0,0001$ ) (Fig. 24D). To confirm that increased anillin levels in HsEct2<sup>ΔBRCT2</sup> are not due to an artifact e.g. caused by increase cell size and thus increased amount of total anillin, I also compared cell sizes in both control and HsEct2<sup>ΔBRCT2</sup> (Fig. 24A+B). Cell size is significantly decreased when BRCT2 domain is deleted. This might be caused by the massive protrusions that originate from the plasma membrane which decreased the size of the cell. This result confirms that anillin levels are elevated in cells when BRCT2 is deleted which is indicative of a hyperactive RhoA at the cell cortex. Together these results suggest that deletion of BRCT2 domain leads to constitutive active HsEct2.

### **3.2.7. The linker region between the BRCT2 and GEF domain is involved in regulating HsEct2 function**

In a previous study it has been shown that deletion of the linker region strongly enhances the transforming activity of HsEct2 (Saito et al., 2004). In addition, it was shown by Yüce et al., 2005 that T342 phosphorylation within the linker region inhibits association with MgcRacGAP in metaphase and that T342A mutation which abolishes phosphorylation of this site allows a premature interaction of Ect2 N-terminus with MgcRacGAP in metaphase. Another study from Niiya et al., 2006 revealed T412 in the linker region as another *in-vivo* phospho-target (Niiya et al., 2006). They showed that T412 site is phosphorylated by Cdk1 and is important for Ect2 function, since the phosphodeficient mutant T412A reduced GTP bound RhoA and lowered membrane blebbing when Ect2 WT was over-expressed. Moreover it was shown by Hara et al., 2006 that when T341 (= T342) is mutated to a phospho deficient mutant T341A, decreased interaction of N-terminal fragments with C-terminal fragments of Ect2 is observed; moreover a phospho-mimetic mutant increased the

interaction of the N-terminal with the C-terminal fragment which supported a model that phosphorylation of the linker region might be important for the catalytic activity of Ect2 since an altered protein structure could inhibit the release of the DH domain from the N-terminal part of Ect2. Another phospho-site was identified (T328) which has been shown to be phosphorylated by Protein kinase C (PKC) which induces Rac1 activation (Justilien and Fields, 2009) . However, T328 has not been implicated to be important for HsEct2 function but rather in HsEct2 related transformation of non-small cell lung cancer cells (Justilien et al., 2017). Lastly, another study showed that the NLS sites in the linker region are not crucial for successful cytokinesis since mutation of these sites results in cytoplasmic HsEct2 but is dispensable for successful cytokinesis (Saito et al., 2003). All these studies hint that the linker region might play a role in the regulation of HsEct2. Therefore, I analyzed the linker region in detail and found that serines and threonines are enriched compared to the entire protein. In the linker region 21% of serines and 9% of threonines can be found vs. 10% of serines and 6% of threonines found in the entire protein (Fig. 25B). Next, I tested whether the linker region of HsEct2 is important for HsEct2 function and I mutated all serines and threonines to alanines in order to block phosphorylation in this region (Fig. 25A+B). By blocking phosphorylation, I wanted to test whether phosphorylation of this region is important for the regulation of HsEct2. In metaphase HsEct2<sup>LinkerAA</sup> (n=20) seems to localize to microtubules and to centrosomes, and slightly to the plasma membrane. In anaphase HsEct2<sup>LinkerAA</sup> localizes to the plasma membrane and to the spindle midzone (Fig. 25C). Cells expressing HsEct2 with the mutated linker region show increased membrane blebbing (7% in metaphase and 70% in anaphase, Fig. 25D). This suggests that the phosphorylation status of the linker in HsEct2 is also involved in the regulation of HsEct2 activity during anaphase.

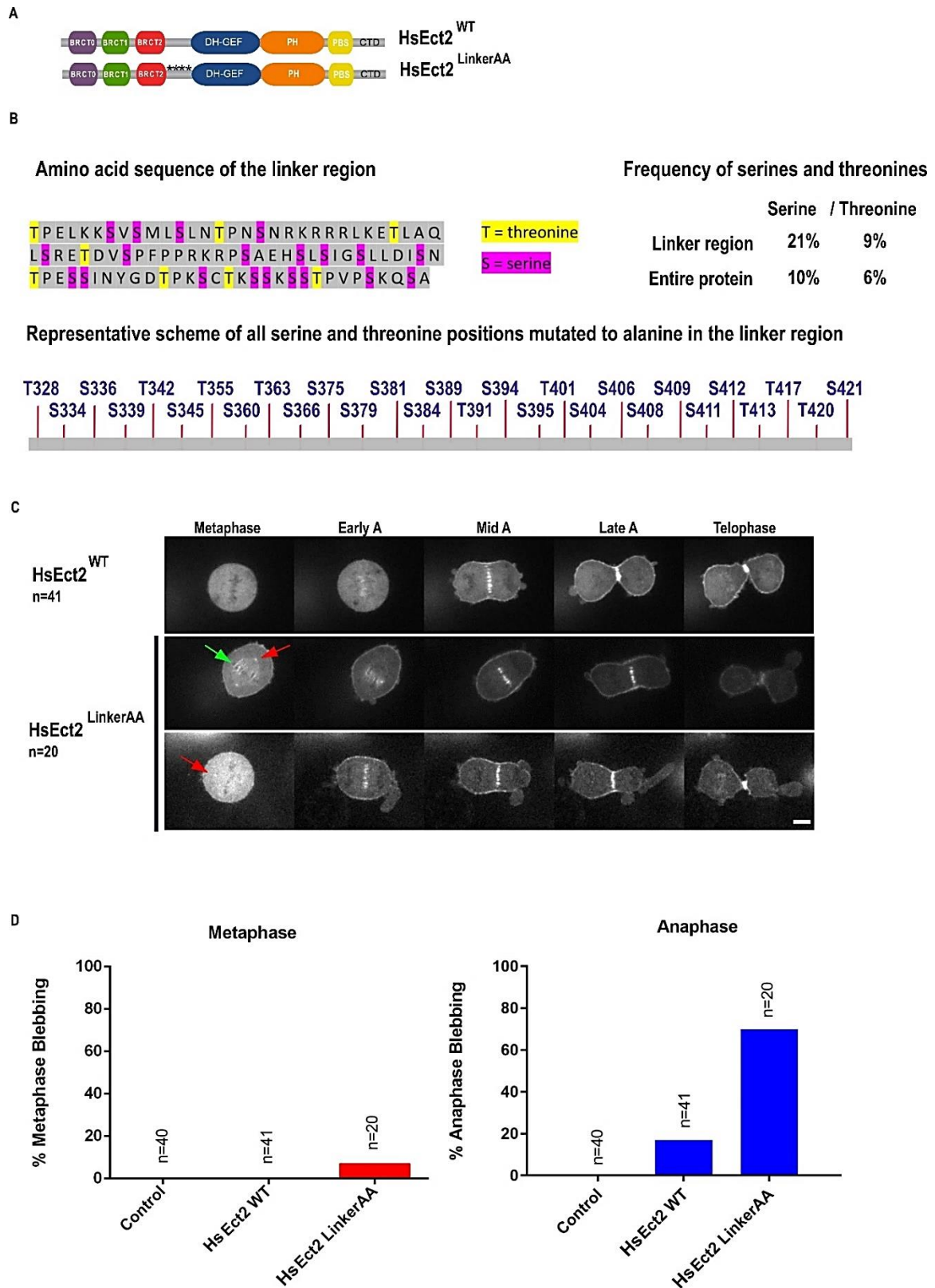


**Fig. 25. HsEct2 linker region is involved in inhibiting HsEct2 GEF activity. (A)** Domain structure of HsEct2<sup>WT</sup> and HsEct2<sup>LinkerAA</sup> transgenes. **(B)** HsEct2 linker sequence indicated with serines (purple) and yellow (threonines). In the panel below all the serines and threonines and their exact positions in the protein are shown and which were mutated to alanines in HsEct2<sup>LinkerAA</sup>. **(C)** Micrographs of live-cell imaging in dividing cells

expressing neongreen-HsEct2<sup>WT</sup> and HsEct2<sup>LinkerAA</sup> (two different cells shown). HsEct2<sup>LinkerAA</sup> localize to centrosomes and to microtubules in metaphase, and to the spindle midzone and the entire cell cortex in anaphase. **(D)** Membrane blebbing during metaphase and anaphase in transgenic HsEct2 cell lines expressing HsEct2<sup>WT</sup> and HsEct2<sup>LinkerAA</sup>. In cells with mutated linker blebbing is dramatically increased during anaphase and slightly increased during metaphase. Blebbing was determined by confocal live-cell imaging. Scale bar = 10  $\mu$ m. n= number of analyzed cells per cell line that expressed the HsEct2 transgenes.

### 3.2.8 Summary

In conclusion I could show that the BRCT0 domain contributes to spindle midzone binding and is required for enriching HsEct2 at the cell equator. Surprisingly I found that the BRCT0 domain is not required for Ect2 function since deletion of BRCT0 does not result in increased bi- and multinucleation.

Furthermore, my studies revealed that BRCT1 is the major spindle midzone binding domain since deletion of BRCT1 completely abolished spindle midzone binding. Similar to the BRCT0 domain, the BRCT1 domain is also required to enrich HsEct2 at the equatorial membrane. Next, I tested the function of BRCT1 and I could show that BRCT1 domain is required for cytokinesis since deletion of BRCT1 results in high bi- and multinucleation. Moreover, BRCT1 is involved in the inhibition of HsEct2 since membrane blebbing is increased when BRCT1 domain is deleted.

Furthermore, I analyzed the role of the BRCT2 domain during cytokinesis and I could show that BRCT2 contributes to spindle midzone binding of HsEct2 since deletion of BRCT2 domain results in a reduction of spindle midzone localization and is required for cytokinesis. However, HsEct2 without the BRCT2 domain seems partially functional. Moreover, I could show that BRCT2 is the major inhibitory domain since expression of HsEct2 <sup>$\Delta$ BRCT2</sup> results in high membrane blebbing during metaphase and increased cortical anillin levels. Lastly, membrane blebbing in cells expressing HsEct2 <sup>$\Delta$ BRCT2</sup> is active RhoA dependent since it can be reduced by inhibition of RhoA by C3 Exoenzyme.

Together my findings suggest that HsEct2 BRCT domains do not act in one module but rather have separate roles during cytokinesis in localizing HsEct2 to the spindle midzone, cell cortex, and in regulating HsEct2 activity *in-vivo*.

## 4. Discussion and outlook

The aim of my thesis was to investigate the distinct roles of three BRCT domains in Ect2 during cytokinesis. In particular I focused on the function of the BRCT domains in the temporal and spatial regulation of Ect2 activity using *in-vivo* structure-function studies in *C. elegans* and human cells.

I started my work in *C. elegans*. The model system of *C. elegans* represented to me a very exciting tool to study CeECT-2 structure and function *in-vivo*, since establishing a molecular replacement system for endogenous and transgenic genes is easy and *in-vivo* analysis by live-imaging allows a straight forward and rapid insight into localization and function of specific transgenes. I generated a molecular replacement system of endogenous and transgenic CeECT-2 with single-copy insertions of the GFP-tagged, RNAi-resistant transgenes. In this system endogenous CeECT-2 could be depleted by RNAi and transgenic CeECT-2 is not affected at the same time, allowing me to study the transgene in absence of endogenous CeECT-2.

In the past, a model was proposed that HsEct2 function is regulated by an autoinhibitory mechanism by binding of the three N-terminal BRCT domains to the GEF domain (Kim et al., 2005; Saito et al., 2004). However, this suggestion was mainly based on *in-vitro* data and biochemical studies in human cells and little was known before how CeECT-2 is regulated in *C. elegans*. To this date, it was known that CeECT-2 localizes to the anterior cortex in early embryos and is important for polarity establishment (Dechant and Glotzer, 2003; Morita et al., 2005). Moreover, it has been shown that CeECT-2 is involved in cytokinesis and targets RHO-1 and Cdc42 (Canevascini et al., 2005; Chan and Nance, 2013; Morita et al., 2005). Furthermore, it has been shown that overexpression of a construct where the N-terminal part of CeECT-2 was deleted in *C. elegans* resulted in bleb formation and resembled the phenotype of a constitutive RHO-1 version suggesting that the N-terminal part of CeECT-2 inhibits the GEF function (Chan and Nance, 2013). However, the defects when N-terminal domain is deleted were only analyzed in interphase and late stage embryos and in presence of endogenous CeECT-2. To exclude that the observed phenotype is resulting from overexpressed mutant CeECT-2, my aim was to test whether deletion of the N-terminal BRCT domains results in membrane blebbing during mitosis when the transgene is expressed at endogenous levels and in absence of endogenous CeECT-2.

To test whether BRCT domains regulate Ect2 activity *in-vivo* by an inhibitory mechanism, I generated transgenic worm strains without all the 3 BRCT domains (CeECT-2<sup>ΔBRCT0+1+2</sup>). I used different approaches to express CeECT-2<sup>ΔBRCT0+1+2</sup>, since the transgene was silenced probably due to cytotoxicity. By two independent approaches, I successfully expressed the transgene, however expression of CeECT-2<sup>ΔBRCT0+1+2</sup> was accompanied with high sterility of the worms. Therefore, very low number of embryos could be analyzed, however I was able to analyze the localization and the cytokinetic phenotype in a few early embryos. In these embryos, CeECT-2<sup>ΔBRCT0+1+2</sup> localized similar as CeECT-2<sup>WT</sup> to the cell cortex and expression of CeECT-2<sup>ΔBRCT0+1+2</sup> did not result in hypercontractility of the cortex.

Expression of CeECT-2<sup>ΔBRCT0+1+2</sup> leads to an enlarged polar body in the 1-cell embryo and to high sterility of the worms. One possibility could be that expression of CeECT-2<sup>ΔBRCT0+1+2</sup> abolishes gonad generation and this might be due to proliferation defects that interfere with gonad growth. In the past it has been shown that CeECT-2 loss of function resulted in high sterility of the worms (Morita et al., 2005). Moreover, it has been shown that CeECT-2 loss of function resulted in developmental defects of the vulva and the authors showed that CeECT-2 activates Ras/MAPK signaling and suggested a cross-talk of CeECT-2 and Ras/MAPK signaling through RHO-1 (Canevascini et al., 2005). Moreover, it has been shown that Ras/MAPK pathway is involved in progression of oogenesis precursors in the pachytene stage of gonadal development and is important for maturation of oocytes (Church et al., 1995). Potentially, like in the vulval development, CeECT-2 and Ras/MAPK pathway could be linked in the process of oocyte production. A possible scenario could be that expression of CeECT-2<sup>ΔBRCT0+1+2</sup> could lead to abnormalities in egg production due to proliferative issues of the oocyte-progenitors that produce the oocytes.

In case GEF function is inhibited via binding of the N-terminal BRCT domains, deletion of the BRCT domains would result in a constitutive active version of CeECT-2. My preliminary data that expression of CeECT-2<sup>ΔBRCT0+1+2</sup> does not induce hypercontractility suggests that Ect2 activity is not elevated when all the three BRCT domains are deleted. These preliminary data are not conclusive with the study of Chan and Nance, 2013 that showed that deletion of the N-terminal part of CeECT-2 results in membrane blebbing resembling a phenotype of hyperactive RhoA (Zanin et al., 2013). A reason for the different results could be the difference in experimental design. In the study of Chan and Nance, they use transient overexpression of CeECT-2<sup>ΔBRCT0+1+2</sup> rather than using single-copy insertions of CeECT-2<sup>ΔBRCT0+1+2</sup> transgene as in my study. Moreover, they only analyzed interphase

cells and did not analyze cells that are in mitosis as shown by my results. Another difference to the previous study of Chan and Nance 2013 is that I only deleted the N-terminal BRCT domains (CeECT-2<sup>ΔBRCT0+1+2</sup>) but did not delete the linker region between the BRCT domains and the GEF domain. The varying results between my study and the study of Chan and Nance could lie in the different protein structure and in the presence of the linker region in my study. In human cells, it has been already shown that deletion of the linker region translocates Ect2 from the nucleus to the cytoplasm in interphase which induces dramatic transforming activity of HsEct2 (Saito et al., 2004). Moreover, my data I obtained in human cells showing that blocking phosphorylation of the linker region in HsEct2 results in hypercontractility support this theory and strongly propose an involvement of the linker region in inhibiting HsEct2 activity. Based on my study and in accordance with the study of Chan and Nance 2013 CeECT-2 could be regulated both via the N-terminal BRCT domains and the linker region and both domains might be important for CeECT-2 activity. One scenario could be that the linker inhibits GEF activity by recruiting mitotic kinases that in turn phosphorylate and inactivate the GEF domain. So, the presence of linker in the CeECT-2<sup>ΔBRCT0+1+2</sup> construct could have prevented hyperactivation even though the N-terminal BRCT domains were deleted. Furthermore, my studies showed that CeECT-2<sup>ΔBRCT0+1+2</sup> localizes to the plasma membrane in early and late stage *C. elegans* embryos which confirms previous observations based on overexpression of CeECT-2<sup>ΔBRCT0+1+2</sup> in late stage embryos with non-mitotic cells in interphase (Chan and Nance, 2013) (Fig. 7). Like in *C. elegans* CeECT-2 it has been shown in human cells that HsEct2<sup>ΔBRCT0+1+2</sup> localizes to the cell cortex but not to the spindle midzone (Su et al., 2011).

A major deficiency in my data lies in the low number of embryos that could be analyzed *in-vivo*, due to high sterility of the worms. Moreover, due to the high sterility of the worms expressing CeECT-2<sup>ΔBRCT0+1+2</sup>, the experiments were very laborious and time-consuming to find embryos that could be imaged. Therefore, on the day where the few embryos were found that expressed CeECT-2<sup>ΔBRCT0+1+2</sup>, unfortunately no controls were imaged in parallel. Whether expression levels in CeEct2<sup>WT</sup> and CeEct2<sup>ΔBRCT0+1+2</sup> are similar could not be compared. Therefore, the lack of hypercontractility in the embryos expressing CeECT-2<sup>ΔBRCT0+1+2</sup> could simply be due to the fact that the expression level was below physiological levels. However due to the small sample size additional studies need to be performed in the future to support this conclusion.

In the future one could test whether the linker is involved in CeECT-2 regulation by deleting the linker in addition of the BRCT domains and test whether the phenotype resembles the results obtained by Chan and Nance, 2013. Another opportunity to test whether the linker is involved in CeECT-2 regulation would be to only delete the linker region or mutate all putative phospho-sites as done in the human construct and then analyze the cytokinetic phenotype and localization in absence of endogenous CeECT-2.

If it is true that expression of CeECT-2<sup>ΔBRCT0+1+2</sup> does not cause hypercontractility, it is still unclear why expression of CeECT-2<sup>ΔBRCT0+1+2</sup> then so strongly interfered with fertility of the worms and why the transgene was always silenced after integration into the genome. In the future one would need to measure and compare expression levels by e.g. Western Blot analysis or live-cell imaging and measuring CeECT-2<sup>ΔBRCT0+1+2</sup> at the cortex and in the cytoplasm in control and CeECT-2<sup>ΔBRCT0+1+2</sup> embryos. The pre-requisite for these experiments will be to find a way to overcome silencing of the transgene and the sterility of the worms to achieve a higher sample number. One possibility could be propagating CeECT-2<sup>ΔBRCT0+1+2</sup> in males under a female promoter. It has been shown before that the promoter *pie-1* is specific only to oocytes, which restricts expression of CeECT-2<sup>ΔBRCT0+1+2</sup> in sperm and has been used to generate transgenic *C. elegans* strains struggling with the expression of cytotoxic transgenes (Mello et al., 1996; Mitchell et al., 2014). Males carrying the CeECT-2<sup>ΔBRCT0+1+2</sup> transgene could then be crossed to wild type hermaphrodites to generate heterozygous F1 offspring that expressed CeECT-2<sup>ΔBRCT0+1+2</sup>. One disadvantage of this approach would be that only heterozygous offspring can be generated carrying one CeECT-2<sup>WT</sup> allele and one CeECT-2<sup>ΔBRCT0+1+2</sup> allele. However, if the hypothesis is true that CeECT-2 BRCT domains inhibit the GEF domain, also in heterozygous animals expression of CeECT-2<sup>ΔBRCT0+1+2</sup> should result in hypercontractility. A big opportunity of this approach could be that enough offspring is generated for subsequent analysis by circumventing sterility of the worm caused by expression of CeECT-2<sup>ΔBRCT0+1+2</sup> in the female gonad.

Another major question of my project was to analyze whether each BRCT domain has a distinct role in regulating CeECT-2 function or whether the BRCT domains function as one module. In 2014 the crystal structure of HsEct2 BRCT domains was resolved by a study from Zou et al., 2014. The study revealed the presence of a third BRCT domain (BRCT0) close to the N-terminus of HsEct2. So far no one in the literature addressed the question

what the role of BRCT0 domain during cytokinesis is. Therefore, I was very excited about testing the localization and function of BRCT0 domain *in-vivo*.

Therefore, I continued my study by deleting BRCT0 (CeECT-2<sup>ΔBRCT0</sup>) and BRCT0+1 (CeECT-2<sup>ΔBRCT0+1</sup>). These transgenic versions of CeECT-2 localize to the plasma membrane similar as wild type CeECT-2 (Fig. 8). Depletion of endogenous CeECT-2 in these strains leads to over 90% embryonic lethality (Fig. 9). The expression of CeECT-2<sup>ΔBRCT0</sup> leads to 16% (n=13) cytokinesis failure in absence of endogenous CeECT-2 when cytokinesis is monitored after 16-20h after the dsRNA injected. Deletion of BRCT0+1 leads to 91% of embryonic lethality and 0% (n=10) of cytokinesis failure after 16-20h RNAi. However, when monitoring first cytokinesis after longer RNAi (30-38h), 63% (n=11) of cytokinesis failure in the 1-cell embryo can be observed (Fig 9). Moreover BRCT0+1 domains are required for normal brood size since deletion of BRCT0 and BRCT1 domain results in dramatic decrease in the number of offspring (Fig. 9). It has been previously shown that expression of the *ect-2(e1178)* allele that harbored deletion of CeECT-2 BRCT1 domain resulted in high sterility and reduction of brood size (Morita et al., 2005). An explanation for the decreased brood size could be that deletion of BRCT0+1 interferes with CeECT-2 function in the germ line and might disrupt gonad function.

Furthermore, deletion of BRCT0 and BRCT0+1 domain result in embryonic lethality since worms expressing CeECT-2<sup>ΔBRCT0</sup> and CeECT-2<sup>ΔBRCT0+1</sup> in absence of endogenous CeECT-2 generate very few and dead embryos. It has been previously shown that generation of mice carrying a homozygous *Ect2* null allele are embryonic lethal and die in the late blastocyst stage showing severe defects in growth (Cook et al., 2011). Immortalized mouse embryonic fibroblasts from these mouse lines showed that *Ect2* loss-of-function resulted in severe defects of cell migration and cell proliferation. A reason why deletion of BRCT0 and BRCT0+1 domains cause embryonic lethality in *C. elegans* could be due to that BRCT0 and BRCT1 domains might impair cell migration in later embryonic stages and could play a role in polarity establishment of different embryonic tissues, e.g. by binding different factors that are expressed in later stages during embryogenesis.

In control embryos no cleavage furrow is formed when endogenous CeECT-2 is depleted. In embryos expressing CeECT-2<sup>ΔBRCT0</sup> a cleavage furrow is formed in the first place, and cytokinesis partially completes in the CeECT-2<sup>ΔBRCT0</sup> and CeECT-2<sup>ΔBRCT0+1</sup> expressing strains. This suggests that BRCT0+1 are mostly important when the cleavage furrow

ingresses. A possible scenario could be that BRCT domains have a role in stabilizing the actomyosin network in the furrow during ingression. One possibility could be that CeECT-2 BRCT0+1 domains bind another factor in the cleavage furrow which further enhances the stability of the actomyosin network during ring ingression.

Together these findings suggest that BRCT0 domain and BRCT1 domains are not important for membrane localization but are required for embryonic viability and cleavage furrow ingression and could hint at separate functions of CeECT-2 during cytokinesis and embryogenesis.

Then I decided to monitor whether CeECT-2 activity changes when the BRCT0 and BRCT1 domains are deleted by using the contractility marker NMY-2. I quantified the signal of mkate2-NMY-2 at the furrow tip in the different strains in presence and absence of endogenous CeECT-2. Before and after depletion of endogenous Ect2 NMY-2 signal is decreased when BRCT0 was deleted (Fig. 10 and Fig. 11). These results suggest that BRCT0 domain promotes NMY-2 recruitment to the furrow. This finding is consistent with a model in which BRCT0 is required for full CeECT-2 activation by recruiting unknown factors to the furrow. Moreover, BRCT0 is only important for furrow ingression but not for formation since a cleavage furrow can be formed without delay. This suggests that BRCT0 has a stabilizing function during furrow ingression. It has been shown that HsEct2 interacts with Anillin via its PH domain and thereby stabilizes actomyosin during ring ingression (Frenette et al., 2012b). One scenario could be that BRCT0 serves as a scaffold, so the PH domain can interact with Anillin and in turn enhance CeNMY-2 in the furrow during ring ingression. The reason that NMY-2 levels are decreased when BRCT0 is deleted even in presence of endogenous could be that CeECT-2<sup>ΔBRCT0</sup> cannot so strongly interact with anillin via its PH domain. Another possibility might be that BRCT0 domain binds an unknown factor and activates it which then recruits anillin to the cleavage furrow. Expression of CeECT-2<sup>ΔBRCT0</sup> might abolish the interaction with this factor and might cause the down-regulation of anillin even in presence of endogenous CeECT-2. In the future one could test whether anillin levels are decreased when CeECT-2<sup>ΔBRCT0</sup> is expressed by analyzing expression of endogenous anillin levels by Western Blot or analyze expression and localization of a fluorescently tagged anillin transgene by live-cell imaging. Furthermore, one could substitute BRCT1 with BRCT0 domain and test whether embryos divide normally and whether the additional BRCT0 domain increases NMY-2 levels in the furrow tip. Moreover, NMY-2 levels were not significantly decreased when BRCT0+1

domains are deleted. However, the control data showed a huge fluctuation which might have caused the lack of significance in the statistical analysis. This might be due to technical reasons, e.g. decrease of laser power of the microscope (UltraViewVOX) over time. In the future, these experiments could be repeated in a shorter time-frame and with a newer confocal spinning disk microscope (Nikon Spinning disk microscope) to test whether these fluctuations can be reduced and to re-analyze whether NMY-2 is indeed decreased when BRCT0+1 domains are deleted.

Finally, I wanted to address the function of the BRCT2 domain in *C. elegans*. Unfortunately, also this transgene was silenced like the CeECT-2<sup>ΔBRCT0+1+2</sup> transgene (not shown). This suggests that BRCT2 domain has a very important role in regulating CeECT-2 activity and that presumably deletion of BRCT2 results in hyperactive CeECT-2 and therefore is cytotoxic.

The major goal of my thesis was to understand whether Ect2 BRCT domains have different roles and how each BRCT domain contributes to temporally and spatially regulating Ect2 activity at the plasma membrane *in-vivo*. Since CeECT-2 and HsEct2 are localized very differently in the dividing cells, I wanted to study whether these differences in localization are connected to different ways of regulation. I used a system in human cancer cells (HeLa cells) where I could express all of the desired transgenes and study their localization and function *in-vivo* (Fig. 14). As in *C. elegans* several HsEct2 transgenes with a fluorescent tag were generated and designed to be RNAi resistance against siRNA targeting endogenous HsEct2. The transgenes were then integrated as a single copy in the same location of the genome and expression was induced with Tetracycline (Fig. 12 and Fig. 13).

I deleted BRCT0 domain and studied the localization, function and cytokinetic phenotype in the cell line expressing HsEct2<sup>ΔBRCT0</sup>. As in HsEct2<sup>WT</sup>, HsEct2<sup>ΔBRCT0</sup> localizes to the plasma membrane (Fig. 15). However, deletion of BRCT0 causes a strong reduction in the localization at the spindle midzone and results in equal distribution of HsEct2<sup>ΔBRCT0</sup> at the cell equator and the cell poles (Fig. 17). This result shows that BRCT0 contributes to spindle midzone localization and is required to enrich HsEct2 at the cell equator. In contrast, in *C. elegans* CeECT-2 does not localize to the spindle midzone; however, deletion of BRCT0 domain does not alter the localization of CeECT-2 at the anterior cell cortex but CeECT-2<sup>ΔBRCT0</sup> appears to be weaker at the cortex when compared to control (Fig. 8). Unfortunately, the weak signal of CeECT-2<sup>ΔBRCT0</sup> made a solid quantification of

the fluorescence intensities at the cell cortex quite difficult. In summary, this shows that in both systems BRCT0 is involved in membrane targeting, in *C. elegans* to the anterior cortex and in human cells to the equatorial plasma membrane.

Then I tested the function of HsEct2 BRCT0 domain and quantified the cytokinetic failure before and after depleting endogenous HsEct2. Cells expressing HsEct2<sup>ΔBRCT0</sup> have no cytokinesis defects in presence and absence of endogenous HsEct2 (Fig. 15). My findings show that BRCT0 domain is not required for HsEct2 function but might play a role in targeting and enriching HsEct2 at the cell equator. However, cytokinesis is successful despite the fact that HsEct2<sup>ΔBRCT0</sup> is not enriched at the equatorial plasma membrane. This suggests that enrichment at the cell equator is dispensable for HsEct2 function. These data are consistent with the *C. elegans* data where I could show that deletion of BRCT0 results in mainly successful cytokinesis after depletion of endogenous CeECT-2 (84% success). Moreover, in *C. elegans* BRCT0 domain is not required for cytokinesis but important for viability (Fig. 9). These results are quite surprising since BRCT0 domain is conserved among *C. elegans* and human cells and one would expect that the conservation results from an important function of this domain during cytokinesis. One possibility could be that BRCT0 has a role besides cytokinesis during tissue development in *C. elegans*, e.g. in polarity establishment. To further proof that BRCT0 domain has no function in HeLa cells, in the future one could over-express BRCT0 domain besides endogenous HsEct2 and test whether overexpression affects the cytokinetic phenotype of the cells.

Lastly, I analyzed membrane blebbing by live-cell imaging in cells expressing HsEct2<sup>ΔBRCT0</sup> and showed that deletion of BRCT0 domain does not increase membrane blebbing *in-vivo* and blebbing is slightly reduced which could be a hint for decreased contractility (Fig.18). This is in accordance of the *C. elegans* data where I showed that deletion of BRCT0 results in decrease of Myosin II levels in the furrow tip which represents a read-out for decreased contractility in this worm strain. These data are consistent with a model where BRCT0 has a positive regulatory function during cytokinesis. Probably BRCT0 simply promotes GEF activity itself by various means. Another possibility could be that BRCT0 binds an unknown factor that enhances contractility during ring ingression. A possible factor could be anillin. In the future, one could test whether cortical anillin levels are decreased when BRCT0 domain is deleted. Lastly one could analyze BRCT0 by a whole-genome proteomic approach with IPs and mass-spectrometry and identify potential binding partners of BRCT0 domain.

Next, I generated transgenic cell lines where I deleted BRCT0+1 and BRCT1 domain to test how Ect2 activity is controlled by BRCT1 (Fig. 19). Former studies showed that when all three BRCT domains are deleted, as well as when specific point mutations are introduced at T153 and K195, spindle midzone localization is abolished (Chalamalasetty et al., 2006; Su et al., 2011). Whether the BRCT0 or BRCT2 domains in addition to BRCT1 domain are involved in spindle midzone and cortical localization has not yet been addressed. HsEct2<sup>ΔBRCT0+1</sup> and HsEct2<sup>ΔBRCT1</sup> do not localize to the spindle midzone (Fig. 19 and Fig. 20). HsEct2<sup>ΔBRCT0+1</sup> evenly distributes over the entire cell cortex, other than in HsEct2<sup>WT</sup> that localizes to the spindle midzone and concentrates at the cell equator (Fig. 20). These data validate the results from Kotýnková et al., 2016 that BRCT1 domain is the major spindle midzone binding domain. Moreover, my data shows that BRCT1 is not only important for spindle midzone localization but is required to enrich HsEct2 at the cell equator. It has been shown that BRCT1 domains binds to MgcRacGAP at the spindle midzone (Tatsumoto et al. 1999; Su, Takaki, and Petronczki 2011; Yüce et al., 2005). The reason why midzone binding is lost might be the fact that HsEct2<sup>ΔBRCT0+1</sup> can no longer bind to MgcRacGAP at the spindle midzone. Since HsEct2<sup>ΔBRCT0+1</sup> does no longer localize to the spindle midzone this might be the reason why HsEct2<sup>ΔBRCT0+1</sup> is not enriched at the cell equator but localizes all around the cortex. It has been shown that the interaction of HsEct2 and MgcRacGAP is not required for successful cytokinesis. One possible scenario could be that the interaction of HsEct2 and MgcRacGAP is not required for successful cytokinesis, but it is required for the enrichment of HsEct2 at the equatorial cortex. Cytokinesis is mainly successful even though HsEct2<sup>ΔBRCT0+1</sup> is not enriched at the equatorial plasma membrane in presence of endogenous HsEct2. However, expression of HsEct2<sup>ΔBRCT0+1</sup> resulted in around 75% of multinucleation in absence of endogenous HsEct2. This suggests that equatorial enrichment is not important for HsEct2 function since expression of HsEct2<sup>ΔBRCT0</sup> also localized all around the cell cortex but did not result in increased multincueation in absence of endogenous HsEct2. However, these data are showing localization and cytokinesis of HsEct2<sup>ΔBRCT0+1</sup> in presence of endogenous HsEct2 and function in presence and absence of endogenous HsEct2. In the future one could analyze localization in absence of endogenous HsEct2 to analyze whether HsEct2<sup>ΔBRCT0+1</sup> still localizes to the membrane since localization could be very different when endogenous HsEct2 is depleted. A reason for this could be that endogenous HsEct2 and transgenic HsEct2<sup>WT</sup> bind to each other. A prerequisite for these experiments is that a broad depletion of endogenous HsEct2 must be achieved. According to my Western Blots showing

expression levels of endogenous HsEct2 depletion levels were very good. However, in my experiments, endogenous Ect2 RNA levels could only be depleted by 79%, in contrast to different studies using the same siRNA oligo which published higher depletion levels (up to 100% percent). Moreover, it has been published that depletion of Ect2 caused complete abolishment of a cytokinetic furrow in almost 100% of analyzed cells (Kim et al., 2005; Yüce et al., 2005). However, no higher depletion levels could be achieved in my experiments and cells showed lower percentage of a “no-furrow formation” phenotype as previously published which suggested that the depletion of endogenous Ect2 is not fully penetrant. I undertook different attempts to increase the depletion level that implied titration of cell number, RNA concentration, different transfection reagents and different time points. One reason why the depletion levels were so variable from the published results could be different cell culture conditions, e.g. different cell maintenance media, cell culture flasks with different coatings that could have increased cell adhesion and supported cell division even though endogenous HsEct2 was depleted. Another reason could be technical issues of used devices, e.g. incubators. In the future, another Ect2 siRNA oligo that has been used in more recent studies could be tested whether it increases *Ect2(RNAi)* depletion levels (Kotýnková et al., 2016; Su et al., 2011). This implies that generated transgenic HsEct2 constructs have to be re-cloned to introduce a new RNAi resistant allele in the BRCT2 domain, so the transgenes will be resistant to endogenous HsEct2 depletion by the different siRNA oligo. In my constructs, the used siRNA oligo targeted BRCT1 domain and therefore RNAi resistance is carried in the same region of BRCT1 domain.

In the past it has been shown that deletion of the GEF domain, the PH domain and the PBS domain increase bi- and multinucleation in human cells (Su et al., 2011). Whether deletion of the BRCT domains increase multinucleation has not yet been answered. Moreover, it has not yet been addressed how cytokinesis is affected when single BRCT domains are deleted. Therefore, I tested the function of BRCT1 domain and counted mono-, bi- and multinucleation in the cells in presence and absence of endogenous HsEct2. Expression of HsEct2<sup>ΔBRCT1</sup> strongly increases bi- and multinucleation in absence of endogenous HsEct2 (Fig. 19). This shows that BRCT1 domain is required for cytokinesis. This data is also consistent with the *C. elegans* data where I showed that deletion of BRCT1 domain interferes with cytokinesis in 63% of embryos (Fig. 9). These data strongly support the hypothesis that BRCT1 domain is crucial for Ect2 function among different animal species like *C. elegans* and human cells.

Moreover, I analyzed contractility of cells expressing Ect2 transgenes without BRCT1 domain. In the past, it has been shown that hyperactive RhoA results in increased membrane blebbing (Zanin et al., 2013). Cells expressing HsEct2<sup>ΔBRCT0+1</sup> and HsEct2<sup>ΔBRCT1</sup> exhibit mild increase in membrane protrusions during anaphase but not during metaphase (Fig. 20). A reason for the difference in membrane blebbing could be that HsEct2<sup>ΔBRCT0+1</sup> is still inactive in metaphase and gets activated in anaphase. Another possibility would be that HsEct2<sup>ΔBRCT0+1</sup> might be mildly hyperactive in metaphase but is not localized to the plasma membrane in metaphase, therefore there is no membrane blebbing. The blebbing in anaphase might be due to amino acids that are deleted in the HsEct2<sup>ΔBRCT0+1</sup> mutant, e.g. T153 and K195. In the mutant expressing HsEct2<sup>T153A, K195M</sup> that has been shown to abolish spindle midzone binding show a mild increase in membrane blebbing as well. HsEct2<sup>T153A, K195</sup> supposedly only disrupt HsEct2 and MgcRacGAP interaction, so it is quite surprising that it induces membrane blebbing. A possible explanation could be that localization of HsEct2 is not important for successful cytokinesis but probably to capture HsEct2 at the spindle midzone in an “inactive” state until HsEct2 then translocates to the plasma membrane. Another scenario could be that HsEct2<sup>T153, K195</sup> are important not only for MgcRacGAP binding but are important amino acids that regulate BRCT1 binding to the GEF domain and thereby controlling Ect2 activity. In the future one has to test whether absence of BRCT1 domain results in membrane blebbing in absence of endogenous Ect2 since the cytokinetic phenotype in the mutants might be very different when endogenous Ect2 is depleted. Moreover, one could analyze whether anillin levels are increased at the cell poles since it has been shown that HsEct2 binds to anillin and HsEct2<sup>ΔBRCT0+1</sup> is equally distributed at the equator and at the cell poles in absence of endogenous HsEct2. Probably HsEct2<sup>ΔBRCT0+1</sup> is more active and this could cause increase in anillin levels at the cell poles. Therefore, one could expect that also anillin is shifted from the cell equator and localizes all around the cell cortex to test whether this interferes with furrow formation. To distinguish whether HsEct2<sup>ΔBRCT0+1</sup> only localizes anillin to the cell poles because of binding to it or by increased activity of HsEct2<sup>ΔBRCT0+1</sup> a possible experiment would be to inhibit RhoA in these cells and analyze whether Anillin levels are decreasing at the cell poles. If anillin localization at the cell poles is independent of an increased activity of HsEct2<sup>ΔBRCT0+1</sup>, anillin levels should not be decreased at the poles when RhoA is inactivated.

The next question I addressed was what the role of BRCT2 domain is during cytokinesis. In the literature this question has yet not been addressed and very little is known about the specific role of BRCT2 domain. I generated different transgenic cell lines where I deleted BRCT2, BRCT1+2 and all three BRCT domains. Deletion of BRCT2 leads to a strong reduction of HsEct2<sup>ΔBRCT2</sup> at the spindle midzone similar to HsEct2<sup>ΔBRCT0</sup> (Fig. 21). Moreover, cells expressing HsEct2<sup>ΔBRCT2</sup> show plasma membrane localization around the cell periphery, in contrast to HsEct2<sup>WT</sup> that is enriched at the cell equator and at the spindle midzone (Fig. 22). As expected HsEct2<sup>ΔBRCT1+2</sup> and HsEct2<sup>ΔBRCT0+1+2</sup> do not localize to the spindle midzone as expected, due to the absence of BRCT1 domain (Fig. 21). Also, they show cortical localization similar to the cells expressing HsEct2<sup>ΔBRCT2</sup>. These data suggest that BRCT2 contributes to spindle midzone localization and is required to enrich HsEct2 to the cell equator. In the literature, it has been suggested that Ect2 BRCT1 domain binds MgcRacGAP that was phosphorylated before by Plk1 (Burkard et al., 2009; Petronczki et al., 2007; Wolfe et al., 2009). Moreover Kotýnková et al., 2016 suggested that T153 and K195 within the BRCT1 domain are important for MgcRacGAP interaction and it has not been clarified whether other BRCT domains are also involved in spindle midzone localization. My data reveals that not only BRCT1 domain is important, but also BRCT2 (and BRCT0 domain as discussed before) are involved in spindle midzone localization. Moreover, it has been suggested that Ect2 PH domain is involved in plasma membrane targeting, but it has not yet been suggested that BRCT2 domain is involved in spindle midzone binding nor in equatorial plasma membrane targeting. Surprisingly, when spindle midzone localization is reduced, equatorial membrane enrichment is lost and Ect2 localizes around the entire cell cortex. Therefore, it seems quite likely that the BRCT domains first target Ect2 to the spindle midzone so it can be loaded and enriched at the equatorial plasma membrane. However, the study of Kotýnková et al. in 2016 showed that neither the binding of Ect2 to MgcRacGAP nor spindle midzone localization is crucial for the success of cytokinesis. Therefore, spindle midzone binding of Ect2 must have a different function than Ect2 activation. One possibility could be that BRCT2 together with BRCT1 domain targets Ect2 to the spindle midzone where Ect2 binds to MgcRacGAP to concentrate it at the spindle midzone, so it can be later more easily enriched at the equatorial plasma membrane. Another scenario would be that by binding of Ect2 to MgcRacGAP at the spindle midzone, Ect2 is captured in a specific site to prevent premature membrane targeting before anaphase starts. A further possibility would be that Ect2 is concentrated at the spindle midzone and captured there for creating a concentrated pool of Ect2 for subsequent activation by mitotic

kinases. Another scenario could be that Ect2 PH domain is masked by BRCT2 domain in an inactive state, so it cannot translocate to the plasma membrane. When Ect2 gets active, BRCT2 domain is no longer masking the PH domain and Ect2 can then translocate to the equatorial plasma membrane.

Next, I studied whether BRCT2 domain is required for cytokinesis and I quantified cytokinetic failure in the cell line expressing the HsEct2<sup>ΔBRCT2</sup> transgene in presence and absence of endogenous HsEct2 (Fig. 21). With my data I could demonstrate that cells expressing HsEct2<sup>ΔBRCT2</sup> show increased bi- and multinucleation but can partially rescue the cytokinesis defect caused by absence of endogenous Ect2 (Fig. 21). Together these data suggest that BRCT2 domain is required for cytokinesis. The data is consistent with former findings that suggested that BRCT1 and BRCT2 domains inhibit GEF activity (Kim et al., 2005; Saito et al., 2004; Yüce et al., 2005) and my data validate the former results that show that BRCT1 and BRCT2 domains are required for cytokinesis. In cell lines expressing HsEct2<sup>ΔBRCT1+2</sup> and HsEct2<sup>ΔBRCT0+1+2</sup> depletion of endogenous HsEct2 cytokinetic failure is higher than when deleting only BRCT2 domain which suggests HsEct2<sup>ΔBRCT2</sup> is partial functional. Surprisingly cells that express HsEct2 where BRCT2 domain was substituted with BRCT1 domain (HsEct2<sup>ΔBRCT1+BRCT1</sup>) the multinucleation is higher than in cells expressing HsEct2<sup>ΔBRCT2</sup> which shows that HsEct2<sup>BRCT1-BRCT1</sup> is not partially functional. A reason why HsEct2<sup>ΔBRCT2</sup> transgene could be partially functional could be that BRCT2 is mostly important for the inhibition of the GEF domain but cells can cope to a certain extent with an increase of Ect2 activity. If BRCT2 is not deleted but replaced, the additional BRCT1 domain in the HsEct2<sup>ΔBRCT1+BRCT1</sup> cells could sterically inhibit the other BRCT1 domain and important factors such as MgcRacGAP could not bind to BRCT1 domain. Another scenario could be that the presence of the second BRCT1 domain additionally enhances Ect2 activity by recruiting unknown factors that enhance contractility of the cells. One caveat of the data is that the transgenes could not be stable and are degraded in absence of endogenous Ect2. Thus, in the future the presence of the transgenes should be analyzed in absence of endogenous Ect2, e.g. by live-cell imaging and western blot analysis to ensure transgenes are stable in absence of endogenous Ect2.

Furthermore, cells expressing HsEct2 transgenes without BRCT2 domain showed massive membrane blebbing during cytokinesis and membrane blebbing already occurred during metaphase (Fig. 22 and Fig. 23). Importantly membrane blebbing in HsEct2<sup>ΔBRCT2</sup> was as strong as in cells HsEct2<sup>ΔBRCT0+1+2</sup> and a cell line where I substituted BRCT2 domain with

BRCT1 domain (Fig. 22). Since it has been shown in the past that hyperactivation of RhoA results in increased membrane protrusions (Zanin et al., 2013), I was interested whether the large protrusions resulted from hyperactive RhoA. Therefore, I used anillin levels as a read-out for active RhoA and I could show that in cells expressing HsEct2<sup>ΔBRCT2</sup> anillin levels are increased at the plasma membrane which suggests that RhoA is hyperactivated in these cells (Fig. 24). Finally, I tested whether inhibition of RhoA by a specific inhibitor for RhoGTPases (C3 Inhibitor) can reduce membrane blebbing in cells expressing HsEct2<sup>ΔBRCT2</sup>. Indeed, inactivation of RhoA reduces membrane blebbing in the cells expressing HsEct2<sup>ΔBRCT2</sup> (Fig. 23). These data are consistent with former findings that Ect2 BRCT domains inhibit the GEF domain. My data further revealed that it is mainly BRCT2 domain that inhibits GEF function. Moreover, these data show that Ect2 BRCT domains do not act as one module but have distinct roles regarding the regulation of Ect2. However, the presented data was generated in presence of endogenous Ect2 since depletion of endogenous Ect2 was not fully penetrant after many approaches to increase the knock-down efficiency. Phenotypes might change after endogenous Ect2 is depleted since transgenes could bind to endogenous Ect2 and transgenes could localize very differently in absence of endogenous Ect2. Therefore, it is a prerequisite for the future to establish RNAi conditions that allow analyzing cytokinetic phenotypes of the transgenes in absence of endogenous Ect2.

It has been proposed that the linker region between the N-terminal BRCT2 domain and the DH domain is important for HsEct2 regulation (Hara et al., 2006; Niiya et al., 2006; Saito et al., 2004; Yüce et al., 2005). It has been shown by a study from Saito et al., 2004, that deletion of the entire linker region leads to a high increase in transforming activity of HsEct2. The authors showed that HsEct2 without the linker localizes in cytoplasm and not in the nucleus in interphase and claimed that this is due to two nuclear localization signals within the linker region that are lost due to deletion of the entire region. Moreover, they claimed that due to loss of the two NLS sites, HsEct2 without the linker is delocalized from the nucleus to the cytoplasm where it can activate RhoA.

To study whether the linker region of HsEct2 is involved in regulating activity of HsEct2, the linker region was analyzed, and I found that serines and threonines are strongly enriched in this region compared to the rest of the protein (Fig.25B). Since serines and threonines are major phospho-targets of specific kinases, such as the mitotic kinases Cdk1 and Plk1, the high content of serines and threonines suggested that the linker might harbor a

regulatory function of HsEct2. Therefore, I generated a cell line where I substituted all serines and threonines with alanines to test whether phosphorylation of these sites is important for HsEct2 function (Fig. 25B). HsEct2<sup>LinkerAA</sup> strongly localizes to the plasma membrane and to microtubules (Fig. 25C). Importantly HsEct2<sup>LinkerAA</sup> localizes to the plasma membrane already in metaphase and also to microtubules before the spindle midzone is established (Fig. 25C). Surprisingly, exchange of serines/threonines to alanines led to a dramatic increase of HsEct2<sup>LinkerAA</sup> activity measured by quantifying membrane blebbing, similar to the phenotype of cells expressing HsEct2<sup>ΔBRCT2</sup> (Fig. 25D).

## Summary of CeECT-2 and HsEct2 localization studies

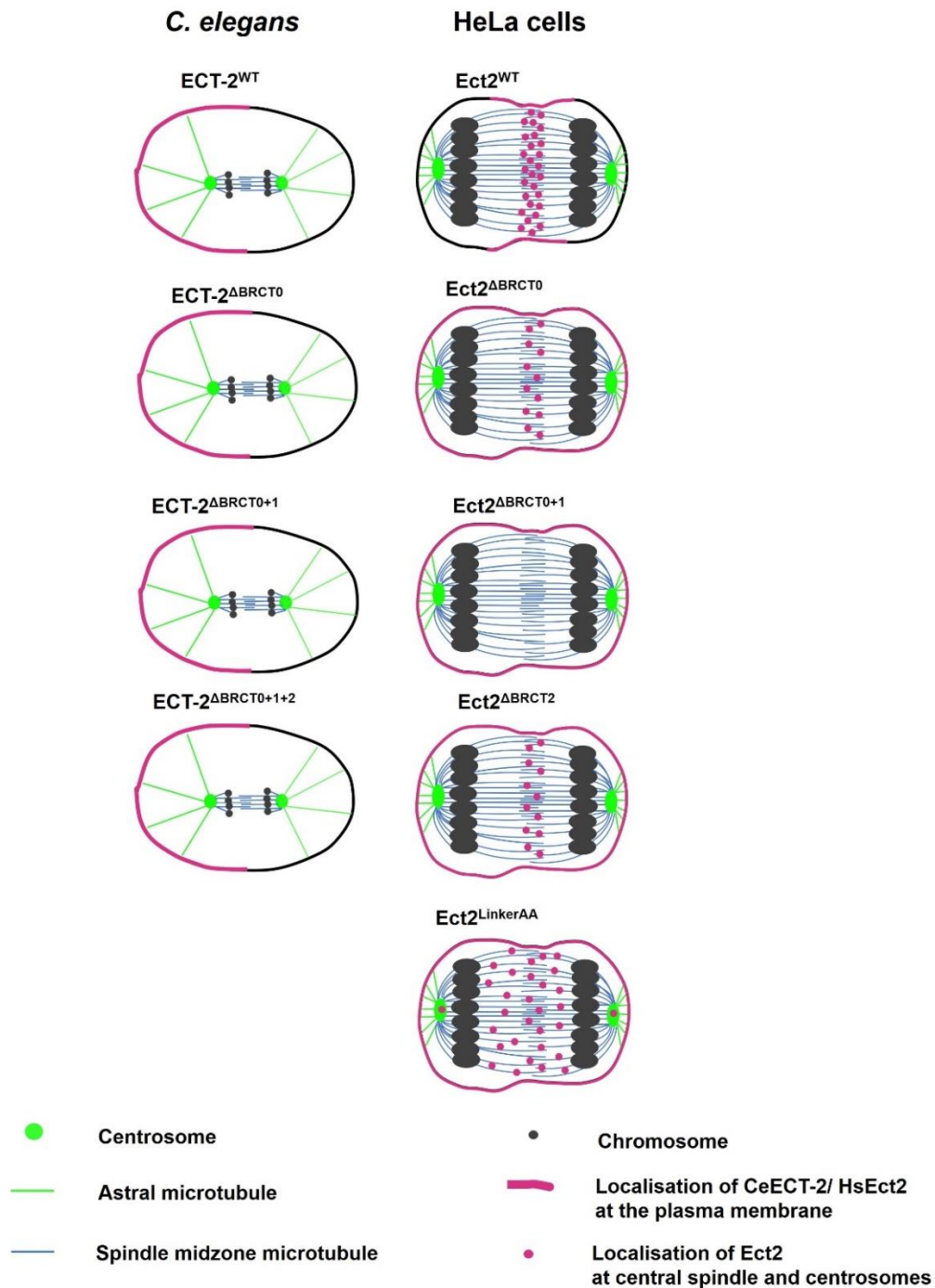


**Fig. 26. BRCT domains are not required for plasma membrane targeting in *C. elegans*, but for equatorial enrichment in human cells.** Summary of CeECT-2 and HsEct2 localization studies in *C. elegans* and human cells. In *C. elegans*, deletion of BRCT0, BRCT0+1 and BRCT0+1+2 domains do not affect cortical localization of CeECT-2. In human cells, deletion of BRCT0 and BRCT2 domains results in reduced spindle midzone binding and localization of the transgenes all around the cell periphery. Deletion of BRCT1 domain abolishes spindle midzone localization completely. Mutation of the linker region also affects equatorial plasma membrane targeting and enriches HsEct2 at the centrosomes and spindle midzone microtubules.

These data suggest a role of the linker in the localization and regulating the activity of HsEct2. In the study of Saito et al., 2004, the authors argue that two NLS sites in the linker region are important for the correct localization of HsEct2 in the nucleus before NEB and deletion of these two NLS sites by deleting the linker leads to a premature release of HsEct2 into the cytoplasm and to a premature activity. In contrast to the deletion construct from Saito et al., 2004, in my HsEct2<sup>LinkerAA</sup> construct I did not delete any amino acid and importantly, I kept the NLS sites in the linker region. It has been shown by another study that anillin is regulated by Ran via its NLS site in the C-terminus and its Rho-binding domain (RBD) by an autoinhibitory mechanism (Beaudet et al., 2017). The model they propose is that the NLS in the C-terminus of anillin is masked and binding of RhoA-GTP to anillin RBD releases the NLS and anillin translocates to the cell cortex where it binds to specific importins. A possibility how Ect2 linker could be involved in regulating Ect2 activity is through its NLS sites that could be masked, e.g. by BRCT2 domain when Ect2 is inactive. When Ect2 is activated by release of BRCT2 domain from the GEF domain, the NLS site could target Ect2 to the plasma membrane where it binds to specific importins. However, this possible scenario does not explain why HsEct2<sup>LinkerAA</sup> shows increased activity. Another possibility could be that phosphorylations in the linker region recruit an unknown factor to Ect2 that binds the linker and thereby masks the NLS site. In cells expressing HsEct2<sup>LinkerAA</sup> phosphorylations of the linker are absent which exposes the NLS site, therefore NLS binds to importins and Ect2 translocate to the cell cortex. This raises the question whether importins are involved in the regulation of Ect2 and one could test in the future whether Ect2 and importins co-localize at the cell equator or analyze by Co-IP studies whether Ect2 linker region binds to importins in mitosis.

The more likely explanation is that Ect2 activity is regulated through phosphorylations of specific sites in the linker. In the past it has been shown that Cdk1 phosphorylates HsEct2 at threonine 342 and prevents the association with MgcRacGAP in metaphase (Yüce et al., 2005). Moreover, it is thought that Cdk1 primes Ect2 at a specific site (threonine 412) for subsequent association with Plk1 (Niiya et al., 2006). It has been shown that a phosphodeficient mutant (T412A) abolished the interaction of Plk1 and Ect2 which leads to a reduced accumulation of GTP-bound RhoA. This showed that phosphorylation of T412 is important for the catalytic activity of Ect2. In my study T412 was also part of the serines and threonines that were exchanged with an alanine to block phosphorylation. However, in my generated linker mutant HsEct2<sup>LinkerAA</sup>, activity seems to be increased and not reduced

since expression leads to massive membrane protrusions similar to the phenotype when RhoA is constitutively active. One possibility how mutation of serines and threonines within the linker region could affect Ect2 activity is that in normal physiological conditions, phosphorylation of these sites by e.g. Cdk1 keeps HsEct2 in an inactive state after NEB and before anaphase onset. When Cdk1 activity declines at metaphase/anaphase transition and phosphorylations are removed, which could lead to a conformational change in the linker region of HsEct2. The conformational change then could open the structure of the N-terminal domain and release the GEF domain so RhoA can then be activated. A caveat of the data is that expression levels in cells expressing HsEct2<sup>LinkerAA</sup> were not measured since these were the last experiments before finishing the study. So, the differences in localization and membrane blebbing could be due to varying expression levels. In the future it has to be tested whether HsEct2<sup>LinkerAA</sup> is functional by performing multinucleation assays in presence and absence of endogenous Ect2. One could also test whether mutation of the NLS changes the localization and activity of Ect2. In addition, one could analyze the different mutated phospho-sites in clusters to determine which region and sites are causing the observed phenotypes. Eventually one would aim to identify single amino acids that are important for regulation of Ect2 activity in the linker region. Moreover, the cytokinetic phenotype of HsEct2<sup>LinkerAA</sup> has to be determined also in absence of endogenous Ect2. One could also test whether shifting the NLS site to another part of the protein, e.g. the C-terminus changes Ect2 activity and localization to test whether the specific position of the NLS site in the linker is important for the phenotype. This could answer the question whether NLS site is masked by another domain, e.g. BRCT2 domain.

In conclusion my results suggest that HsEct2 is regulated via an inhibitory two-step process: the BRCT2 domain mainly binds the GEF domain *in-vivo*. Additionally, phosphorylation of the linker region by e.g. Cdk1 helps to keep HsEct2 in an inactive state. At anaphase onset when Cdk1 is inactivated HsEct2 gets dephosphorylated and undergoes a conformational change the BRCT2 domain unbinds from the GEF domain so RhoA can be activated and the contractile ring can assemble. It has been shown that Ect2 is targeted to the plasma membrane via its PH domain (Su et al., 2011) and a speculative scenario could be that Ect2 is enriched at the equatorial plasma membrane by either its BRCT domains, or by the binding of the BRCT domains to a yet unknown factor that is localized to the cell equator. A potential candidate would be the scaffold protein anillin that localizes to the equatorial plasma membrane and which is a crucial protein of the contractile ring

that interacts with many different components of the contractile ring, such as Ect2, RhoA and Myosin II. This proposed mechanism is consistent with the current model proposed by Kotýnková et al., 2016 which showed neither spindle midzone localization nor MgcRacGAP interaction is important for regulating HsEct2 activity *in-vivo*. My study adds to the current model and revealed that mainly BRCT2 domain is the inhibitory domain of Ect2. Moreover, my data added Ect2 linker region as another regulatory region during mitosis that has not yet been implied by the past studies and suggests that Ect2 activation is controlled at multiple levels.

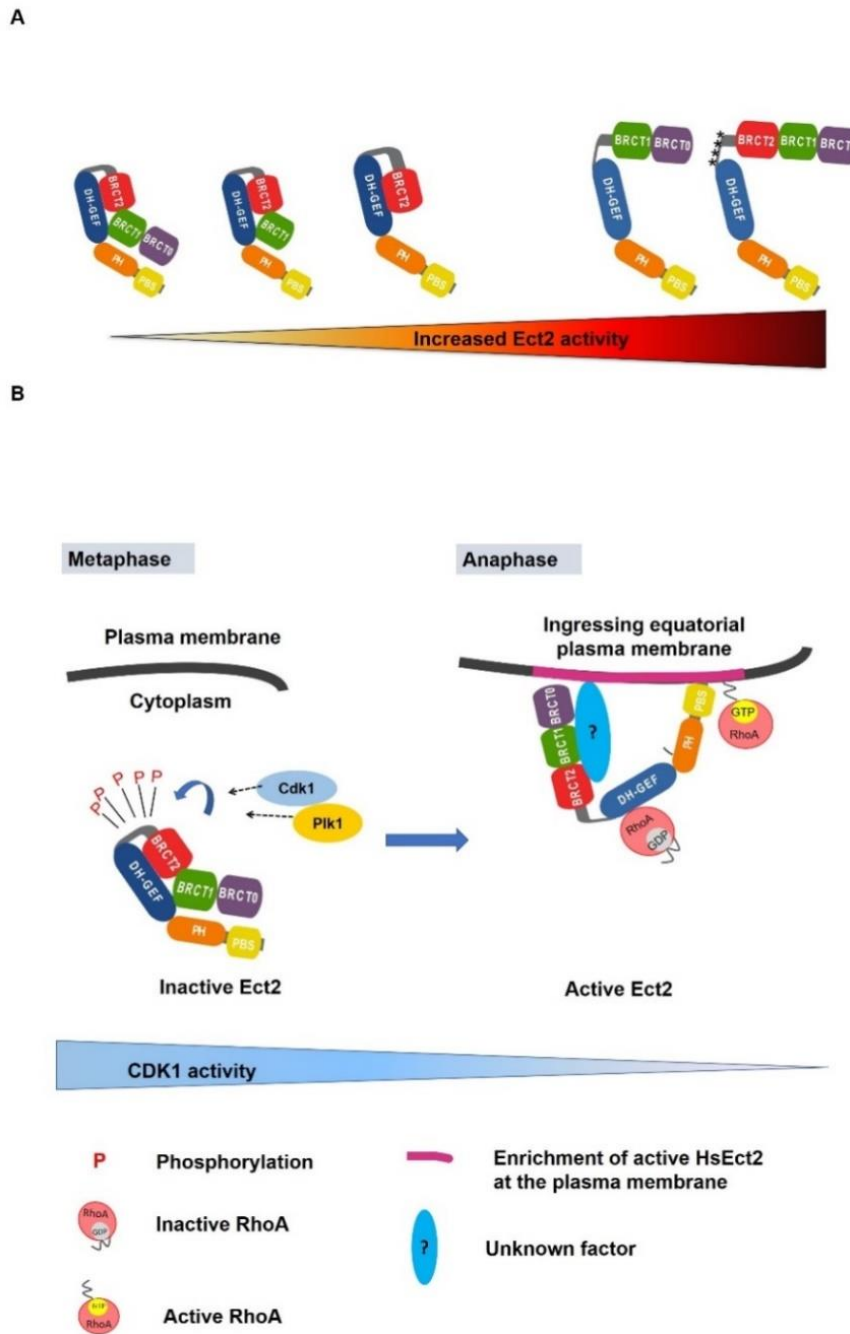


**Fig. 27. Model of HsEct2 activity regulation.** (A) HsEct2 activity is regulated by the binding of HsEct2 BRCT1 and BRCT2 domain to the GEF domain. BRCT2 domain is the major inhibiting domain of the GEF domain. Deletion of BRCT0 slightly decreases HsEct2 activity, deletion of BRCT0+1 slightly increases HsEct2 activity. When BRCT2 domain is deleted, HsEct2 hyperactive. Mutation of the linker region also results in hyperactivity. (B) Model of HsEct2 regulation. In metaphase, binding of BRCT2 domain to the GEF domain and phosphorylation of the linker region keeps HsEct2 in an inactive state. At metaphase to anaphase transition when Cdk1 levels decline and the linker is dephosphorylated, HsEct2 gets active. HsEct2 is targeted to the plasma membrane via its PH-PBS domain and enriched at the equatorial plasma membrane by the binding of the BRCT domains to a yet unknown factor that is localized to the cell equator. Another possibility could be that the BRCT domains themselves could contribute to enrich Ect2 at the equatorial plasma membrane by targeting the Ect2 to the spindle midzone.

## Literature

Addi, C., Bai, J., and Echard, A. (2018). Actin, microtubule, septin and ESCRT filament remodeling during late steps of cytokinesis. *Curr. Opin. Cell Biol.* *50*, 27–34.

Aktories, K., Braun, U., Rösener, S., Just, I., and Hall, A. (1989). The rho gene product expressed in *E. Coli* is a substrate of botulinum ADP-ribosyltransferase C3. *Biochem. Biophys. Res. Commun.* *158*, 209–213.

Beudet, D., Akhshi, T., Phillipp, J., Law, C., and Piekny, A. (2017). Active Ran regulates anillin function during cytokinesis. *Mol. Biol. Cell* *28*, 3517–3531.

Bement, W.M., Miller, A.L., and Von Dassow, G. (2006). Rho GTPase activity zones and transient contractile arrays. *BioEssays* *28*, 983–993.

Berens, C. (1994). Mechanisms Underlying Expression of Tn10-Encoded Tetracycline Resistance. *Annu. Rev. Microbiol.* *48*, 345–369.

Bringmann, H., and Hyman, A.A. (2005). A cytokinesis furrow is positioned by two consecutive signals. *Nature* *436*, 731–734.

Burkard, M.E., Maciejowski, J., Rodriguez-Bravo, V., Repka, M., Lowery, D.M., Clauser, K.R., Zhang, C., Shokat, K.M., Carr, S.A., Yaffe, M.B., et al. (2009). Plk1 Self-Organization and Priming Phosphorylation of HsCYK-4 at the Spindle Midzone Regulate the Onset of Division in Human Cells. *PLoS Biol.* *7*, e1000111.

Canevascini, S., Marti, M., Fröhli, E., and Hajnal, A. (2005). The *Caenorhabditis elegans* homologue of the proto-oncogene *ect-2* positively regulates RAS signalling during vulval development. *EMBO Rep.* *6*, 1169–1175.

Casamayor, A. (2002). Bud-site selection and cell polarity in budding yeast. *Curr. Opin. Microbiol.* *5*, 179–186.

Chalamalasetty, R.B., Hümmer, S., Nigg, E. a, and Silljé, H.H.W. (2006). Influence of human *Ect2* depletion and overexpression on cleavage furrow formation and abscission. *J. Cell Sci.* *119*, 3008–3019.

Chan, E., and Nance, J. (2013). Mechanisms of CDC-42 activation during contact-induced cell polarization. *J. Cell Sci.* *126*, 1692–1702.

Church, D.L., Guan, K.L., and Lambie, E.J. (1995). Three genes of the MAP kinase cascade, mek-2, mpk-1/sur-1 and let-60 ras, are required for meiotic cell cycle progression in *Caenorhabditis elegans*. *Development* *121*, 2525–2535.

Cook, D.R., Solski, P.A., Bultman, S.J., Kauselmann, G., Schoor, M., Kuehn, R., Friedman, L.S., Cowley, D.O., van Dyke, T., Yeh, J.J., et al. (2011). The Ect2 Rho Guanine Nucleotide Exchange Factor Is Essential for Early Mouse Development and Normal Cell Cytokinesis and Migration. *Genes and Cancer* *2*, 932–942.

Crest, J., Concha-Moore, K., and Sullivan, W. (2012). RhoGEF and Positioning of Rappaport-like Furrows in the Early *Drosophila* Embryo. *Curr. Biol.* *22*, 2037–2041.

D'Avino, P. (2015). Cytokinesis in Animal Cells. *Cold Spring Harb Perspect Biol.* *7(4)*, a015834.

Dambournet, D., Machicoane, M., Chesneau, L., Sachse, M., Rocancourt, M., El Marjou, A., Formstecher, E., Salomon, R., Goud, B., and Echard, A. (2011). Rab35 GTPase and OCRL phosphatase remodel lipids and F-actin for successful cytokinesis. *Nat. Cell Biol.* *13*, 981–988.

von Dassow, G. (2009). Concurrent cues for cytokinetic furrow induction in animal cells. *Trends Cell Biol.* *19*, 165–173.

Dechant, R., and Glotzer, M. (2003). Centrosome separation and central spindle assembly act in redundant pathways that regulate microtubule density and trigger cleavage furrow formation. *Dev. Cell* *4*, 333–344.

Dephoure, N., Zhou, C., Villen, J., Beausoleil, S.A., Bakalarski, C.E., Elledge, S.J., and Gygi, S.P. (2008). A quantitative atlas of mitotic phosphorylation. *Proc. Natl. Acad. Sci.* *105*, 10762–10767.

Drechsel, D.N., Hyman, A.A., Hall, A., and Glotzer, M. (1997). A requirement for Rho and Cdc42 during cytokinesis in *Xenopus* embryos. *Curr. Biol.* *7*, 12–23.

Elia, A.E.H. (2003). Proteomic Screen Finds pSer/pThr-Binding Domain Localizing Plk1 to Mitotic Substrates. *Science* (80-. ). *299*, 1228–1231.

Elia, N., Fabrikant, G., Kozlov, M.M., and Lippincott-Schwartz, J. (2012). Computational Model of Cytokinetic Abscission Driven by ESCRT-III Polymerization and Remodeling. *Biophys. J.* *102*, 2309–2320.

- Emoto, K., Inadome, H., Kanaho, Y., Narumiya, S., and Umeda, M. (2005). Local Change in Phospholipid Composition at the Cleavage Furrow Is Essential for Completion of Cytokinesis. *J. Biol. Chem.* *280*, 37901–37907.
- Evangelista, M., Pruyne, D., Amberg, D.C., Boone, C., and Bretscher, A. (2002). Formins direct Arp2/3-independent actin filament assembly to polarize cell growth in yeast. *Nat. Cell Biol.* *4*, 32–41.
- Field, S.J., Madson, N., Kerr, M.L., Galbraith, K.A.A., Kennedy, C.E., Tahiliani, M., Wilkins, A., and Cantley, L.C. (2005). PtdIns(4,5)P<sub>2</sub> Functions at the Cleavage Furrow during Cytokinesis. *Curr. Biol.* *15*, 1407–1412.
- Frenette, P., Haines, E., Loloyan, M., Kinal, M., Pakarian, P., and Piekny, A. (2012a). An Anillin-Ect2 Complex Stabilizes Central Spindle Microtubules at the Cortex during Cytokinesis. *PLoS One* *7*, e34888.
- Frøkjær-Jensen, C., Davis, M.W., Hopkins, C.E., Newman, B.J., Thummel, J.M., Olesen, S.-P., Grunnet, M., and Jørgensen, E.M. (2008). Single-copy insertion of transgenes in *Caenorhabditis elegans*. *Nat. Genet.* *40*, 1375–1383.
- Gai, M., Camera, P., Dema, A., Bianchi, F., Berto, G., Scarpa, E., Germena, G., and Di Cunto, F. (2011). Citron kinase controls abscission through RhoA and anillin. *Mol. Biol. Cell* *22*, 3768–3778.
- Ganem, N.J., Cornils, H., Chiu, S.Y., O'Rourke, K.P., Arnaud, J., Yimlamai, D., Théry, M., Camargo, F.D., and Pellman, D. (2014). Cytokinesis failure triggers hippo tumor suppressor pathway activation. *Cell* *158*, 833–848.
- Gibson, D.G., Young, L., Chuang, R.-Y., Venter, J.C., Hutchison, C.A., and Smith, H.O. (2009). Enzymatic assembly of DNA molecules up to several hundred kilobases. *Nat. Methods* *6*, 343–345.
- Glotzer, M. (2004). Cleavage furrow positioning. *J. Cell Biol.* *164*, 347–351.
- Glotzer, M. (2005). The Molecular Requirements for Cytokinesis. *Science* (80-. ). *307*, 1735–1739.
- Green et al., 2012 (2012). Cytokinesis in animal cells. *Annu. Rev. Cell Dev. Biol.* *28*:12.1–12.30.

Guizetti, J., and Gerlich, D.W. (2012). ESCRT-III polymers in membrane neck constriction. *Trends Cell Biol.* 22, 133–140.

Haeusler, L.C., Blumenstein, L., Stege, P., Dvorsky, R., and Ahmadian, M.R. (2003). Comparative functional analysis of the Rac GTPases. *FEBS Lett.* 555, 556–560.

Hakem, A. (2005). RhoC is dispensable for embryogenesis and tumor initiation but essential for metastasis. *Genes Dev.* 19, 1974–1979.

Hancock, J.F., Paterson, H., and Marshall, C.J. (1990). A polybasic domain or palmitoylation is required in addition to the CAAX motif to localize p21ras to the plasma membrane. *Cell* 63, 133–139.

Hara, T., Abe, M., Inoue, H., Yu, L.-R., Veenstra, T.D., Kang, Y.H., Lee, K.S., and Miki, T. (2006). Cytokinesis regulator ECT2 changes its conformation through phosphorylation at Thr-341 in G2/M phase. *Oncogene* 25, 566–578.

Hartwell, L.H., Mortimer, R.K., Culotti, J., and Culotti, M. (1973). Genetic control of the cell division cycle in yeast: V. Genetic analysis of cdc mutants. *Genetics* 74, 267–286.

Heo, W. Do, Inoue, T., Park, W.S., Kim, M.L., Park, B.O., Wandless, T.J., and Meyer, T. (2006). PI(3,4,5)P3 and PI(4,5)P2 Lipids Target Proteins with Polybasic Clusters to the Plasma Membrane. *Science* (80-. ). 314, 1458–1461.

Hu, C.-K., Coughlin, M., and Mitchison, T.J. (2012). Midbody assembly and its regulation during cytokinesis. *Mol. Biol. Cell* 23, 1024–1034.

Jantsch-Plunger, V., Gönczy, P., Romano, A., Schnabel, H., Hamill, D., Schnabel, R., Hyman, A.A., and Glotzer, M. (2000). CYK-4: A Rho family GTPase activating protein (GAP) required for central spindle formation and cytokinesis. *J. Cell Biol.* 149, 1391–1404.

Jenkins, N. (2006). CYK-4/GAP Provides a Localized Cue to Initiate Anteroposterior Polarity upon Fertilization. *Science* (80-. ). 313, 1298–1301.

Jordan, S.N., and Canman, J.C. (2012). Rho GTPases in animal cell cytokinesis: An occupation by the one percent. *Cytoskeleton* 69, 919–930.

Justilien, V., and Fields, A.P. (2009). Ect2 links the PKC $\zeta$ -Par6 $\alpha$  complex to Rac1 activation and cellular transformation. *Oncogene* 28, 3597–3607.

Justilien, V., Ali, S.A., Jamieson, L., Yin, N., Cox, A.D., Der, C.J., Murray, N.R., and

- Fields, A.P. (2017). Ect2-Dependent rRNA Synthesis Is Required for KRAS-TRP53 - Driven Lung Adenocarcinoma. *Cancer Cell* 31, 256–269.
- Kechad, A., Jananji, S., Ruella, Y., and Hickson, G.R.X. (2012). Anillin Acts as a Bifunctional Linker Coordinating Midbody Ring Biogenesis during Cytokinesis. *Curr. Biol.* 22, 197–203.
- Kim, J.E., Billadeau, D.D., and Chen, J. (2005). The tandem BRCT domains of Ect2 are required for both negative and positive regulation of Ect2 in cytokinesis. *J. Biol. Chem.* 280, 5733–5739.
- Kishi, K. (1993). Regulation of cytoplasmic division of *Xenopus* embryo by rho p21 and its inhibitory GDP/GTP exchange protein (rho GDI). *J. Cell Biol.* 120, 1187–1195.
- Kotýnková, K., Su, K.-C., West, S.C., and Petronczki, M. (2016). Plasma Membrane Association but Not Midzone Recruitment of RhoGEF ECT2 Is Essential for Cytokinesis. *Cell Rep.* 17, 2672–2686.
- Lacroix, B., and Maddox, A.S. (2012). Cytokinesis, ploidy and aneuploidy. *J. Pathol.* 226, 338–351.
- Larochelle, D.A., Vithalani, K.K., and De Lozanne, A. (1996). A novel member of the rho family of small GTP-binding proteins is specifically required for cytokinesis. *J. Cell Biol.* 133, 1321–1329.
- Lehner, C.F. (1992). The pebble gene is required for cytokinesis in *Drosophila*. *J. Cell Sci.* 103 ( Pt 4, 1021–1030.
- Liu, A. -x., Cerniglia, G.J., Bernhard, E.J., and Prendergast, G.C. (2001). RhoB is required to mediate apoptosis in neoplastically transformed cells after DNA damage. *Proc. Natl. Acad. Sci.* 98, 6192–6197.
- Llamazares, S., Moreira, A., Tavares, A., Girdham, C., Spruce, B.A., Gonzalez, C., Karess, R.E., Glover, D.M., and Sunkel, C.E. (1991). polo encodes a protein kinase homolog required for mitosis in *Drosophila*. *Genes Dev.* 5, 2153–2165.
- Mabuchi, I., Hamaguchi, Y., Fujimoto, H., Morii, N., Mishima, M., and Narumiya, S. (1993). A rho-like protein is involved in the organisation of the contractile ring in dividing sand dollar eggs. *Zygote* 1, 325–331.

Maduro, M., and Pilgrim, D. (1995). Identification and cloning of *unc-119*, a gene expressed in the *Caenorhabditis elegans* nervous system. *Genetics* *141*, 977–988.

Mangal, S., Sacher, J., Kim, T., Osório, D.S., Motegi, F., Carvalho, A.X., Oegema, K., and Zanin, E. (2018). TPXL-1 activates Aurora A to clear contractile ring components from the polar cortex during cytokinesis. *J. Cell Biol.* *217*, 837–848.

Manke, I. a (2009). BRCT Repeats As Phosphopeptide-Binding Modules. *Science* (80-. ). *636*, 636–640.

Mello, C.C., Kramer, J.M., Stinchcomb, D., and Ambros, V. (1991). Efficient gene transfer in *C.elegans*: extrachromosomal maintenance and integration of transforming sequences. *EMBO J.* *10*, 3959–3970.

Mello, C.C., Schubert, C., Draper, B., Zhang, W., Lobel, R., and Priess, J.R. (1996). The PIE-1 protein and germline specification in *C. elegans* embryos. *Nature* *382*, 710–712.

Merritt, C., Rasoloson, D., Ko, D., and Seydoux, G. (2008). 3' UTRs Are the Primary Regulators of Gene Expression in the *C. elegans* Germline. *Curr. Biol.* *18*, 1476–1482.

Mierzwa, B., and Gerlich, D.W. (2014). Review Cytokinetic Abscission : Molecular Mechanisms and Temporal Control. *Dev. Cell* *31*, 525–538.

Miki, T., Fleming, T.P., Bottaro, D.P., Rubin, J.S., Ron, D., and Aaronson, S.A. (1991). Expression cDNA cloning of the KGF receptor by creation of a transforming autocrine loop. *Science* *251*, 72–75.

Mishima, M., Kaitna, S., and Glotzer, M. (2002). Central Spindle Assembly and Cytokinesis Require a Kinesin-like Protein/RhoGAP Complex with Microtubule Bundling Activity. *Dev. Cell* *2*, 41–54.

Mitchell, D.M., Uehlein-Klebanow, L.R., and Bembenek, J.N. (2014). Protease-Dead Separase Is Dominant Negative in the *C. elegans* Embryo. *PLoS One* *9*, e108188.

Moon, S. (2003). Rho GTPase-activating proteins in cell regulation. *Trends Cell Biol.* *13*, 13–22.

Morita, K., Hirono, K., and Han, M. (2005). The *Caenorhabditis elegans* *ect-2* RhoGEF gene regulates cytokinesis and migration of epidermal P cells. *EMBO Rep.* *6*, 1163–1168.

Motegi, F., and Sugimoto, A. (2006). Sequential functioning of the ECT-2 RhoGEF, RHO-

1 and CDC-42 establishes cell polarity in *Caenorhabditis elegans* embryos. *Nat. Cell Biol.* 8, 978–985.

Mullins, J. (1977). Terminal phase of cytokinesis in D-98S cells. *J. Cell Biol.* 73, 672–684.

Murthy, K., and Wadsworth, P. (2008). Dual role for microtubules in regulating cortical contractility during cytokinesis. *J. Cell Sci.* 121, 2350–2359.

Nigg, E. a, Blangy, a, and Lane, H. a (1996). Dynamic changes in nuclear architecture during mitosis: on the role of protein phosphorylation in spindle assembly and chromosome segregation. *Exp. Cell Res.* 229, 174–180.

Niiya, F., Tatsumoto, T., Lee, K.S., and Miki, T. (2006). Phosphorylation of the cytokinesis regulator ECT2 at G2/M phase stimulates association of the mitotic kinase Plk1 and accumulation of GTP-bound RhoA. *Oncogene* 25, 827–837.

Nishimura, Y., and Yonemura, S. (2006). Centralspindlin regulates ECT2 and RhoA accumulation at the equatorial cortex during cytokinesis. *J. Cell Sci.* 119, 104–114.

Otomo, T., Otomo, C., Tomchick, D.R., Machius, M., and Rosen, M.K. (2005). Structural Basis of Rho GTPase-Mediated Activation of the Formin mDia1. *Mol. Cell* 18, 273–281.

Petronczki, M., Glotzer, M., Kraut, N., and Peters, J.M. (2007). Polo-like Kinase 1 Triggers the Initiation of Cytokinesis in Human Cells by Promoting Recruitment of the RhoGEF Ect2 to the Central Spindle. *Dev. Cell* 12, 713–725.

Piekny, A.J., and Glotzer, M. (2008). Anillin Is a Scaffold Protein That Links RhoA, Actin, and Myosin during Cytokinesis. *Curr. Biol.* 18, 30–36.

Piekny, A., Werner, M., and Glotzer, M. (2005). Cytokinesis: welcome to the Rho zone. *Trends Cell Biol.* 15, 651–658.

Prokopenko, S.N., Brumby, A., O’Keefe, L., Prior, L., He, Y., Saint, R., and Bellen, H.J. (1999). A putative exchange factor for Rho1 GTPase is required for initiation of cytokinesis in *Drosophila*. *Genes Dev.* 13, 2301–2314.

Prokopenko, S.N., Saint, R., and Bellen, H.J. (2000). Tissue distribution of PEBBLE RNA and Pebble protein during *Drosophila* embryonic development. *Mech. Dev.* 90, 269–273.

Rappaport, R. (1985). Repeated furrow formation from a single mitotic apparatus in cylindrical sand dollar eggs. *J. Exp. Zool.* 234, 167–171.

Rhind, N., and Russell, P. (2012). Signaling pathways that regulate cell division. *Cold Spring Harb. Perspect. Biol.* 4, 1–15.

Rose, L.S., Lamb, M.L., Hird, S.N., and Kemphues, K.J. (1995). Pseudocleavage Is Dispensable for Polarity and Development in *C. elegans* Embryos. *Dev. Biol.* 168, 479–489.

Rossman, K.L., Der, C.J., and Sondek, J. (2005). GEF means go: turning on RHO GTPases with guanine nucleotide-exchange factors. *Nat. Rev. Mol. Cell Biol.* 6, 167–180.

Saito, S., Tatsumoto, T., Lorenzi, M. V., Chedid, M., Kapoor, V., Sakata, H., Rubin, J., and Miki, T. (2003). Rho Exchange Factor ECT2 Is Induced by Growth Factors and Regulates Cytokinesis Through the N-Terminal Cell Cycle Regulator-Related Domains. *J. Cell. Biochem.* 90, 819–836.

Saito, S., Liu, X.F., Kamijo, K., Raziuddin, R., Tatsumoto, T., Okamoto, I., Chen, X., Lee, C.C., Lorenzi, M. V., Ohara, N., et al. (2004). Deregulation and Mislocalization of the Cytokinesis Regulator ECT2 Activate the Rho Signaling Pathways Leading to Malignant Transformation. *J. Biol. Chem.* 279, 7169–7179.

Schmutz, C., Stevens, J., and Spang, A. (2007). Functions of the novel RhoGAP proteins RGA-3 and RGA-4 in the germ line and in the early embryo of *C. elegans*. *Development* 134, 3495–3505.

Schonegg, S., Constantinescu, A.T., Hoegge, C., and Hyman, A.A. (2007). The Rho GTPase-activating proteins RGA-3 and RGA-4 are required to set the initial size of PAR domains in *Caenorhabditis elegans* one-cell embryos. *Pnas* 104, 1–6.

Severson, A.F., Baillie, D.L., and Bowerman, B. (2002). A Formin Homology Protein and a Profilin Are Required for Cytokinesis and Arp2/3-Independent Assembly of Cortical Microfilaments in *C. elegans*. *Curr. Biol.* 12, 2066–2075.

Siderovski, D.P., and Willard, F.S. (2005). The GAPs, GEFs, and GDIs of heterotrimeric G-protein alpha subunits. *Int. J. Biol. Sci.* 1(2), 51–66.

Spencer, A.G., Orita, S., Malone, C.J., and Han, M. (2001). A RHO GTPase-mediated pathway is required during P cell migration in *Caenorhabditis elegans*. *Proc. Natl. Acad. Sci.* 98, 13132–13137.

Su, K.C., Takaki, T., and Petronczki, M. (2011). Targeting of the RhoGEF Ect2 to the

Equatorial Membrane Controls Cleavage Furrow Formation during Cytokinesis. *Dev. Cell* 21, 1104–1115.

Sulston, J.E., and Brenner, S. (1974). The DNA of *Caenorhabditis elegans*. *Genetics* 77, 95–104.

Sunkel, C.E., and Glover, D.M. (1988). polo, a mitotic mutant of *Drosophila* displaying abnormal spindle poles. *J Cell Sci* 89, 25–38.

Suzuki, K., Sako, K., Akiyama, K., Isoda, M., Senoo, C., Nakajo, N., and Sagata, N. (2015). Identification of non-Ser/Thr-Pro consensus motifs for Cdk1 and their roles in mitotic regulation of C2H2 zinc finger proteins and Ect2. *Sci. Rep.* 5, 7929.

Takaishi, K., Sasaki, T., Kameyama, T., Tsukita, S., and Takai, Y. (1995). Translocation of activated Rho from the cytoplasm to membrane ruffling area, cell-cell adhesion sites and cleavage furrows. *Oncogene* 11, 39–48

Tatsumoto, T., Xie, X., Blumenthal, R., Okamoto, I., and Miki, T. (1999). Human ECT2 is an exchange factor for Rho GTPases, phosphorylated in G2/M phases, and involved in cytokinesis. *J. Cell Biol.* 147, 921–927.

Taylor, R.M., Wickstead, B., Cronin, S., and Caldecott, K.W. (2004). Role of a BRCT domain in the interaction of DNA ligase III- $\alpha$  with the DNA repair protein XRCC1. *Curr. Biol.* 8, 877–880.

Tcherkezian, J., and Lamarche-Vane, N. (2007). Current knowledge of the large RhoGAP family of proteins. *Biol. Cell* 99, 67–86.

Tighe, A. (2004). Truncating APC mutations have dominant effects on proliferation, spindle checkpoint control, survival and chromosome stability. *J. Cell Sci.* 117, 6339–6353.

Tse, Y.C., Werner, M., Longhini, K.M., Labbe, J.-C., Goldstein, B., and Glotzer, M. (2012). RhoA activation during polarization and cytokinesis of the early *Caenorhabditis elegans* embryo is differentially dependent on NOP-1 and CYK-4. *Mol. Biol. Cell* 23, 4020–4031.

Watanabe, N., Madaule, P., Reid, T., Ishizaki, T., Watanabe, G., Kakizuka, A., Saito, Y., Nakao, K., Jockusch, B.M., and Narumiya, S. (1997). p140mDia, a mammalian homolog of *Drosophila* diaphanous, is a target protein for Rho small GTPase and is a ligand for profilin. *EMBO J.* 16, 3044–3056.

- Wilde, C., and Aktories, K. (2001). The Rho-ADP-ribosylating C3 exoenzyme from *Clostridium botulinum* and related C3-like transferases. *Toxicon* 39, 1647–1660.
- Wolfe, B.A., Takaki, T., Petronczki, M., and Glotzer, M. (2009). Polo-Like Kinase 1 Directs Assembly of the HsCyk-4 RhoGAP/Ect2 RhoGEF Complex to Initiate Cleavage Furrow Formation. *PLoS Biol.* 7, e1000110.
- Yao, F., and Eriksson, E. (2002). A Novel Tetracycline-Inducible Viral Replication Switch. *Hum. Gene Ther.* 10, 419–427.
- Yonemura, S., Hirao-Minakuchi, K., and Nishimura, Y. (2004). Rho localization in cells and tissues. *Exp. Cell Res.* 295, 300–314.
- Yoshizaki, H., Ohba, Y., Kurokawa, K., Itoh, R.E., Nakamura, T., Mochizuki, N., Nagashima, K., and Matsuda, M. (2003). Activity of Rho-family GTPases during cell division as visualized with FRET-based probes. *J. Cell Biol.* 162, 223–232.
- Yüce, Ö., Piekny, A., and Glotzer, M. (2005). An ECT2-centralspindlin complex regulates the localization and function of RhoA. *J. Cell Biol.* 170, 571–582.
- Zanin, E., Desai, A., Poser, I., Toyoda, Y., Andree, C., Moebius, C., Bickle, M., Conradt, B., Piekny, A., and Oegema, K. (2013). A conserved RhoGAP limits M phase contractility and coordinates with microtubule asters to confine RhoA during Cytokinesis. *Dev. Cell* 26, 496–510.
- Zeiser, E., Frøkjær-Jensen, C., Jorgensen, E., and Ahringer, J. (2011). MosSCI and gateway compatible plasmid toolkit for constitutive and inducible expression of transgenes in the *c. elegans* germline. *PLoS One* 6, 3–8.
- Zhao, W. -m., and Fang, G. (2005). MgcRacGAP controls the assembly of the contractile ring and the initiation of cytokinesis. *Proc. Natl. Acad. Sci.* 102, 13158–13163.
- Zou, Y., Shao, Z., Peng, J., Li, F., Gong, D., Wang, C., Zuo, X., Zhang, Z., Wu, J., Shi, Y., et al. (2014). Crystal structure of triple-BRCT-domain of ECT2 and insights into the binding characteristics to CYK-4.

## Acknowledgement

Ich möchte mich bedanken bei ...

Meiner Betreuerin Dr. Esther Zanin. Vielen Dank für die große Chance, meine Doktorarbeit in deiner aller ersten Arbeitsgruppe durchführen zu dürfen, und für das Vertrauen, mich mit Jennifer Sacher und Sriyash Mangal als deine ersten Doktoranden in dein Team zu holen. Vielen Dank für die großartige Ausbildung und die konstante Unterstützung während meiner gesamten Zeit. Es war ein großes Privileg eine Betreuerin zu haben, die trotz ihrer neuen und stressigen Aufgabe als PI jederzeit ansprechbar und erreichbar war. Durch dein großes fachliches und technisches Know-How habe ich den allerbesten Support für meine Doktorarbeit bekommen.

Bei meinen Kollegen Jennifer und Sriyash. Danke für eure großartige Unterstützung und die schöne Zeit mit euch im Labor. Es war eine Freude mit euch zu arbeiten. Gerade der Anfang einer Doktorarbeit ist nicht einfach, und ich hätte mir keine besseren Team Kollegen als euch vorstellen können. Auf euch war immer Verlass und das werde ich euch nie vergessen. Danke auch an unsere fleißige und liebe Hiwi Isabel für Ihre große Leistung.

Meinen Studenten Seren Baygun, Pedro Barbosa, Lisa Plenninger, Ricarda Trapp und Marcus Springer. Vielen Dank für eure super Leistung und euren großen Einsatz, um mir bei meiner Doktorarbeit zu helfen.

Bei Prof. Dr. Barbara Conradt und Dr. Eric Lambie. Vielen Dank, dass ihr uns, der AG Zanin, die Möglichkeit gegeben habt, in euren Räumlichkeiten unsere Arbeit zu verrichten und uns durch euer vielfältiges, technisches, Equipment so viele wichtige Experimente möglich gemacht wurden.

Bei der gesamten AG Conrad für die Unterstützung und unseren technischen Assistenten Melanie Schwarz, Nadja Lebedeva, Michaela Bauer und Linda Jocham für die tolle Organisation vom Labor.

Bei unseren Spülfrauen Silvia und Tatjana für all die Mühe und Ihren Einsatz, die täglichen Laborabläufe für uns so reibungslos zu ermöglichen

Bei meinen TAC Members:

- Prof. Dr. Heinrich Leonhardt für den konstanten Support und das ehrliche, realistische und wegweisendes Feedback für meine Experimente, basierend auf Ihrem jahrelangen und großen Erfahrungsschatz. Es ist ein großes Privileg, so einen erfahrenen PI wie Sie in meinem TAC Committee sitzen zu haben und ich bin sehr dankbar für diese große Möglichkeit, die ich hatte.
- Dr. Annette-Müller Taubenberger für ihre großartige Betreuung und Unterstützung. Danke für all dein feedback, dass du stets erreichbar warst, immer ein offenes Ohr für mich hattest und mich sowohl mit vielen fachlichen Tipps und so viel Herz begleitest hast.
- Dr. Tamara Mikeladze-Dvali für zahlreiche, experimentelle Ideen und Vorschläge.

Bei Dr. Hartmann Harz. Vielen Dank für den konstanten, technischen Support, für deinen großen Einsatz, die vielen Stunden an Einweisungen und Hilfe bei der Optimierung meiner zahlreichen Mikroskopie-Experimente. Ohne dich wäre so vieles nicht möglich geworden und dank dir konnte ich so viele schöne Aufnahmen machen.

Bei der AG Leonhardt für euren konstanten Support, und dafür, dass ihr so oft ausgeholfen habt, wenn mal was ausging und es sonst irgendwo gehakt hat.

Bei meinen Eltern, meinem Bruder Thomas und meiner Oma für ihre großartige Unterstützung und bedingungslose Liebe. Mama und Papa, ihr habt mich zu dem Menschen gemacht, der ich heute bin. Ich danke euch für alles, was ihr für mich getan habt. Ohne euch wäre ich niemals so weit im Leben gekommen und ich kann mir keine besseren Eltern als euch vorstellen.

Bei meinem Freund Marcus Jung. Vielen Dank für all deine Unterstützung und deine unendliche Liebe, die du mir in all den Jahren gegeben hast. Du hast mich durch alle Höhen und Tiefen begleitet, mir stets Mut gemacht und immer an mich geglaubt. Du hast mir so unglaublich viel Kraft gegeben, um all dies zu schaffen und warst mir der allerbeste Partner und Freund, den ich mir jemals hätte wünschen können.

Bei meiner lieben Ute Broß. Danke für deine Unterstützung seit so vielen Jahren.

Bei meinen Freunden für die große Unterstützung und die Schönen und lustigen Jahre an tiefer Freundschaft: Elisa, Basti, Christoph, Chrissy, Chrissi, Steffi, Madi und Jenny.

